NORTHWESTERN UNIVERSITY

Characterization of Three Activity Domains Within the Multifunctional RTX Toxin from *Vibrio cholerae*

A DISSERTATION

SUBMITTED TO THE GRADUATE SCHOOL
IN PARTIAL FULFILLMENT OF THE REQUIREMENTS

for the degree

DOCTOR OF PHILOSOPHY

Field of Immunology and Microbial Pathogenesis
Integrated Graduate Program in the Life Sciences

By

Kerri-Lynn Sheahan

EVANSTON, ILLINOIS

December 2006

Abstract

Characterization of Three Activity Domains within the Multifunctional

RTX Toxin from *Vibrio cholerae*

Kerri-Lynn Sheahan

The Gram-negative bacterium *Vibrio cholerae* elicits disease through the export of enterotoxins. The *V. cholerae* RTX toxin was identified due its ability to cause cell rounding. Characterization of the RTX toxin demonstrated that this cell rounding was due to the depolymerization of the actin cytoskeleton through the novel mechanism of covalent actin cross-linking. In this study, three functional domains were identified and characterized within the RTX toxin. Expression of a 47.8 kDa domain from the RTX toxin mediated the covalent cross-linking of actin. An in-frame deletion of this domain within the RTX toxin abrogated the cross-linking activity of the toxin but not cell rounding. Further investigation revealed that this second cell rounding activity was due to RTX inactivation of the Rho GTPases. This activity was mapped to a 548 amino acid region within RTX. Characterization of a third domain from RTX demonstrated that it was a novel cysteine protease domain, which is speculated to autoproces the toxin. Mutation of the catalytic cysteine on the *V. cholerae* chromosome inhibited the actin cross-linking activity of the toxin suggesting that autoprocessing of the RTX toxin is important for activity. Analysis of this cysteine protease domain revealed that it is conserved in large clostridial glucosylating toxins TcdB, TcdA, TcnA, and TcsL; putative toxins from *V. vulnificus*, *Yersinia sp.*, *Photorhabdus sp.*, and *Xenorhabdus sp.*; and a filamentous/hemagglutinin-like protein FhaL from *Bordetella sp.* which suggests that autoprocessing is a common mechanism

utilized by these proteins. Altogether, the studies presented in this thesis have further characterized the mechanism of the *V. cholerae* RTX toxin.

Acknowledgements

I think I finally see the light at the end of this very long tunnel. There were times when this long journey appeared never-ending but the last six months disappeared in the blink of an eye. I would just like to acknowledge everyone that contributed to my success during these last five years.

I thank my advisor Dr. Karla Satchell for allowing me to independently pursue this interesting project. I was encouraged to undertake this risky and overall more challenging project that has made me a better scientist.

I also thank my thesis committee, Drs. Hank Seifert, Greg Smith, Kathy Green and Kasturi Haldar, for asking challenging questions and providing input into this project.

I would like to thank the girls in the Satchell lab for always providing an entertaining environment to work in everyday. Amanda Bonebrake for her excellent technical assistance, helping me with annoying minipreps and pouring all those SDS-PAGE gels. Verena Olivier for her help with statistics as well as teaching me those key German phrases that will come in handy if I ever go to Germany. Bethany Boardman for encouraging my dream to be on American Idol. And of course to Tina Cordero for all our shopping excursions, nights drinking beer and watching baseball at O'Tooles, and all those fabulous dinner parties you had that I already miss dearly.

To the new members of the lab, Burt- I mean Brett- and Rehman, for your bravery in joining an all female lab and making these last few months fun.

Also I would like to acknowledge my friend Francesca Garcia. I cannot believe we have been friends for over 11 years. It feels like yesterday we were sitting in our dorm room

procrastinating studying for finals. I probably would not have moved halfway across the country to Chicago to go to Northwestern if she did not live here. She has always been an incredibly supportive friend during the good and bad times of my life.

To my sisters, brothers and sister-in-law, Gail, Allie, Kathy, Tommy, Lisa and Paula, I am very lucky to be the youngest of six. Thanks for all the encouragement, the fancy dinners and vacations that you have provided this poor graduate student.

Lastly, I thank my parents, Charles and Elizabeth Sheahan, for providing me with opportunities and encouragement to pursue my goals over the last thirty years. To my mom, thank you for all the airline tickets, care packages, shopping trips and vacations over the last five years. To my dad, I wish you were here to see this accomplishment but I know you are somewhere watching.

Table of Contents

List of Figures

List of Tables

Chapter 1

Introduction

Overview of Cholera

The devastating diarrheal disease cholera has significantly impacted history through the emergence of seven global pandemics (Kaper 1995). For 2005, the World Health Organization reports a total of 131,943 cases of cholera resulting in 2272 deaths from 52 countries. However, the overall number of cases and deaths resulting from cholera are expected to be higher but are underreported due to many limitations. The majority of these cases are from endemic regions with approximately 95% occurring in Africa with the second highest incidence occurring in southern Asia (WHO, 2006). Sporadic incidences of disease occur in other areas, including the United States where 4 cases were reported in 2005 associated with Hurricane Katrina (CDC, 2005).

The causative agent of cholera is the Gram-negative bacterium *Vibrio cholerae*. This rod-shaped bacterium is motile by means of a single polar flagellum. *V. cholerae* inhabits estuarine environments throughout the world as part of the normal bacterial flora. Transmission of the bacterium to the host occurs through the consumption of contaminated water or food, most notably, raw shellfish obtained from contaminated waters. Once ingested the bacteria colonizes the mucosa of the upper intestinal epithelium. Upon colonization, *V. cholerae* elicits disease through the export of enterotoxins (Kaper 1995). After an incubation period, which can range from hours to days, the symptoms of disease are abrupt and include rice-water diarrhea and

vomiting. Severe cholera results in the rapid loss of fluid leading to severe dehydration. Without proper rehydration therapy, cholera has a 50% fatality rate (Sack et al., 2004).

Only the O1 or O139 strains of *V. cholerae* cause epidemic cholera even though there are numerous reported serotypes. The *V. cholerae* O1 serotype is further classified into the classical biotype, which is associated with the sixth and most likely the fifth pandemics, and the El Tor biotype, currently associated with the seventh pandemic (Kaper 1995). Identification of the O139 serogroup in the early 1990's in India as the cause of explosive outbreaks of disease suggests that this new strain may correspond to the emergence of an eighth pandemic of cholera (Hisatsune et al., 1993; Ramamurthy et al., 1993; Swerdlow and Ries, 1993). Non-O1/non-O139 *V. cholerae* strains exist in the environment and are reported to cause sporadic outbreaks associated with milder diarrheal disease and extraintestinal infections (Bhattacharya et al., 1998; Faruque et al., 2004; Sharma et al., 1998).

Previous studies revealed that volunteers experimentally infected with a *V. cholerae* O1 classical strain had full protection for a minimum of 3 years against subsequent infection with other classical strains of *V. cholerae* (Levine et al., 1981; Levine et al., 1979). Similar studies with a *V. cholerae* O1 El Tor strain exhibited 90% protection against subsequent infection (Levine et al., 1979). These studies demonstrate that protective immunity was established after infection with *V. cholerae* indicating that development of a vaccine could be useful in the prevention of massive outbreaks of disease (Levine et al., 1981). However, early attempts in vaccine production had severe side effects, did not establish lasting immunity, and were not cost effective for the people that would benefit most from them (Mosley et al., 1972; Sack et al., 2004). In order to develop a safe effective vaccine that will establish long lasting immunity, the

contribution of *V. cholerae* virulence factors to the disease cholera needs to be extensively characterized.

Virulence Factors

The major virulence factor of *V. cholerae* is cholera toxin (CT) (Kaper 1995). After colonization of the intestine, the bacterium secretes this bipartite toxin where a pentamer of cholera toxin B-subunits bind to the ganglioside G_{M1} on the surface of the cell to facilitate the entry of the catalytic A-subunit into the cell (Hirst, 1999; Svennerholm, 1976). Once inside the cell, the toxin catalyzes the ADP-ribosylation of the α-subunit of the Gs GTP-binding protein causing the constitutive activation of adenylate cyclase (Cassel and Selinger, 1977; Moss and Vaughan, 1977). This increase in adenylate cyclase activity leads to elevated levels of the secondary messenger 3'-5'-cyclic AMP (cAMP) in the cell. High levels of cAMP cause increased secretion of Cl^- and decreased adsorption of NaCl resulting in the efflux of water into the lumen (Field et al., 1972). This fluid accumulation in the intestine produces the profuse watery diarrhea associated with cholera disease (Speelman et al., 1986).

Another major virulence factor of *V. cholerae* is the type IV bundle forming pilus known as the toxin co-regulated pilus (TCP). The TcpA subunit assembles into long filaments that are further associated laterally into bundles to form the pilus (Taylor et al., 1987). Biogenesis of TCP is hypothesized to occur in a manner similar to type II secretion (Kirn et al., 2003). The function of TCP is to aid in the adherence of the bacterium to epithelial cells and previous studies reveal the importance of TCP in mediating bacterial interactions to promote microcolony formation (Kirn et al., 2000) . Mouse studies as well as studies in human volunteers demonstrate that a

disruption in the *tcpA* gene encoding the pilin subunit completely abolishes colonization of *V. cholerae* (Herrington et al., 1988; Taylor et al., 1987).

Analysis of *V. cholerae* O1 isolates revealed that the genes encoding CT and TCP are not found in all isolates. These data and further sequence analysis indicated that through evolution these genes were acquired by the bacterium through horizontal gene transfer (Faruque and Mekalanos, 2003). In fact, CT is encoded by a filamentous phage, CTXΦ, that has integrated on the *V. cholerae* chromosome (Waldor and Mekalanos, 1996). The genes required for TCP structure and biosynthesis are encoded within an operon located within the TCP-ACF element also known as the *Vibrio* pathogenicity island (VPI) (Faruque and Mekalanos, 2003; Kovach et al., 1996). Overall, the acquisition of these two major virulence factors significantly contributed to the pathogenicity of *V. cholerae*.

Since the production of CT is responsible for the manifestation of the massive diarrhea associated with *V. cholerae*, it was proposed that deletion of these genes would yield a strain for use as a live attenuated vaccine. However, both clinical isolates and genetically modified strains of *V. cholerae* that lack the *ctx* genes still cause mild diarrheal disease (Levine et al., 1988; Morris, 2003). These *V. cholerae* strains also produce a more inflammatory diarrheal disease than observed in the presence of cholera toxin (Silva et al., 1996). In addition, *V. cholerae* O1 strains that lack CT as well as non-O1/non-O139 strains can be invasive leading to bacteremia with severe sepsis (Crump et al., 2003; Ninin et al., 2000). These findings suggest that other enterotoxins secreted by *V. cholerae* are contributing to the overall disease.

Linkage of Accessory Toxins of *V. cholerae* to Pathogenesis

Other accessory toxins secreted by *V. cholerae*, the hemagglutinin protease (HAP), hemolysin (HlyA) and the repeats-in-toxin (RTX), are hypothesized to be coordinately contributing to this milder form of cholera disease (Fullner et al., 2002). Experiments utilizing a murine pulmonary model reveal that a *V. cholerae* strain with a deletion of the *ctxAB* genes causes diffuse pneumonia as demonstrated by infiltration of polymorphonuclear leukocytes, tissue damage and hemorrhage. However, a *V. cholerae* strain that has a deletion of the *ctxAB* genes in combination with the *hlyA, hap*, and *rtxA* genes could still colonize the lung but is avirulent producing limited inflammation. In this model, a *V. cholerae* strain with a combined deletion of the *ctxAB* and *rtxA* genes yields a decrease in the pathology and inflammatory response (Fullner et al., 2002). This study clearly suggests that these three accessory toxins contribute to the pathogenesis of *V. cholerae*.

Understanding the mechanism of action of these toxins will help define their role in pathogenesis. HAP is a zinc-metalloprotease that has both hemagglutinating and proteolytic activity (Hase and Finkelstein, 1993). *In vitro* studies demonstrate that HAP degrades occludin in the tight junctions disrupting the endothelial monolayer (Wu et al., 2000). HlyA causes vacuolation of epithelial cells in culture eventually leading to cell lysis (Coelho et al., 2000; Figueroa-Arredondo et al., 2001; Mitra et al., 2000). The studies presented in this thesis will focus on characterization of the activities of the RTX toxin from *V. cholerae*.

Discovery of the RTX Toxin

The RTX toxin gene cluster was discovered in 1999 through a combination of genomic sequence analysis, genetic mapping and representational difference analysis. The *rtxA* gene is a 13,635-bp-long ORF located adjacent to the *ctx* genes on the large chromosome of *V. cholerae*. The deduced RTX protein is 4,545 amino acids in length, with a predicted molecular mass of 484 kDa, making it the second largest polypeptide toxin reported. Initial characterization of RTX revealed that this toxin causes the rapid rounding of human laryngeal epithelial cells (HEp-2) (Lin et al., 1999). RTX is expressed by El Tor O1 and O139 *V. cholerae* strains responsible for the current cholera pandemic (Chow et al., 2001; Lin et al., 1999). The O1 classical biotype strains of *V. cholerae* do not produce the RTX toxin due to a 7 kilobase deletion in the RTX gene cluster (Lin et al., 1999). This toxin is also expressed by non-O1/non-O139 isolates, and is believed to contribute to the emergence of these strains as pathogens (Dalsgaard et al., 2001; Faruque et al., 2004). All recent isolates of *V. cholerae* contain an intact *rtxA* gene as determined by PCR, RFLP, and microarray analysis (Bina et al., 2003; Chow et al., 2001; Dalsgaard et al., 2001; Xu et al., 2003). A recent study by Chow et al. demonstrates that 166 recent isolates of *V. cholerae* caused HEp-2 cell rounding which was correlated by PCR analysis to the presence of the *rtx* genes (Chow et al., 2001).

The *V. cholerae* RTX toxin was classified as a member of the repeats-in-toxin (RTX) family, which is a diverse family of proteins secreted by Gram-negative bacteria. The bacterial protein toxins initially characterized in this family were pore-forming hemolysins and leukotoxins but other toxins assigned to this family include proteases and lipases. Members of this family include *Escherichia coli* hemolysin, *Pasturella haemolytica* and *Actinobacillus actinomycetemcomitans* leukotoxins, and *Bordetella pertussis* adenylate cyclase-hemolysin

toxin. The general characteristics shared by this toxin family are as follows: the presence of Ca^{2+} binding nonapeptide glycine rich amino acid repeats at the C-terminus of the protein, secretion by the bacterium through a type I secretion system and post-translational maturation of the toxin (Welch, 2001).

RTX Secretion by an Atypical Type I Secretion System

The *V. cholerae* RTX toxin is secreted from the bacterium by an atypical Type I secretion system (Boardman and Satchell, 2004). A type I secretion apparatus typically has three general components, which include a homodimer of an inner membrane transport ATPase, a trimer of a transmembrane linker protein and a trimer of an outer membrane porin (Andersen et al., 2000). Analysis of the *V. cholerae* RTX operon reveals a type I secretion apparatus that is divergently transcribed from the *rtxA* toxin gene (Lin et al., 1999). This operon contains genes for two transport ATPases with 60% similarity (*rtxB* and *rtxE*) and the transmembrane linker (*rtxD*). Experimental evidence indicates that instead of the typical homodimer inner membrane transport ATPase, the *V. cholerae* RTX toxin has two distinct transport ATPases that are required for export of the toxin from the bacterium. The outer membrane porin TolC, which is not linked to the RTX gene cluster, is essential for secretion of the *V. cholerae* RTX toxin. Therefore, the *V. cholerae* RTX toxin utilizes an atypical four component type I secretion system unlike other members of the RTX toxin family (Boardman and Satchell, 2004).

RTX Toxin Structure

The *V. cholerae* RTX toxin is predicted to be 484 kDa which is 2-3 times larger than other RTX toxin family members (Figure 1-2). Analysis of the primary structure of the RTX toxin revealed that approximately one-quarter of this large toxin is comprised of 3 distinct classes of 18-20 amino acid glycine rich repeats with the common central motif of G-7x-GxxN localized at the extreme N- and C-terminus of RTX. The first class of repeats are the A repeats that are 20 residue repeats with the consensus sequence [GxxG(N/D)(L/I)(T/S)FxGAG(A/G)xNx(L/Ix(RH)] (central motif double underlined). There are 16 copies of these repeats located at the extreme N-terminus of RTX as depicted in Figure 1-1. The B repeats are a second class of repeats also located within the N-terminus of RTX following the A repeats. There are 34 consecutive copies of these repeats with the consensus sequence [T(K/H)VGDGx(ST)VAVMxGxAN(I/V)x] (central motif double underlined).

Figure 1-1: Schematic representation of RTX toxin.
Model of RTX toxin depicting the A repeats, B repeats and C repeats. The location of two cysteine residues are marked with C above. Numbers along the bottom correspond to the amino acids.

The third class of repeats are the C repeats and represent the RTX like repeats that initially classified this toxin as a member of the RTX toxin family. These 18 amino acid repeats are located at the C-terminus and have similarities to both the nonapeptide RTX repeats as well as the A and B repeats located in the N-terminus of the toxin. There are 15 copies of the C repeats with the consensus sequence [GGxG(N/D)Dxx(V/I)(L/V/I)xGxxNxxx] (central motif

double underlined) (Figure 1-1). Additional analysis of the amino acid sequence of RTX interestingly reveals that there are only two cysteine residues within all of the 4545 amino acids suggesting that these two amino acids could be important in toxin function (Figure 1-1).

RTX Toxin Activity

As stated above the RTX toxin was initially characterized to cause the rounding of a broad range of cells grown in culture including HEp-2, A549 lung epithelial carcinoma cells, Henle 407 intestinal epithelial cells, L6 rat fibroblastoma cells, Chinese hamster ovary cells, Raw264.7 and J774 macrophages. Experiments revealed that this observed cytotoxic activity was not due to pore forming activity described by other RTX family members as demonstrated by no elevated increase of lactate dehydrogenase or sodium^{51} chromate in the culture media of these cells. These rounded cells also excluded the membrane impermeant dye DEAD-RED, trypan blue and propidium iodide further confirming that the membranes of cells exposed to the RTX toxin are intact. Additional experiments using alamar blue dye determined that cells rounded by RTX are still biochemically active 24 hours after exposure to the toxin (Fullner and Mekalanos, 2000).

Cells rounded by the RTX toxin stained with fluorescently-labelled phalloidin revealed that the actin cytoskeleton was extensively depolymerized after 1 hour of incubation with RTX and ceased to bind phalloidin after 2 hours of incubation. This depolymerization of actin was identified to occur by a mechanism unique to this toxin, the cross-linking of actin monomers, as shown by the appearance of actin dimers, trimers and higher-order multimers in cells exposed to bacteria expressing the RTX toxin. Biochemical analysis of purified 84 kDa cross-linked protein

confirmed that this protein was a homodimer of actin. These cross-linked actin multimers were observed even after the proteins were boiled for 10 minutes in SDS-PAGE buffer containing 0.2 M dithiothreitol, 5% β-mercaptoehanol, 6 M urea or 1 % Triton X-100 indicating that these stable cross-linked actin proteins are covalently cross-linked (Fullner and Mekalanos, 2000).

Recent evidence also demonstrates that the RTX toxin disrupts the integrity of the polarized intestinal epithelial cell monolayer. *In vivo* columnar epithelial cells line the intestine establishing a barrier through the formation of tight junctions and adherens junctions. These junctions maintain cell shape through association of their respective transmembrane proteins with the actin cytoskeleton. *In vitro* T84 cells grown in transwell dishes establish a polarized monolayer composed of basolateral and apical surfaces mimicking what occurs *in vivo*. The addition of *V. cholerae* secreting the RTX toxin to both the apical and basolateral surfaces of the cell monolayer causes an 80% reduction in electrical resistance across the monolayer. Additionally, incubation with RTX results in a 6-fold increase in the permeability of 3000 Da dextran across the monolayer (Fullner et al., 2001). Therefore the RTX toxin activity contributes to the disease cholera possibly through disruption of the intestinal epithelial monolayer.

V. cholerae RTX Toxin Represents New Family of *Vibrio*-type RTX Toxins

Characterization of the *V. cholerae* RTX toxin distinguished this toxin as a unique member of the RTX family of toxins. This conclusion was made due to the presence of three glycine rich repeat regions, the large size of this RTX toxin, the secretion of RTX by an atypical type I secretion system and the unique activities of this toxin. Genomic sequencing projects

discovered putative RTX toxins with structural features similar to the unique *V. cholerae* RTX toxin indicating that these toxins may represent a new *Vibrio* type family of RTX toxins. These putative RTX toxins were identified in a close relative organism *V. vulnificus* as well as in the insect pathogens *Xenorhabdus bovienii, X. nematophila* and four proteins from *Photorhabdus luminescens* (Duchaud et al., 2003; Gulig et al., 2005). The presence of a putative RTX toxin in *V. vulnificus* was particularly interesting since this bacterium causes gastrointestinal disease and necrotizing fasciitis resulting in rapid mortality (Hlady and Klontz, 1996; Musher, 1989). Recent studies demonstrated that a *V. vulnificus* strain with a deletion of the *vvhA, vvpE* and *rtxA* genes, which are similar to the HAP, HlyA and RTX toxins of *V. cholerae*, significantly attenuated the lethality of this organism in mice (Dhakal et al., 2006).

Analysis of these putative toxins revealed that all of these toxins were greater that 3500 amino acids with the putative RTX toxin from *V. vulnificus* representing the largest toxin encoding 5206 amino acids. These putative toxins were also located within gene clusters organized similar to the *V. cholerae rtx* locus putatively encoding a type I secretion system with two independent transport ATPases. Sequence alignment of these putative RTX toxins with the *V. cholerae* RTX toxin demonstrated that there is high sequence conservation within the N- and C-terminus including the repeat regions described above (Figure 1-2). However the internal regions of these proteins exhibited sequence divergence as well as conservation among the eight members of the *Vibrio* type RTX proteins (Figure 1-2). From this analysis, the conserved N- and C-terminal regions were hypothesized to be involved in delivery of the toxin to the cell with the divergent internal regions responsible for mediating different cytotoxic activities.

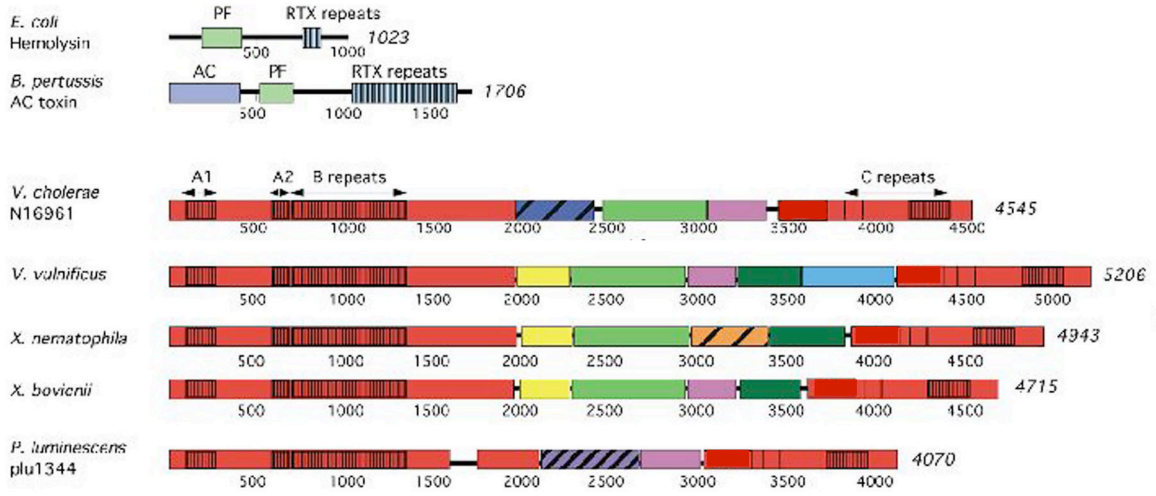

Figure 1-2: Comparison of the *V. cholerae* RTX toxin with other putative RTX toxins.
Diagrams of representative RTX pore-forming toxins from *E. coli* and *B. pertussis* marking the RTX repeats, the pore forming region (PF) and the adenylate cyclase region (AC). Diagram of *Vibrio* type RTX toxins marking the conserved N- and C-terminal regions of all eight RTX toxins including the A, B, and C repeats in red. Regions that share homology with one or more, but not all proteins are color-coded to show the mosaic structure of the internal domains.

Bacterial Toxins Target the Rho GTPase Signaling Pathway

Many bacterial toxins have adapted mechanisms to advantageously manipulate the actin cytoskeleton by targeting the small Rho GTPase signaling proteins, which coordinately regulate the actin dynamics within the cell. As depicted in Figure 1-3, the Rho GTPases cycle between an active membrane-localized GTP-bound state and an inactive GDP-bound state. The activation state is regulated by guanine nucleotide exchange factors (GEFs) that mediate exchange of GDP for GTP and GTPase activating proteins (GAPs) that stimulate the intrinsic GTPase activity of the Rho family proteins. The inactive GDP-bound form can also be sequestered in the cytosol in complex with guanine nucleotide dissociation inhibitors (GDI), adding an additional level of regulation for GTPase activation. In the active GTP-bound state, the Rho GTPases can bind to effector proteins to activate signaling pathways in the cell (Etienne-Manneville and Hall, 2002).

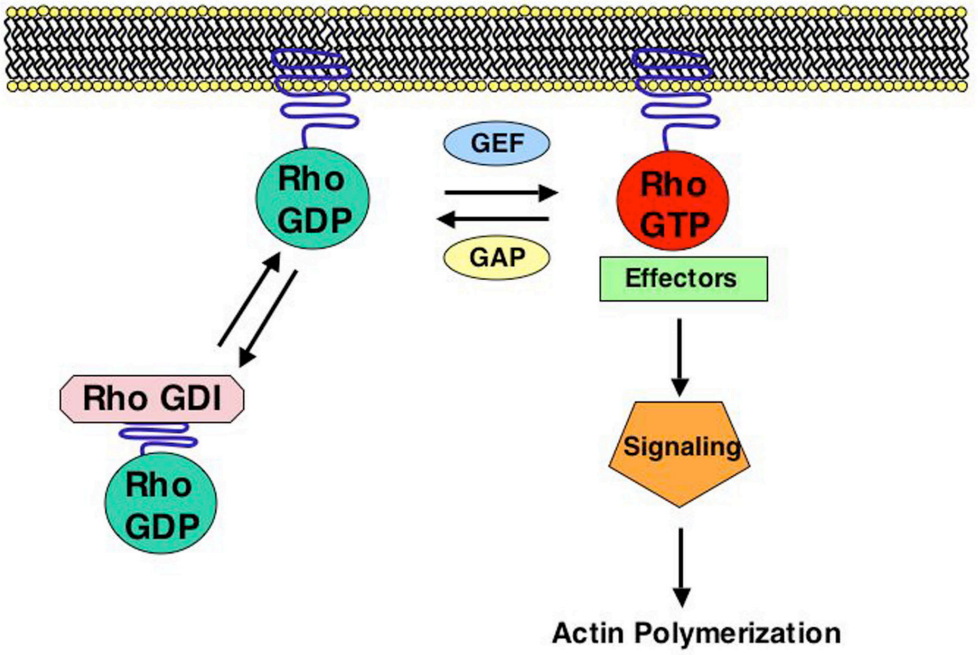

Figure 1-3: Schematic depicting the Rho GTPase signaling pathway.
Adapted from *Nature Reviews Microbiology* 3, 397-410 (2005).

Approximately twenty members have been identified for the family of Rho GTPases (Etienne-Manneville and Hall, 2002). The three most extensively characterized members of this family are Rho, Rac and Cdc42, each controlling distinct organization of the actin cytoskeleton. Activation of Rho leads to the assembly of contractile actin stress fibers across the cell as well as the associated focal adhesion complexes (Ridley and Hall, 1992). Rac activation induces the polymerization of actin at the cell periphery producing lamellipodia and membrane ruffling (Ridley et al., 1992). The activation of Cdc42 causes actin-rich surface protrusions that appear as microspikes at the surface of the cell called filopodia (Nobes and Hall, 1995). Besides regulating the actin cytoskeleton, these signaling proteins also control other cellular activities (Hall and Nobes, 2000).

The Rho GTPase signaling pathways are critical for the maintenance of the epithelial barrier through their regulation of junctional complexes, which include the tight junctions and the adherens junctions (Braga *et al.*, 1997; Nusrat *et al.*, 1995). These signaling proteins are also important for other cellular events including cell motility, membrane trafficking as well as transcriptional regulation, which are all important for the host adaptive and innate immune responses. Previous studies have shown that the Rho GTPases play a essential role in leukocyte migration, macrophage phagocytosis, and expression of cytokines and chemokines (Aktories and Barbieri, 2005; Vicente-Manzanares and Sanchez-Madrid, 2004). Due to the crucial role of the actin cytoskeleton and the Rho GTPases in these cellular functions, bacterial toxins target these molecules in order to promote the pathogenesis of their respective organism.

Bacterial toxins can irreversibly modify the members of the small Rho GTPase family resulting in either activation or inactivation of these signaling proteins. The C3 exoenzyme from *C. botulinum* as well as Toxin A and B from *C. difficile* directly target these signaling proteins through an irreversible covalent modification (Chardin et al., 1989; Just et al., 1995a; Just et al., 1995b). These covalent modifications disrupt the ability of the Guanine exchange factors (GEFs) to exchange GDP for GTP rendering these GTPases in the inactive conformation (Sehr *et al.*, 1998). Conversely covalent modification by the Dermonecrotizing toxin from *Bordetella spp.* and the Cytotoxic Necrotizing Factor 1 from *E. coli* constitutively activate the Rho GTPases blocking the intrinsic as well as the GTPase activating proteins stimulation of the hydrolysis of GTP (Fiorentini *et al.*, 1997; Horiguchi *et al.*, 1997; Schmidt *et al.*, 1997).

Bacterial toxins have also evolved to mimic host cell proteins involved in the regulation of the activation state of the Rho GTPases to either reversibly activate or inactivate these signaling proteins (Aktories and Barbieri, 2005). *Salmonella spp.* coordinately translocates the

opposing Type III effectors SopE and SptP. SopE is a GEF that promotes the activation of the Rho GTPases to facilitate the entry of the bacteria into non-phagocytic intestinal epithelial cells (Hardt et al., 1998; Stender et al., 2000). SptP, which exhibits dual functionality mimicking mammalian GAP proteins and tyrosine phosphatases, then inactivates the GTPases Rac and Cdc42 in order to return the cell to normal morphology (Fu and Galan, 1999). *Pseudomonas aeruginosa* ExoS and ExoT and *Yersinia spp*. YopE are also examples of bacterial toxins that mimic host GAP proteins to inactivate the Rho GTPases blocking phagocytosis of their respective organisms (Black and Bliska, 2000; Goehring et al., 1999; Krall et al., 2000). Essentially, bacterial toxins have developed many different mechanisms to target the actin cytoskeleton to promote the pathogenesis of their organism.

Adaptation of Anthrax Toxin Lethal Factor to Deliver Recombinant Proteins to Cytosol

The *Bacillus anthracis* anthrax toxin utilizes a well-characterized entry mechanism to intoxicate the cell. Anthrax toxin is comprised of three components, which include Protective Antigen (PA) that assists in the entry of either catalytic component lethal factor (LF) or edema factor (EF) (Abrami et al., 2005). As depicted in Figure 1-4, Protective antigen (PA) binds to the anthrax toxin receptor (1) (Bradley et al., 2001). Once bound the extracellular protease furin cleaves PA to its active form PA_{63} on the surface of the cell (2) (Molloy et al., 1992). PA_{63} undergoes oligomerization into a heptamer (3) (Milne et al., 1994). Then three molecules of EF or LF can bind to $[PA_{63}]_7$ (4) and the complex enters the cell through receptor-mediated endocytosis (5) (Gordon et al., 1988; Mogridge et al., 2002). Acidification of the vacuole

triggers PA to form a pore and translocate either EF or LF into the cytosol (6) (Elliott et al., 2000; Koehler and Collier, 1991).

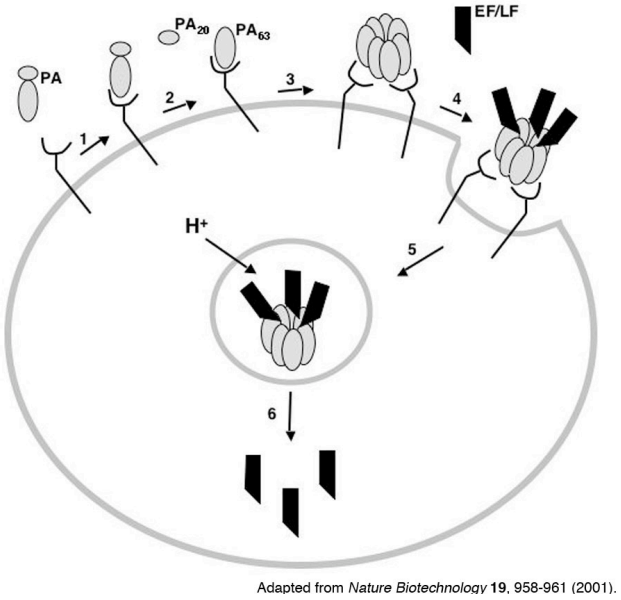

Figure 1-4: Schematic depicting Anthrax toxin entry
The steps of toxin entry are described in text. Adapted from Nature Biotechnology 19, 958-961 (2001).

Previous studies demonstrated that the N-terminal 254 amino acids of either EF or LF were sufficient to bind to PA and facilitate the entry of proteins fused to this region (Arora and Leppla, 1993). The catalytic chain of diphtheria toxin from *Corynebacterium diphtheriae* fused to the N-terminal 254 amino acids of lethal factor (LF_N) was delivered to the cytosol of the cell dependent on the presence of PA (Milne et al., 1995). This method was also employed to facilitate the entry of enzymatic domains from the bacterial toxins *C. difficile* Toxin B, *Pseudomonas* exotoxin A, and Shiga toxin from *Shigella dysenteriae* indicating that it is a useful tool to study enzymatic domains of bacterial toxins (Arora and Leppla, 1993; Arora and Leppla, 1994; Spyres et al., 2001).

Clostridium difficile Toxin B is Autoprocessed after Translocation into the Cell

The *Clostridium difficile* Toxin B (TcdB) is a member of the large clostridial glucosylating family of toxins whose members are all greater than 250 kDa. The TcdB toxin is comprised of three functional domains (Voth and Ballard, 2005). The N-terminal enzymatic domain binds and glucosylates Rho, Rac and Cdc42 (Hofmann et al., 1997). The middle domain of the toxin is a putative membrane insertion-translocation domain proposed to facilitate the translocation of the N-terminal enzymatic fragment into the cytosol of the cell. The C-terminal receptor-binding domain of TcdB represents approximately one-third of the toxin and contains 38 repeating CROP modules that hypothesized to bind a saccharide on the surface of the cell (Voth and Ballard, 2005).

Intoxication of cells by TcdB requires the N-terminal domain to access the cytosol in order to glucosylate the Rho GTPase proteins (Florin and Thelestam, 1983). TcdB binds to an unidentified receptor on the surface of the cell, undergoes receptor-mediated endocytosis and upon acidification of the vacuole a channel is formed in the lipid bilayer translocating the toxin into the cytosol (Barth et al., 2001; Florin and Thelestam, 1986; Voth and Ballard, 2005). Until recently it was not known whether the full-length toxin or just the N-terminal region was released into the cytosol. However, recent experiments demonstrate that following proteolytic cleavage the N-terminal region is released into the cytosol of the cell (Pfeifer et al., 2003). Further *in vitro* characterization of the TcdB proteolytic cleavage reveals that a host cell lysate can stimulate the cleavage of purified toxin between L543 and G544 (Rupnik et al., 2005). The RTX toxin has sequence similarity to this region of TcdB including the conservation of a His and Cys (Fullner and Mekalanos, 2000). Interestingly, these conserved residues corresponding to His654 and Cys699 in TcdB were previously shown to be important for cytotoxicity of the toxin

(Barroso et al., 1994). This region conserved between RTX and TcdB is further characterized in chapter 5.

Summary of Thesis Results

The goal of this work was to identify functional domains of the *V. cholerae* RTX toxin in order to further understand the mechanism of action of this toxin. Through a combination of molecular biological, cell biological and biochemical techniques three functional domains of the RTX toxin were identified and characterized. The identification of the domain responsible for actin cross-linking unveiled a second cell rounding activity. This cell rounding activity was determined to be due to the inactivation of the Rho GTPases. Further studies identified the region of RTX that inactivates the Rho GTPases. Lastly, a third functional domain was discovered within RTX that is a novel cysteine protease hypothesized to cleave the RTX toxin after stimulation by a host cell factor. Analysis of this region revealed that this domain is conserved in other large bacterial toxins suggesting that autoprocessing by a cysteine protease domain is a common mechanism shared by these bacterial toxins.

Chapter 2

Materials and Methods

Cell lines, bacterial strains and reagents

Human laryngeal epithelial cells (HEp-2) and African green monkey kidney fibroblasts (COS-7) were cultured at 37°C with 5% CO_2 in Dulbeccos Modified Eagle's Medium (DMEM) containing 50 U/mL penicillin, 50 µg/mL streptomycin, and 10% Fetal Bovine Serum (Invitrogen, Carlsbad, CA). T84 intestinal epithelial cells were cultured at 37°C with 5% CO_2 in T84 medium (low-glucose DMEM mixed 1:1 with Ham's F-12 nutrient mixture with l-glutamine).

The *Vibrio cholerae* strains, KFV92, KFV102 and KFV119, were previously made by Karla Satchell. KFV119 was derived from KFV43 (Fullner and Mekalanos, 1999) (Table I); a streptomycin-resistant isolate of the *V. cholerae* O1 El Tor Inaba strain N16961 with a deletion in the *hapA* gene. KFV92 was constructed from CW128 a strain isogenic to KFV43 with a deletion in the *rtxA* gene. KFV102 was derived from the strain KFV70 (P4 Δ*hapA*) (Table I). KFV43, KFV70 and CW128 were modified to delete the gene *hlyA* by double homologous recombination using the plasmid pCWΔ*hlyA* and the *sacB*-lethality counter selection method as previously described (Fullner et al., 2002)(Table I). Strains were grown at 30°C in Luria broth (LB) containing streptomycin (100 µg/mL). The *V. vulnificus* strains FLA400 (VvRTX-) and MO6-24/0 (VvRTX+), obtained from P. Gulig (University of Florida, Gainesville), were grown at 30°C in Luria broth (LB).

All restriction enzymes were obtained from New England Biolabs (Beverly, MA) and Invitrogen (Carlsbad, CA). All chemicals were purchased from Sigma (St. Louis, MO) except N-ethylmaleimide was from Pierce (Rockford, IL), Calpeptin, E64, and Pepstatin were from Calbiochem (La Jolla, CA), and isopropyla-beta-D-thiogalactopyranoside (IPTG) was from Denville Scientific (Metuchen, NJ). Oligonucleotides as listed in Table II were obtained from either Qiagen (Germantown, MD), Sigma (St. Louis, MO) or IDT (Coralville, IA).

Construction of EGFP plasmids

Primers used to make the following constructs are listed in Table II. Table III contains detailed descriptions of the regions expressed by the EGFP plasmids constructed in these studies. For all constructs, plasmid DNA prepared using the Qiaprep Spin Miniprep kit (Qiagen, Valencia, CA) was sequenced at either the CRC DNA Sequencing Facility at the University of Chicago or the Northwestern University Biotechnology Core facility to confirm gene sequence and *gfp* fusion.

Actin Cross-linking Domain (ACD) Constructs

Primers VgrG1963 and VgrG*Eco*RI were designed to amplify the DNA corresponding to amino acids (aa) 1963-2419 of RTX with flanking *Bgl* II and *Eco* RI sites from N16961 genomic DNA. The five N-terminal ACD deletions were constructed using the following forward primers NΔ30, NΔ90. NΔ168, NΔ254, and NΔ328 and the VgrG*Eco*RI reverse primer. The two C-terminal ACD truncations were made using the VgrG1963 forward primer with the CΔ129 and CΔ45 reverse primers. To construct the pVC1416-EGFP expression plasmid, primers VC1416F and VC1416R were used to amplify the DNA corresponding to amino acids 716-1161 of the VC1416

ORF. PCR products were then cloned into the pCR-BluntII-TOPO vector (Invitrogen, Carlsbad, CA) and then subcloned into the pEGFP-N3 vector (Clontech, Mountain View, CA) as a *Bgl* II- *Eco* RI fragment in order to create an in-frame fusion to the *gfp* gene.

Rho GTPase Inactivation Domain (RID) Constructs

To construct the plasmid pYP-Tox, primers YPF and CPD-*Eco*RI were used to amplify the DNA corresponding to aa 2420-3637 of RTX from N16961 genomic DNA. After cloning into the *Eco*RV site of pBluescript, the resulting plasmid was digested with *Spe*I and *Apa*I and the resulting fragment corresponding to the aa 2420-3443 was sub-cloned into the *Nhe*I and *Apa*I sites on the pEGFP-N1 vector (Clontech, Mountain View, CA). The vector was digested again with *Apa*I, incubated with the Klenow fragment from DNA polymerase I and re-ligated in order to create an in-frame fusion with the *gfp* gene. Plasmid pKS76 was constructed by digesting pYP-Tox with *Bam*HI and *Pst*I and cloning the resulting fragment into the *Bgl*II and *Pst*I sites pf pEGFP-C3 (Clonetech, Mountain View, CA) to create an in-frame N-terminal fusion to the *gfp* gene. To construct plasmid pKS77, pYP-Tox was digested with *Sac*I and *Pst*I and the resulting fragment was cloned into the *Sac*I and *Pst*I sites of pEGFP-C3 (Clonetech, Mountain View, CA) as an in-frame N-terminal fusion to the *gfp* gene.

The plasmids pKS80, pKS82 and pKS84 were constructed using the YPF primer with the RID384R, RID346R, and RID326R respectively. Plasmids pKS86, pKS88 and pKS90 were constructed using the RID-*Nhe*I primer with the RID384R, RID346R, and RID326R respectively. Plasmids pKS92, pKS94, pKS96 were constructed using the RID170F primer with the RID384R, RID346R, and RID326R respectively. Plasmids pKS98, pKS100, and pKS102 were constructed using the RID210F with the RID384R, RID346R, and RID326R respectively.

PCR products were cloned into the *Eco*RV site of pBluescript. The resulting plasmids were either digested with *Spe*I and *Pst*I (for pKS80, pKS82 and pKS84) or *Nhe*I and *Pst*I and subcloned in-frame into the *Nhe*I and *Pst*I restriction sites of pEGFP-N3 (Clonetech, Mountain View, CA).

To construct pYP, the PCR product generated with the primers YPF and YPR was cloned into pCR-BluntII-TOPO (Invitrogen, Carlsbad, CA) and the fragment produced by digestion with *Bgl*II and *Pst*I was subcloned in-frame into pEGFP-N3 (Clontech, Mountain View, CA). The plasmid pKS107 and pABHY were constructed using either the primer RTX8410F or ABHY-*Bgl*II in the forward direction with the primer ABHY-*Eco*RI in the reverse direction introducing flanking *Bgl*II and *Eco*RI sites. Plasmids pRID and pKS111 were constructed using the RID-*Nhe*I primer in the forward direction and either the primer RID-*Bam*H1 or RTX9627R in the reverse direction introducing flanking *Nhe*I and *Bam*HI sites. PCR products were cloned into the *Eco*RV site of pBluescript and then subcloned into pEGFP-N3 (Clontech, Mountain View, CA) as either an *Bgl*II-*Eco*RI or *Nhe*I-*Bam*H1 fragment to create an in-frame fusion to *gfp*.

Cysteine Protease Domain Constructs

For the plasmid pCPDc, the primers CPDc-*Bgl*II and CPD-*Eco*RI were used to amplify the DNA corresponding to aa 3376-3637 of RTX with flanking *Bgl*II and *Eco*RI from N16961 genomic DNA. Six N-terminal truncations of CPD were constructed using the following forward primers CPDNΔ36, CPDNΔ58, CPDNΔ65, CPDNΔ85, CPDNΔ120, and CPDNΔ157 with the CPD-*Eco*RI reverse primer. The plasmid pCPDcCΔ20 was made with the forward primer CPDc-*Bgl*II and the reverse primer CPDCΔ20. To construct pxlCPDc and pCPDn, PCR products were

generated using primers xlCPDc-*Bgl*II and CPDn-*Bgl*II in the forward direction and CPD-*Eco*RI in the reverse direction. All PCR products were cloned into the pCR-BluntII-TOPO vector and the *Bgl*II-*Eco*RI fragments were then subcloned into either pEGFP-N3 or pEGFP-C3 (Clontech, Mountain View, CA) to create in-frame fusions to *gfp*.

Mutagenesis of the EGFP Constructs

Point mutations within pRID and pCPDc were engineered using the Quickchange Mutagenesis kit (Stratagene, La Jolla, CA). The Cys residue on the pRID plasmid corresponding to Cys3022 of RTX was mutated to a Met using the primers C3022M-sense and C3022M-antisense incorporating a *Mfe*I site to aid in screening. The Cys residue on the pCPDc plasmid corresponding to Cys3568 of RTX was mutated to a Ser using the primers C3568S-sense and C3568S-antisense incorporating a *Bam*HI site. Plasmids pxlCPDc C-S and pCPDn C-S were construct by Heather Howell by using the restriction enzyme *Apa*I to excise a fragment from pCPDc C-S containing the C3568S point mutation for religation into similarly digested pxlCPDc and pCPDn. The Lys3482A and the Glu3543A mutations of pCPDc were generated with primers K3482A-sense and K3482A-antisense and E3543A-sense and E3543A-antisense incorporating a *Sac*I and *Nsi*I restriction site, respectively. The H3519A mutation was made by Heather Howell using primers H3519A-sense and H3519A-antisense incorporating a *Bsa*HI restriction site.

Mutagenesis of the *rtxA* gene on *V. cholerae* chromosome

The in-frame deletion of the ACD and the Cys3568 point mutation within the *rtxA* gene on the *V. cholerae* chromosome were created by double homologous recombination using the *sacB*-lethality counterselection method as described below (Metcalf et al., 1996).

In-frame deletion of the ACD within RTX

The strain CCO5 was made by C. Cordero. Briefly, an 877 base pair (bp) fragment upstream and 967 bp fragment downstream of the ACD was amplified from N16961 genomic DNA and the two fragments were separately cloned into the pCR-BluntII-TOPO vector (Invitrogen, Carlsbad, CA). An in-frame fusion of these two regions was generated using engineered *Ava* I restriction sites on the respective fragments and ligation into the pCR-BluntII-TOPO vector (Invitrogen, Carlsbad, CA). The fused fragments were then moved into the pWM91 vector, which contains the *sacB* counterselection gene (Metcalf et al., 1996), utilizing the *Spe* I and *Xho* I sites. The donor bacterium *E. coli* SM10λpir was transformed with the resulting plasmid pTCO16 and mated with the recipient strains KFV119. The plasmid pTCO16 was also mated with KFV102 to generate the strain SAV2 by Sarah Antinone. Colonies containing the co-integrated plasmid were subjected to counterselection on sucrose. The colonies obtained after this selection process were then screened by PCR to detect the 1587 nucleotide deletion on the *V. cholerae* chromosome removing aa 1913-2441. The plasmid pTCO16 as well as the PCR product from the mutant strain were sequenced at the CRC DNA Sequencing Facility at the University of Chicago to confirm gene sequence.

Cys3568 point mutation on the *rtxA* gene of *V. cholerae*

A 2097 bp fragment corresponding to RTX codons for aa 3201-3899 was amplified from N16961 genomic DNA and cloned into the pCR-BluntII-TOPO vector (Invitrogen, Carlsbad, CA). The Cys3568S point mutation was generated on this plasmid using the Quickchange Mutagenesis kit (Stratagene, La Jolla, CA) with the primers C3568S-sense and C3568S-antisense. After mutagenesis the fragment was moved into the *sacB*-counterselection vector pWM91 (Metcalf et al., 1996). The resulting plasmid was transformed into *E coli* SM10λpir and mated into the recipient strain KFV119. Colonies containing the cointegrated plasmid were subjected to counterselection on sucrose. The colonies obtained after selection were screened by digestion of PCR products with *Bam*HI to detect the incorporation of the point mutation and by DNA sequencing.

Cloning, Expression, and Purification of Recombinant CPD and RID

Primers CPD-LICF and CPD-LICR were used to amplify the CPD from the *V. cholerae* strains KFV119, KSV10 and the plasmid pCPDc K-A. Ligation independent cloning (LIC) was then used to construct overexpression plasmids pHisCPD, pHisCPDC-S, and pHisCPDK-A respectively, according to the manufacturer recommended protocol for the pET30-XA-LIC vector (Novagen, Madison, WI) using modified vector pMCSG7 (Stols et al., 2002).

Primers RID-LF_NF and RID-LF_NR were used to amplify the RID from the *V. cholerae* N16961 genomic DNA with flanking BamHI sites (underlined). This fragment was cloned into pBluescript and then subcloned into pABII as an N-terminal fusion to amino acids 1-254 of *Bacillus anthracis* Lethal Factor. Plasmids pABII and PA-pET15B obtained from J. Ballard

(University of Oklahoma Health Sciences Center) were used for purification of the proteins PA and LF_N (Spyres *et al.*, 2001).

All recombinant proteins were expressed in *E. coli* strain BL21 (λ DE3). Overnight cultures were diluted 1:500 into LB containing 100 μg/ml ampicillin and grown at 37°C to a density of OD_{600}=0.6. Protein expression was induced with 0.2 mM IPTG for 2 h. Bacterial pellets were resuspended in 20 mM Tris, 500 mM NaCl and 5 mM imidazole pH 8.0, 1 mg/ml lysozyme and incubated on ice for 30 min. Triton X-100 was added to a concentration of 1% and lysates were sonicated with a Bronson Digital Sonifier 450 at 40% amplitude for 2 min. Insoluble debris was pelleted at 27,000*g*, and the 6xHis tagged proteins were purified by affinity chromatography using a HisTrap HP column on the ÄKTA purifier (GE Healthcare, Piscataway, NJ). The column was washed with 20 mM Tris, 500 mM NaCl, and 60 mM imidazole pH 8.0 and eluted with 250 mM imidazole. Proteins were then dialyzed into 20 mM Tris, 500 mM NaCl pH 7.5. Protein purity was assessed on Coomassie Blue R250 stained SDS-PAGE gel and concentration was determined by using a Bicinchoninic Acid (BCA) acid protein assay kit (Pierce, Rockford, IL).

Purification of Cytotoxic Necrotizing Factor 1 (CNF1)

CNF1 was purified using the pCNF24 plasmid obtained from A. O'Brien (Uniformed Services University of the Health Services) as previously described with minor modifications (Mills *et al.*, 2000). Briefly, CNF1was expressed in *E. coli* strain XL1-Blue. Overnight cultures were diluted 1:500 into LB containing 100 μg/ml ampicillin and grown at 37°C to a density of OD_{600}=0.5. Protein expression was induced with 0.1 mM IPTG for 4 h at room temperature.

Bacterial pellets were resuspended in 50 mM NaH_2PO_4, 300 mM NaCl and 10 mM imidazole pH 8.0, 1 mg/ml lysozyme and incubated on ice for 30 min. Triton X-100 was added to a concentration of 1% and lysates were sonicated with a Bronson Digital Sonifier 450 at 40% amplitude for 2 min. Insoluble debris was pelleted at 10,000*g*, and the 6xHis tagged proteins were purified by affinity chromatography using a HisTrap HP column on the ÄKTA purifier (GE Healthcare, Piscataway, NJ). The column was washed with 50 mM NaH_2PO_4, 300 mM NaCl, and 20 mM imidazole pH 8.0 and eluted with 250 mM imidazole. The eluted proteins were precipitated by 60% ammonium sulfate fractionation for 30 min at 4°C followed by centrifugation at 12000*g* for 30 min at 4°C. Precipitated proteins were then resuspended in Phosphate-buffered saline (PBS) pH 7.4 and dialyzed against the same buffer overnight. Protein purity was assessed on Coomassie Blue R250 stained SDS-PAGE gel and concentration was determined by using a BCA acid protein assay kit (Pierce, Rockford, IL). In experiments using CNF1, cells were either pre-incubated with 0.9 mg/mL or recovered in the presence 1.5 mg/mL after incubation with RTXΔACD.

Transient Transfection

Approximately 2 x 10^5 cells, COS-7 or HEp-2, were seeded in a 6-well dish 24 h prior to transfection. Experiments in chapter 3 were performed utilizing lipofectamine (Invitrogen, Carlsbad, CA) as follows. The media was changed to DMEM without serum and antibiotics and the lipofectamine reaction (2 μg DNA, 8 μg lipofectamine, 18 μg PLUS reagent in DMEM alone) was incubated with the cultured cells at 37°C with 5% CO_2 for 3-5 h. DMEM containing

10% FBS, 50 U/mL penicillin, and 50 μg/mL streptomycin was then added to the cells for continued incubation.

Experiments in chapters 4 and 5 were performed using the FuGene 6 reagent (Roche Applied Sciences, Indianapolis, IN) as follows. COS-7 or HEp-2 cells were plated at approximately 50% confluency in either six-well dishes or on coverslips 24 h before transfection. Cells were transfected using the FuGene 6 reagent mixed with plasmid DNA at a 3:1 reagent:DNA ratio for COS-7 cells or a 3:2 reagent:DNA ration for HEp-2 cells in DMEM. This mixture was preincubated for 45 min before addition to cultured cells followed by incubation at 37°C with 5% CO_2 for 24 h.

Microscopy

Cells grown in 6-well dishes were washed with PBS and fixed with 4% paraformaldehyde. Cells transfected with ACD constructs were observed after 24 h for expression of EGFP at 400x magnification with fluorescence microscopy at 550-575 nm. Phase contrast images were acquired at 200x magnification of HEp-2 cells that had been incubated with PBS, KFV119, KFV92 and CCO5 or with 28 nM PA with either 12 nM LF_N or LF_NRID.

For the RID and CPD constructs, cells grown on coverslips were washed with PBS, fixed with 4% paraformaldehyde and stained with 0.5 μg/ml Hoechst 33342 24 h after transfection. The coverslips were mounted using Anti-Fade mounting media (Molecular Probes, Eugene, OR). Transfected cells were observed for expression of EGFP at either 630x or 1000x magnification under fluorescence microscopy at 550-575 nm and 440-470 nm to visualize nuclei.

For actin staining, fixed cells were permeabilized with 0.1% Triton X-100 for 10 minutes and then incubated with 0.1 ug/ml of Tetramethylrhodamine B iso-Thiocyanate (TRITC)-labeled Phalloidin conjugate for 30 minutes at RT. Phalloidin stained cells were visualized under fluorescence microscopy at 610-675 nm at either 400x or 1000x magnification. All images were captured using an inverted Leica DMIRE2 microscope with a C4742-95-12ERG digital charge-coupled device (CCD) camera (Hamamatsu Photonics, Tokyo) in conjunction with the OPENLAB software (Improvision, Coventry, UK) for image processing.

Polarized T84 Epithelial Cells

T84 cells were cultured in collagen-treated commercially available 0.33 cm^2 Transwell inserts (Costar Laboratories, Cambridge, MA). Experiments were performed 2 weeks after plating, when resistances consistently reached >1000 Ω cm^2. Cells were rinsed in Hanks' balanced salt solution containing $CaCl_2$ and were transferred into T84 medium without serum or antibiotics. Transwells were kept in the incubator for the course of the experiments. The resistance was measured at 10-15 minute intervals for 4 h using an Epithelial Voltohmmeter (World Precision Instruments, Sarasota, FL). The *V. cholerae* strains KFV101, KFV102, and SAV2 were grown overnight at 30°C in Lb and washed twice with PBS. After three baseline electrical readings, 10 ul of PBS-washed bacteria (PBS as negative control) were added to the apical chamber of the Transwell. Numbers were derived by dividing the recorded resistance value by the mean of three initial resistance values before addition of bacteria.

Western Blotting for Actin Cross-linking and EGFP Expression

Cultures of *V. cholerae* were grown for 16 h in LB containing streptomycin at 30°C, washed with PBS and added to the media of HEp-2 cells at a multiplicity of infection (M.O.I.) of 200. Cells exposed to KFV92, KFV119, CCO5 and KSV10 were collected 90 and 180 min after addition of bacteria to detect actin cross-linking. Cells transiently transfected were collected 24 h after transfection. All cells were washed with PBS, collected by scraping, centrifuged at 4,500*g*, and resuspended in SDS-PAGE sample buffer. Proteins in boiled cell lysates were separated on SDS-PAGE and transferred to Hybond-C nitrocellulose (GE Healthcare, Piscataway, NJ). EGFP expression was detected using a monoclonal anti-GFP antibody at 1:1000 dilution (Santa Cruz Biotechnology, Santa Cruz, CA) followed by the anti-mouse IgG HRP secondary antibody at 1:5000 dilution (Sigma, St. Louis, MO). Actin cross-linking was detected by Western blotting with a polyclonal anti-actin antibody at 1:1000 dilution (Sigma, St. Louis, MO) and a 1:5000 dilution of anti-rabbit IgG HRP (Jackson Immuno Research, West Grove, PA). All westerns represent a typical result of at least three independent experiments.

Inhibitor studies of RTX activity

HEp-2 cells were pre-incubated with either 20 and 200 μM of Nocodazole or 10 μM of Colchicine which were empirically determined to be sufficient to depolymerize microtubules as assessed by immunofluoresence using an anti-tubulin antibody. Cells were pre-incubated with 50 nM of Bafilomycin A1 which was experimentally determined to block acidification of vacuoles in HEp-2 cells by staining with Acridine Orange. The following inhibitors were used at concentrations previously characterized in the literature: Chlorpromazine HCl at 10 μg/mL,

Nystatin at 100 μg/mL, and Methyl-β-Cyclodextrin at 5 and 10 mM (Akula et al., 2003; Rodal et al., 1999). HEp-2 cells were incubated with inhibitors for 1 h at 37°C followed by the addition of PBS-washed bacteria at an M.O.I. of 200 for 90 min. RTX toxin entry was measured by the detection of actin cross-linking.

Cytotoxicity Assays

Cytotoxicity assays were performed on HEp-2 cells that had been incubated at 37 °C for 3 and 6 h in the presence of PBS-washed bacteria at an M.O.I. of 200. The release of lactate dehydrogenase into the medium was assessed using the Promega CytoTox96 Non-radioactive Cytotoxicity kit according to the manufacturer's instructions. Membrane integrity was measured using the fluorophores SYTO10 and DEAD-RED provided in the Molecular Probes Live/Dead Reduced Biohazard Viability/Cytotoxicity kit following the instructions provided by the manufacturer. Cells were then visualized under fluorescence microscopy at 550-575 nm (SYTO10) and 610-675 nm (DEAD-RED).

Affinity Precipitation Assay

Approximately 10^7 HEp-2 cells were incubated with either PBS, KFV92, KFV119, CCO5 or in the presence of PA with either LF_NRID or LF_N at a molar ratio of 7:3 for 4 h at 37 °C. Cells were washed with cold PBS, collected and lysed in 1 ml of Rho assay buffer (25 mM HEPES, pH 7.5, 150 mM NaCl, 1% NP-40, 10 mM $MgCl_2$, 1 mM EDTA, 2% glycerol, 10 μg/mL aprotinin and leupeptin). Lysates were centrifuged at 14,000*g* for 5 min at 4°C to remove insoluble debris. Lysates (800 μl) were then incubated with 40 μg of GST-RBD (glutathione-s-

transferase Rho binding domain from Rhotekin) agarose beads (Cytoskeleton, Denver, CO) for 1 h at 4°C to measure Rho-GTP levels. Beads were collected, washed 3x with Rho assay buffer, resuspended in SDS-PAGE buffer, and boiled for 5 min. Total Rho was measured from 40 μl of lysate. Samples were resolved by SDS-PAGE (15%) and transferred to Hybond-C nitrocellulose (GE Healthcare, Piscataway, NJ). Total Rho and Rho-GTP levels were detected by Western blotting with anti-RhoA (Santa Cruz Biotechnology, Santa Cruz, CA) at 1:500 dilution followed by anti-mouse IgG HRP secondary antibody at 1:5000 dilution (Sigma, St. Louis, MO) and chemiluminescent detection.

Subcellular Localization

Approximately 10^7 HEp-2 cells were incubated with PBS, KFV92, KFV119 or CCO5 for 4 h at 37 °C. Cells were washed with cold PBS, collected and resuspended in 1 ml of homogenization buffer (250 mM sucrose, 3 mM imidazole pH 7.4, 0.5 mM EDTA and complete EDTA-free protease inhibitor mixture (Roche Applied Sciences, Indianapolis, IN)). The cells were lysed by 3 pulses of 10 s with a Sonicel disrupter and then centrifuged at 2,000*g* for 5 min at 4°C. The post-nuclear supernatant was then fractionated by centrifugation at 100,000*g* for 30 min at 4°C. The supernatant (cytosolic fraction) was removed, and the insoluble pellet (membrane fraction) was resuspended in an equivalent volume of homogenization buffer containing 1% Triton X-100. SDS-PAGE loading buffer was added to the cytosolic and membrane fractions and then the fractions were boiled for 5 min. Equivalent volumes of samples were resolved by SDS-PAGE (15%) and transferred to Hybond-C nitrocellulose (GE Healthcare, Piscataway, NJ). Western blotting was then performed with anti-RhoA (Santa Cruz Biotechnology, Santa Cruz, CA), anti-Rac, or anti-Cdc42 (Upstate Biotechnology, Lake Placid, NY) at 1:500 dilution. The anti-mouse

IgG HRP secondary antibody was used at 1:5000 dilution (Sigma, St. Louis, MO) followed by chemiluminescent detection. Densitometric analysis was performed using NIH ImageJ 1.36b software (http://rsb.info.nih.gov/ij/).

GAP Assay

The GAP assay was performed as previously described (Self and Hall, 1995). Briefly, recombinant His-RhoA (Cytoskeleton, Denver, Co) was loaded with [γ-^{32}P]GTP (6000 Ci/mmol, 10μCi/μl) (Perkin Elmer NEN, Wellesley, MA) in loading buffer (20 mM Tris-HCl pH 7.5, 0.1 mM DTT, 25 mM NaCl, and 4 mM EDTA) for 5 min at 37° C followed by the addition of $MgCl_2$ to a final concentration of 17 mM. To test for GAP activity, 2 μM [γ-^{32}P]GTP-loaded RhoA was incubated alone, with LF_NRID (100 nM), or with positive control p50RhoGAP (100 nM) (Cytoskeleton, Denver, CO) in hydrolysis buffer (20 mM Tris-HCl pH 7.5, 0.1 mM DTT, 1 mM GTP, 1 mg/mL BSA) for 10 min at 37° C followed by dilution into 1 mL of cold assay buffer (50 mM Tris-HCl pH 7.5, 50 mM NaCl and 5 mM $MgCl_2$). Samples were analyzed by a filter binding assay and then reported as bound GTP remaining at T=10 min as a percentage of the initial bound GTP at T=0.

pNPP Hydrolysis Assay

LF_N (1μg), LF_NRID (1μg) and as a positive control calf intestinal alkaline phosphatase (CIP) (1μL) (Invitrogen, Carlsbad, CA) were incubated with 120 μg of p-Nitrophenyl phosphate (pNPP) in pNPP hydrolysis buffer (25 mM HEPES pH 7.4, 50 mM NaCl, 5 mM DTT, 2.5 mM

EDTA supplemented with 5 μg of BSA). After 15 min of incubation at 37°C, the reaction was stopped with 13% K_2HPO_4. Samples were then measured at absorbance of 405 nm.

In Vitro Cleavage Assay

Cell lysate was prepared from approximately 10^7 COS-7 cells that were washed with PBS, collected and suspended in 1 ml of homogenization buffer (250 mM sucrose, 3 mM imidazole pH 7.5). The cells were lysed by 3 pulses of 10 s using a Sonicel disrupter and then were centrifuged at 2,000*g* for 5 min at 4°C. For subcellular fractionation, the lysate was then fractionated by centrifugation at 100,000*g* for 30 min at 4°C. The supernatant (cytosolic fraction) was removed and the insoluble pellet (membrane fraction) was resuspended in an equivalent volume of homogenization buffer containing 1% Triton X-100. The *in vitro* cleavage assay was performed using 2 μg rCPD, rCPD C-S or rCPD K-A plus cell lysate in a buffer of 20 mM Tris pH 7.5, 250 mM sucrose and 3 mM imidazole at 37°C for time indicated. For inhibitor studies rCPD was pre-incubated for 30 min with 1 mM NEM, E-64, Calpeptin, or Phenylmethylsulphonylfluoride, 100 μM Pepstatin, 200 μM Leupeptin, or 2 mM $MgCl_2$, $CaCl_2$, or $MnCl_2$. Samples were heated at 95°C in SDS-PAGE loading buffer for 5 min and proteins were separated by SDS-PAGE (15% gel) and staining with Coomassie Blue R250.

GTP Binding Assay

Fluorescence binding assays were performed with rCPD and rCPD K-A (200 μM) in 20 mM Tris (pH 7.5), 50 mM NaCl, and 0.2% $C_{12}E_8$ with 0.5 μM 2'-(or-3')-O-(N-methylanthraniloyl) (mant)-GTP or mant-GDP (Invitrogen, Carlsbad, CA) in the presence or absence of 2 mM

$MgCl_2$. The assay mixture was incubated at 37°C for 30 min. An emission scan was performed from 400 nm - 550 nm (bandwidth 10 nm) after excitation λ= 350nm using the Safire 2 spectrofluorometer (Tecan, Durham, NC). Binding was measured as the change in relative fluorescent intensity at 440 nm between mant-GTP (or mant-GDP) measured alone or with recombinant protein. Statistical analyses were performed using the GraphPad InStat software (GraphPad Software, Inc., San Diego, CA) for unpaired t-tests, assuming the populations have different standard deviations. P values < 0.05 were determined to be statistically significant.

Fourier Transform Mass Spectrometry

FT-MS was performed at Chicago Biomedical Consortium Proteomic Facility at the University of Illinois at Chicago. 100 pmol rCPD cleaved in the absence of lysate was separated on an Agilent Zorbax C-8 (300A pore size, 3.5 um particle size) 2.1 x 50 mm id column run at a flow rate of 200 μL/min in 90% 0.1% Formic acid:water/10% Acetonitrile to 50:50 in 10 min. Eluted samples were run on a Thermo LTQ-FT mass spectrometer using FTMS + p ESI Full MS scanning mode, mass range 450-2000, FT resolution 100000, scan speed approx 0.9 second/scan. The molecular weight of eluted peptides was determined by deconvolving multiply charge peaks to the proteins effective mass using the charge state determination afforded by the instrument high resolution capability. The measured mass was compared to the predicted m.w. of possible peptide cleavage fragments determined from the primary sequence of rCPD using PROTPARAM (http://ca.expasy.org/tools/protparam.html) (Gasteiger et al., 2005).

Bioinformatics

Proteins with CPDs were identified by searching GenBank and the nonredundant protein database through the National Center for Biotechnology Information (NCBI) (http://www.ncbi.nlm.nih.gov) and San Diego Supercomputing Center (SDSC) (http://sdsc.edu) using PSI-BLAST (Altschul et al., 1997) and MEME/MAST (Bailey and Elkan, 1994; Bailey and Gribskov, 1998), respectively. Protein sequences identical to YPTB3219 and FhaL from other related species were excluded from analysis. The CPD from the *V. cholerae* RTX was further searched against the MEROPS peptidase database (http://merops.sanger.ac.uk) (Rawlings et al., 2006). CLUSTALW alignments were prepared using the identity weight matrix followed by preparation of PHYLIP rooted phylogenetic tree in DRAWGRAM and alignment in TeXshade using the Biology WorkBench V. 3.2 program at SDSC (Beitz, 2000; Felsenstein, 1989; Thompson et al., 1994). Primary aa sequences used were from NCBI GenBank except *Xenorhabdus* sequences were acquired by FTP from the Donald Danforth Plant Science Center. Accession numbers are listed in Table IV.

Table I List of *Vibrio* strains used in study.

Strain	Genotype	Published
Vibrio cholerae		
KFV92	N16961 Δ*hapA* Δ*hlyA* Δ*rtxA*	This work
KFV119	N16961 Δ*hapA* Δ*hlyA*	This work
CCO5	N16961 Δ*hapA* Δ*hlyA* RTXΔ1913-2441	This work
KSV10	N16961 Δ*hapA* Δ*hlyA* RTX C3568S	This work
KFV101	P4 Δ*hapA* Δ*hlyA* Δ*rtxA*	(Fullner et al.,2002)
KFV102	P4 Δ*hapA* Δ*hlyA*	This work
SAV2	P4 Δ*hapA* Δ*hlyA* RTXΔ1913-2441	This work
Vibrio vulnificus		
MO6-24/0	Clinical isolate	(Wright et al., 1990)
FLA 400	MO6-24/0 w/ Kan cassette disrupting *rtxA*	(Gulig et al., 2005)

N16961 is a streptomycin resistant isolate of *V. cholerae* O1 El Tor Inaba.

P4 is derived from P27459 a streptomycin resistant isolate of *V. cholerae* O1 El Tor Inaba engineered mutation replacing *ctxA* and *ctxB* with a gene for kanamycin resistance as previously described (Mekalanos, 1983)

Table II List of oligonucleotides used for plasmid construction.

Oligonucleotide	Sequence
VgrG1963	5’ GAAGATCTCGCCACCATGGGAAGTCAACCAACGGGTCAA 3’
VgrG*Eco*RI	5’ CGGAATTCGTCTCATGGTTATCAGTATAAG 3’
ACD NΔ30	5’ GAAGATCTCGCCACCATGTCCGGTCTGGTGGTGGTTTTA 3’
ACD NΔ90	5’ GAAGATCTCGCCACCATGGAACTCGTTACATATCCTAGT 3’
ACD NΔ168	5’ GAAGATCTCGCCACCATGACCCCTAGTGGCCAACAA 3’
ACD NΔ254	5’ GAAGATCTCGCCACCATGCCTGCCTCTGAAGGTTTTTCA 3’
ACD NΔ328	5’ GAAGATCTCGCCACCATGGTCGCTGGACATGGAATCAAT 3’
ACD CΔ129	5’ CGGAATTCACTTCTCCACCATATTGGAA 3’
ACD CΔ45	5’ CGGAATTCCTTGCTCGATACTCCTGATA 3’
VC1416F	5’ GAAGATCTCGCCACCATGAACGCGCAGCCTAATCTTGGAAGA 3’
VC1416R	5’ CGGAATTCGCGCGTTGCCATTCTTGAGGATT 3’
RID-*Nhe*I	5’ GAGCTAGCCGCCACCATGGGTGCATGGCAATACAACGCCACA 3’
RID-*Bam*H1	5’ GCCGGATCCATTTTCAATCGCCACGTTTTC 3’
ABHY-*Bgl*II	5’ GAAGATCTCGCCACCAATGGGTACGCCACCGCGCGATAAA 3’
ABHY-*Eco*RI	5’ CGGAATTCCGCAAACGGTTGCTTGCTTCGTG 3’
YPF	5’ GAAGATCTCGCCACCATGTCTACCAAGCTTGCTTCT 3’
YPR	5’ GCCTGCAGGCTCAGCAACTGACAGCAGTGA 3’
C3022M-sense	5' CGTTATCAATTGCTGACCAAGAACATGTCCAGCACAGTGGCT 3'
C3022M-antisense	5' AGCCACTGTGCTGGACATGTTCTTGGTCAGCAATTGATAACG 3'
RID170F	5' GAGCTAGCCGCCACCATGGCATTGACTGATTACCACGCCAGC 3'
RID210F	5' GAGCTAGCCGCCACCATGGGCCGTGTTGAAGCGATGAATTCA 3'
RID326R	5' GCGGTACCAACCCCTTTACCGTCTTTGGCAA 3'
RID346R	5' GCGGTACCGACAGGTGACAGATGCTGTTCAA 3'
RID384R	5' GCGGTACCGTTAAAATCAGCTGCAGCTTGAC 3'
RTX8410F	5' GAAGATCTCGCCACCATGCAGCAAAATTACGTAAGCTGGTGG 3'
RTX9627R	5' GCCGGATCCGATACCTTGCTTCTGGTAGTGA 3'
RID-LF_NF	5’ GAGGATCCCCGGGAGGTGCATGGCAATACAACGCCACA 3’
RID-LF_NR	5’ GAGGATCCCTAATTTTCAATCGCCACGTTTTC 3’
CPDc-*Bgl*II	5’ GAAGATCTCGCCACCATGAGTCAATATGCGGATCAAATTGTC 3’
CPD-*Eco*RI	5’ CGGAATTCGGACCTTGCGCGTCCCAGCTTAG 3’
xlCPDc-*Bgl*II	5’ GAAGATCTCGCCACCAATGGGTACGCCACCGCGCGATAAA 3’
CPDn-*Bgl*II	5’ GAAGATCTCATGAGTCAATTATGCGGATCAAATTGTC 3’

Table II: Cont.

Oligonucleotide	Sequence
CPD NΔ36	5' GAAGATCTCGCCACCATGATCTCAAATAAGAATGATCATCTG 3'
CPD NΔ58	5' GAAGATCTCGCCACCATGCTCCATAATCAAAATGTTAATAGC 3'
CPD NΔ65	5' GAAGATCTCGCCACCATGAGCTGGGGCCCGATTACGGTTACA 3'
CPD NΔ85	5' GAAGATCTCGCCACCATGGGTCAAATCATCGTTCAAATGGAA 3'
CPD NΔ120	5' GAAGATCTCGCCACCATGGGCAACTATCGCGTGGTGTATGGC 3'
CPD NΔ157	5' GAAGATCTCGCCACCATGGGTTACAGTGCCGATGAGTTG 3'
CPD CΔ20	5' CGGAATTCGGATTCGCGTCCTTGGTATGCT 3'
CPD C+12	5' CGGAATTCGGACCATTGCGAATACGTTCAT 3'
C3568S-sense	5' CATCAGTATTGTTGGATCCTCTTTGGTGACG 3'
C3568S-antisense	5' CGTCACTCACCAAAGAGGATCCAACAATACTGATG 3'
H3519A-sense	5' TTGGCAGTTGGTGGGCGCCGGTCGCGACCACTCAG 3'
H3519A-antisense	5' CTGAGTGGTCGCGACCGGCGCCCACCAACTGCCAA 3'
K3482A-sense	5' GCGGCAGCCAATTTAGCAGGAGCTCATGCTGAAAGCAGTGTG 3'
K3482A-antisense	5' CACACTGCTTTCAGCATGAGCTCCTGCTAAATTGGCTGCCGC 3'
E3543A-sense	5' TTAAGTGGTTACAGTGCCGATGCATTGGCCGTGAAATTGGCC 3'
E3543A-antisense	5' GGCCAATTTCACGGCCAATGCATCGGCACTGTAACCACTTAA 3'
CPD-LICF	5' **TACTTCCAATCCAATGCT**ATGCAATATGCGGATCAAATTGTC 3'
CPD-LICR	5' **TTATCCACTTCCAATG**ACCTTGCGCGTCCCAGCTTAG 3'

Underlined - restriction sites Double underlined – Kozak sequences Bold – LIC sequences

Table III List of plasmids constructed for these studies.

Plasmid	Vector	Brief Description
pACD	pEGFP-N3	RTXaa 1963-2419 w/ C-terminal EGFP fusion
pACDNΔ30	pEGFP-N3	RTXaa 1994-2419 w/ C-terminal EGFP fusion
pACDNΔ90	pEGFP-N3	RTXaa 2054-2419 w/ C-terminal EGFP fusion
pACDNΔ168	pEGFP-N3	RTXaa 2131-2419 w/ C-terminal EGFP fusion
pACDNΔ254	pEGFP-N3	RTXaa 2217-2419 w/ C-terminal EGFP fusion
pACDNΔ328	pEGFP-N3	RTXaa 2291-2419 w/ C-terminal EGFP fusion
pACDCΔ129	pEGFP-N3	RTXaa 1963-2291 w/ C-terminal EGFP fusion
pACDCΔ45	pEGFP-N3	RTXaa 1963-2372 w/ C-terminal EGFP fusion
pVC1416	pEGFP-N3	VC1416 aa 716-1161 w/ C-terminal EGFP fusion
pRID	pEGFP-N3	RTXaa 2552-3099 w/ C-terminal EGFP fusion
pRID C-M	pEGFP-N3	C3022M mutation on pRID
pLF_NRID	pABII	RTXaa 2552-3099 w/ N-terminal fusion to LF_N
pYP	pEGFP-N3	RTXaa2420-2650 w/ C-terminal EGFP fusion
pYP-Tox	pEGFP-N1	RTXaa2420-3443 w/ C-terminal EGFP fusion
pABHY	pEGFP-N3	RTXaa3209-3375 w/ C-terminal EGFP fusion
pKS76	pEGFP-N3	RTX aa2500-2799 w/ N-terminal EGFP fusion
pKS77	pEGFP-N3	RTX aa2528-2799 w/ N-terminal EGFP fusion
pKS80	pEGFP-N3	RTX aa2420-2803 w/ C-terminal EGFP fusion
pKS82	pEGFP-N3	RTX aa2420-2765 w/ C-terminal EGFP fusion
pKS84	pEGFP-N3	RTX aa2420-2745 w/ C-terminal EGFP fusion
pKS86	pEGFP-N3	RTX aa2552-2803 w/ C-terminal EGFP fusion
pKS88	pEGFP-N3	RTX aa2552-2765 w/ C-terminal EGFP fusion
pKS90	pEGFP-N3	RTX aa2552-2745 w/ C-terminal EGFP fusion
PKS92	pEGFP-N3	RTX aa2589-2803 w/ C-terminal EGFP fusion
pKS94	pEGFP-N3	RTX aa2589-2765 w/ C-terminal EGFP fusion
pKS96	pEGFP-N3	RTX aa2589-2745 w/ C-terminal EGFP fusion
pKS98	pEGFP-N3	RTX aa2629-2803 w/ C-terminal EGFP fusion
pKS100	pEGFP-N3	RTX aa2629-2765 w/ C-terminal EGFP fusion
pKS102	pEGFP-N3	RTX aa 2629-2745 w/ C-terminal EGFP fusion
pKS107	pEGFP-N3	RTX aa 2804-3375 w/ C-terminal EGFP fusion
pKS111	pEGFP-N3	RTX aa 2552-3209 w/ C-terminal EGFP fusion

Table III Cont.

Plasmid	Vector	Brief Description
pCPDc	pEGFP-N3	RTXaa 3376-3637 w/ C-terminal EGFP fusion
pCPDn	pEGFP-C3	RTXaa 3376-3637 w/ N-terminal EGFP fusion
pxlCPDc	pEGFP-N3	RTXaa 3101-3637 w/ C-terminal EGFP fusion
pCPDcC-S	pEGFP-N3	C3568S mutation in pCPDc
pCPDnC-S	pEGFP-C3	C3568S mutation in pCPDn
pxlCPDcC-S	pEGFP-N3	C3568S mutation in pxlCPDc
pCPDcH-A	pEGFP-N3	H3519A mutation in pCPDc
pCPDcK-A	pEGFP-N3	L3482A mutation in pCPDc
pCPDcE-A	pEGFP-N3	G3542A mutation in pCPDc
pCPDcNΔ36	pEGFP-N3	RTXaa 3411-3637 w/ C-terminal EGFP fusion
pCPDcNΔ58	pEGFP-N3	RTXaa 3434-3637 w/ C-terminal EGFP fusion
pCPDcNΔ65	pEGFP-N3	RTXaa 3441-3637 w/ C-terminal EGFP fusion
pCPDcNΔ85	pEGFP-N3	RTXaa 3461-3637 w/ C-terminal EGFP fusion
pCPDcNΔ120	pEGFP-N3	RTXaa 3496-3637 w/ C-terminal EGFP fusion
pCPDcNΔ157	pEGFP-N3	RTXaa 3533-3637 w/ C-terminal EGFP fusion
pCPDcCΔ20	pEGFP-N3	RTXaa 3376-3617 w/ C-terminal EGFP fusion
pHisCPD	pMCSG7	RTXaa 3378-3637 w/ N- and C-terminal 6xHis tag
pHisCPD C-S	pMCSG7	RTXaa 3378-3637 C3658A w/ N- and C-terminal6xHis tag
pHisCPD K-A	pMCSG7	RTXaa 3378-3637 K3482A w/ N- and C-terminal 6xHis tag

Table IV Accession numbers for primary amino acid sequences used to generate phylogenetic tree and alignment in Figure 5-1.

Protein	Abbreviation	Accession number[a]	Amino acids used in analysis
Group 1: *Vibrio*-type RTX toxins			
V. cholerae RTX toxin	VcRtx	gi|4455065	aa 3420-3619
V. vulnificus RTX toxin	VvRtx	gi|37676690	aa 4110-4288
V. splendidus putative RTX toxin	VsRtx	gi|84386478	aa 3751-3975
P. luminescens putative RTX toxins	Plu1341	gi|37525303	aa 2579-2764
	Plu1344	gi|36784731	aa 2965-3163
	Plu3217	gi|36786533	aa 2425-2620
	Plu3324	gi|37686635	aa 2440-2626
X. nematophila putative RTX toxin	XnRtx	DDPSC	aa 3823-4042
X. bovienii putative RTX toxin	XbRtx	DDPSC	aa 3601-3816
Group 2: Putative toxins from *Yersinia*			
Y. pseudotuberculosis putative toxin	YpRtx	gi|51590811	aa 1058-1271
Y. mollaretti putative toxin	YmMfp2	gi|77962640	aa 1-224
Group 3: Clostridial glucosylating toxins			
C. difficile Toxin A	TcdA	gi|98593	aa535-769
C. difficile Toxin B	TcdB	gi|761714	aa536-768
C. noveyi alpha toxin	TcnA	gi|755724	aa532-813
C. sordellii cytotoxin L	TcsL	gi|1000695	aa526-825

Table IV: Cont.

Protein Abbreviation	Accession number[a]	Amino acids used	Amino acids used in analysis
Group 4. Type V secreted adhesin			
Bordetella pertussis putative adhesin FhaL	cpd1	gi|33563918	aa 2551-2716
	cpd2	gi|33563918	aa 3079-3119
	cdp3	gi|33563918	aa3375-3971
	cpd4	gi|33563918	aa3397-3562

[a] All sequences from National Center for Biotechnology Information GenBank except *Xenorhabdus* sequences acquired by FTP from Donald Danforth Plant Science Center (DDPSC) at http://xenorhabdus.danforthcenter.org

Chapter 3

Identification of a Domain Within the Multi-functional *Vibrio cholerae* RTX Toxin that Covalently Cross-links Actin

Abstract

The Gram-negative pathogen *Vibrio cholerae* causes diarrheal disease through the export of enterotoxins. The *V. cholerae* RTX toxin was previously identified and characterized by its ability to round human laryngeal epithelial (HEp-2) cells. Further investigation determined that cell rounding is due to the depolymerization of actin stress fibers, through the novel mechanism of covalent actin cross-linking. In this study, a domain was identified within the full-length RTX toxin that is capable of mediating the cross-linking reaction when transiently expressed within eukaryotic cells. A structure/function analysis of the actin cross-linking domain (ACD) reveals that 412 amino acids, or a 47.8 kDa, region is essential for cross-linking activity. When this domain is deleted from the full-length toxin gene actin cross-linking, but not cell rounding, is eliminated indicating that this toxin carries multiple dissociable activities. The ACD shares 59% amino acid identity with a hypothetical protein from *V. cholerae*, VC1416, and transient expression of the C-terminal domain of VC1416 also results in actin cross-linking in eukaryotic cells. The presence of this second ACD linked to an *Rhs*-like element suggests that *V. cholerae* acquired the domain by horizontal gene transfer and the ACD was inserted into the RTX toxin by gene duplication through the evolution of *V. cholerae*.

Introduction

The *Vibrio cholerae* RTX toxin is a unique member of the repeats-in-toxin family. This large bacterial toxin was previously characterized to cause the covalent cross-linking of actin monomers into dimers, trimers and higher multimers of cross-linked actin. However, many questions remain concerning the precise mechanism of the RTX toxin. The secreted toxin could gain entry into the host cells where it can access the cellular pool of G-actin to either directly catalyze the cross-linking of actin or activate a host cell cross-linking protein to covalently cross-link actin. Alternatively, the RTX toxin may not enter the cell but rather activate a signaling pathway from outside the cell leading to activation of a cellular protein to cross-link actin (Fullner and Mekalanos, 2000).

The *V. cholerae* RTX toxin is the second largest reported bacterial toxin while the closely related RTX toxin from *V. vulnificus* RTX toxin is the largest (Figure 3-1C). It is not known whether the whole toxin or just a region of this toxin is responsible for the actin cross-linking activity of the toxin. Approximately 25% of RTX is comprised of three distinct repeat regions located at the N- and C-terminus, which are possibly involved in toxin entry. The remaining internal region of RTX representing approximately 75% of this large 484 kDa toxin could be responsible for the catalytic properties of the toxin.

Using comparative sequence analysis, a unique domain was identified within the *V. cholerae* RTX toxin that was capable of mediating the covalent cross-linking of actin when expressed as a transgene within eukaryotic cells. A deletion of this domain from the full-length *rtxA* gene completely abolishes the ability of the toxin to cross-link actin. However, this deletion did not disrupt the cell rounding activity of the RTX toxin. Lastly, VC1416, a hypothetical protein from *V. cholerae* that is homologous to this unique domain, can also mediate the covalent

cross-linking of actin when expressed in eukaryotic cells. Discovery of this unique domain within the *V. cholerae* RTX toxin is critical for future studies focusing on delineating the catalytic mechanism of covalently cross-linking actin.

Results

V. cholerae and V. vulnificus RTX toxins have unique domains.

Sequence alignment of the primary amino acid sequences from the *V. cholerae* RTX toxin and the *V. vulnificus* RTX toxin reveal approximately 80-90% identity throughout most regions of the two toxins. The *V. cholerae* RTX toxin causes cell rounding, actin cytoskeleton depolymerization, and the covalent cross-linking of actin monomers 60-90 minutes after addition of either partially purified toxin or live bacteria to epithelial cells (Fullner and Mekalanos, 2000; Lin et al., 1999). Actin cross-linking is visualized as an "actin ladder" of monomers, dimers, trimers and tetramers by Western blotting of cell extracts with an anti-actin antibody. To investigate whether these two RTX toxins have common activities, human laryngeal epithelial (HEp-2) cells were incubated with RTX+ and RTX- strains of *V. cholerae* and *V. vulnificus* at an multiplicity of infection (M.O.I.) of 200. After 90 minutes of incubation, cell rounding was observed in the presence of the RTX toxin from both *V. cholerae* and *V. vulnificus* (Figure 3-1A). However, actin cross-linking was only detected in the lysates of cells incubated with the RTX toxin from *V. cholerae* (Figure 3-1B). The cell rounding observed in the presence of the *V. vulnificus* RTX toxin could be due to rapid cell lysis correlated with the presence of this toxin (Gulig et al., 2005). These data indicate that even though the primary amino acid sequences of these two toxins are highly conserved, they have different catalytic activities.

Analysis of the sequence alignment revealed that although most regions of these two toxins are highly conserved, there is extensive sequence divergence at two internal regions. As shown in Figure 3-1C, the *V. cholerae* RTX toxin contains a novel domain, Vc1, at amino acids 1963-2419 (according to annotation Lin et al., 1999, GenBank gi|4455065), which is absent in the *V. vulnificus* RTX toxin. There are also two novel domains within the *V. vulnificus* RTX toxin, Vv1, located at the same relative location of Vc1, and Vv2, located at amino acids 3204-4095 (according to annotation by Chen *et al.* 2003, Genbank gi|37676690). Therefore, these distinct domains may confer different catalytic activities of these toxins on an otherwise highly conserved protein backbone.

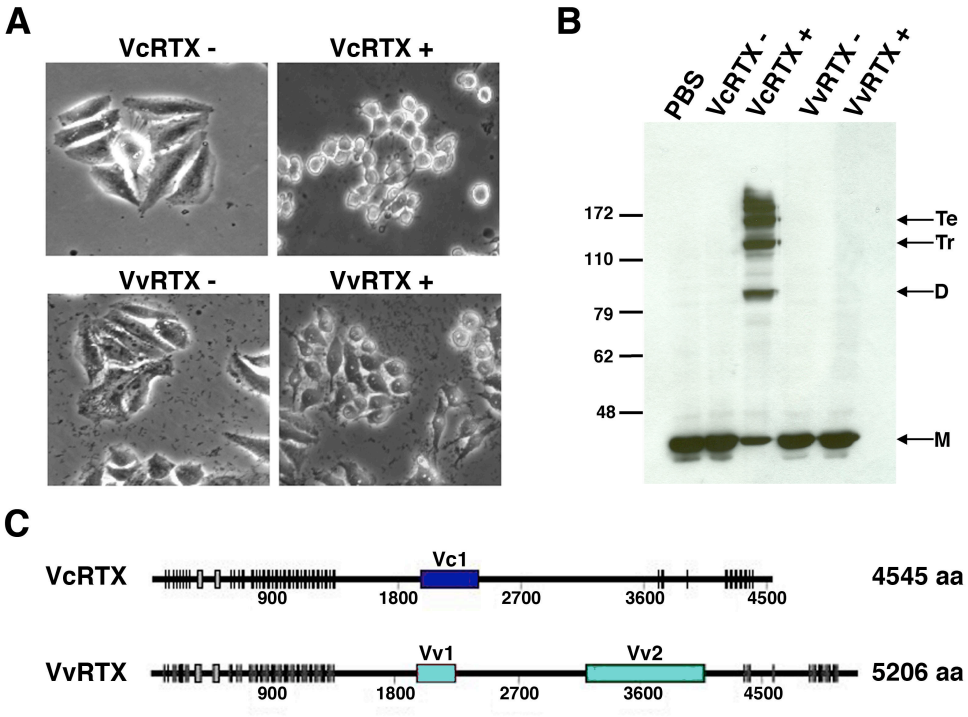

Figure 3-1: Comparison of the RTX toxins from *V. cholerae* and *V. vulnificus*.
HEp-2 cells were incubated with PBS or *V. cholerae* and *V. vulnificus* strains with an intact *rtxA* gene (VcRTX+, VvRTX+) or a null mutation in *rtxA* (VcRTX-, VvRTX-). After 90 minutes of incubation, cells were either (A) fixed for microscopic analysis at 200x or (B) harvested to measure actin cross-linking by Western blotting with an anti-actin antibody. Lines at right mark monomer (M), dimer (D), trimer (Tr), and Tetramer (Te) forms of actin. (C) Comparative analysis of the primary amino acid sequences of VcRTX and VvRTX reveals that the two toxins are similar. The domains unique to each toxin are depicted as boxes.

Discovery of the Actin Cross-linking Domain (ACD)

In order to investigate whether the novel domain Vc1 is responsible for catalyzing the covalent cross-linking of actin, DNA from the *V. cholerae* chromosome corresponding to residues 1963-2419 of RTX was amplified by PCR and cloned into the eukaryotic expression vector pEGFP-N3, such that the novel Vc1 domain is expressed with EGFP fused to the C-terminus. As shown in Figure 3-2C, African green monkey kidney fibroblasts (COS-7) transiently transfected with the resulting plasmid pACD express an EGFP fusion protein of 76.8 kDa, while cells transfected with vector pEGFP-N3 express the 27 kDa EGFP protein.

24 hours after transfection, COS-7 cells expressing the Vc1-EGFP fusion were identified by fluorescence microscopy. Nearly all the cells expressing the Vc1-EGFP fusion protein appear rounded by phase microscopy while untransfected neighboring cells appear similar to cells expressing EGFP alone (Figure 3-2B). These data demonstrate that Vc1 is associated with cell rounding.

To determine if Vc1-specific cell rounding occurs due to covalent actin cross-linking, COS-7 cells expressing this Vc1-EGFP fusion protein as well as EGFP were collected and lysed in SDS sample buffer. When subjected to Western blotting using anti-actin antibody, the actin from cells expressing the Vc1-EGFP fusion appears as a ladder of cross-linked forms of actin (Fig. 3-2D). These data demonstrate that Vc1 carries the actin cross-linking activity of RTX and this region of the protein was named the actin cross-linking domain and will be referred throughout this study as ACD.

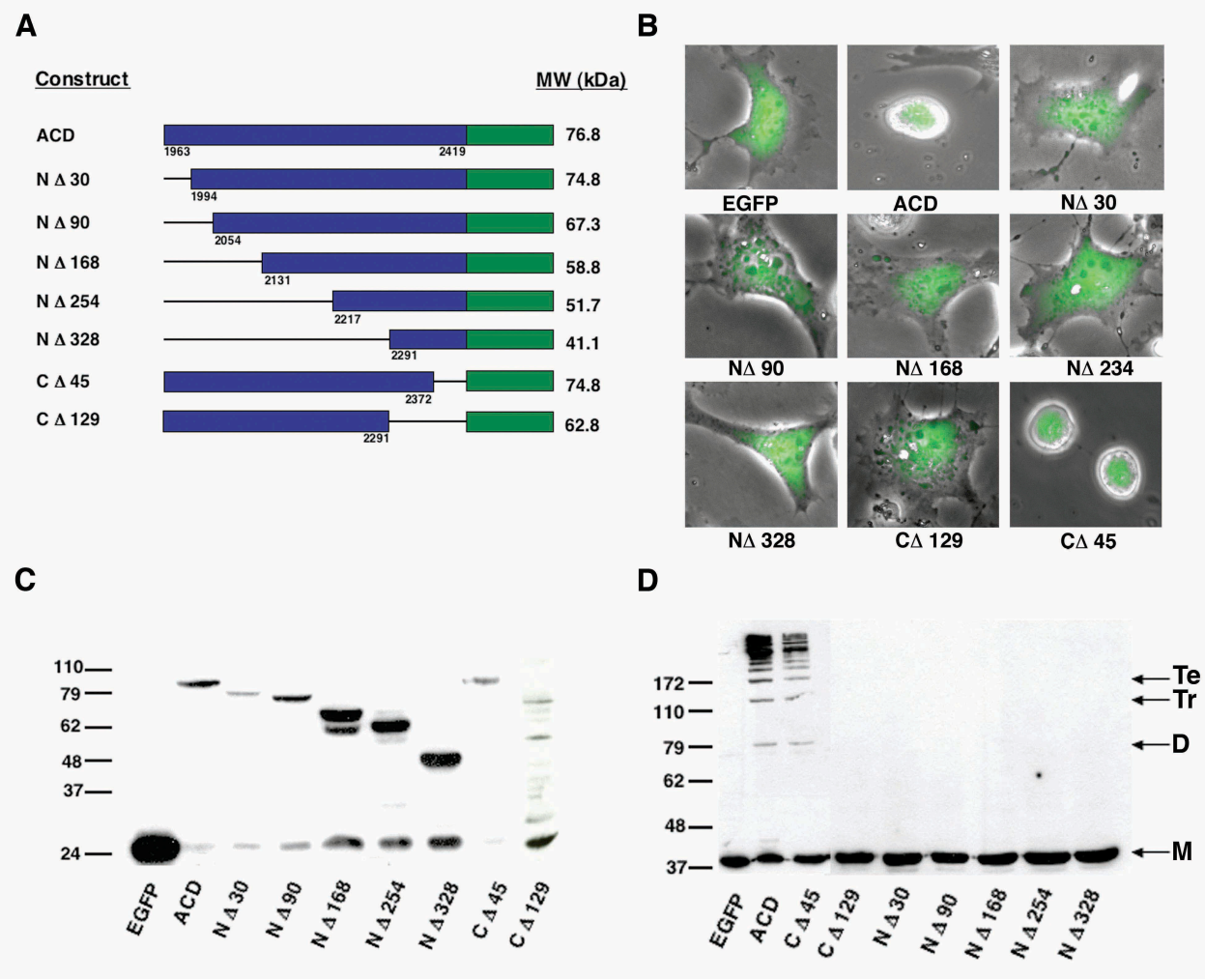

Figure 3-2: Identification of actin cross-linking domain within RTX toxin.
(*A*) Schematic representation of the ACD-EGFP full-length and truncated constructs used in this study. The predicted molecular weights of each fusion protein are stated to the right of the construct. (Numbers at bottom correspond to the amino acids of the translated product according to the annotation of Lin *et al*. 2003, GenBank no. gi |4455065). (*B,C,D*) Cell rounding, EGFP-fusion expression and actin cross-linking were detected in COS-7 cells transiently transfected with pEGFP-N3, pACD and truncated pACD constructs 24 hours post transfection. (B) Representative images were acquired as an overlay of the phase contrast image with the fluorescence micrograph measured at 550-575 nm of a single field viewed at 400x magnification. Collected cells were resuspended in SDS buffer, boiled, subjected to SDS-PAGE and Western blotting with either anti-GFP (C) or anti-actin antibody (D). Lines at right mark monomer (M), dimer (D), trimer (Tr), and tetramer (Te) forms of actin.

Structure/Function Analysis of ACD.

A Chou-Fasman secondary structure prediction performed using the MacVector software (Oxford Molecular Group) showed that the 457 amino acids of ACD contains both α-helices and β strands. Based on the predicted structure, a series of primers were designed to create truncated forms of the ACD. Five 5' deletion constructs were created resulting in proteins with truncations of 30 (NΔ30), 90 (NΔ90), 168 (NΔ168), 254 (NΔ254), and 328 (NΔ328) amino acids. Similarly, two 3' deletions were constructed resulting in 129 (CΔ129) and 45 (CΔ45) amino acid truncations from the C-terminus of the ACD representing the last two predicted α-helices. The truncated DNA sequences were amplified from the N16961 chromosomal DNA and cloned into the pEGFP-N3 vector to create C-terminal fusions with EGFP (Figure 3-2A).

The truncated ACD constructs were transiently transfected into COS-7 cells and protein expression was detected through Western blotting and fluorescence microscopy. As shown in Figure 3-2C, all of the truncated ACD proteins are expressed at their respective predicted molecular weights. Cells expressing the ACD truncations NΔ30, NΔ90, NΔ168, NΔ254, NΔ328 and CΔ129 (Figure 3-2B) do not produce the rounded phenotype generated by actin depolymerization. In contrast, all the cells expressing the CΔ45 truncated ACD protein are rounded after 24 hours (Figure 3-2B).

To associate cell rounding with actin cross-linking, lysates from the COS-7 cells transiently expressing the truncated proteins were assessed by Western blotting using an anti-actin antibody to measure actin cross-linking. As observed above, the ACD CΔ45 is the only truncated protein that retains the ability to cross-link actin comparable to cells expressing the full-length construct (Figure 3-2D).

In order to ensure that the actin cross-linking measured in COS-7 cells is not due to the over-expression of the ACD constructs or is cell type specific, the ACD constructs were tested in another cell line. HEp-2 cells, which do not express the small T antigen necessary for plasmid replication, were also transiently transfected with plasmids encoding the ACD constructs. Similar to COS-7 cells, transiently transfected HEp-2 cells appear rounded under phase microscopy only when expressing full-length ACD and ACD CΔ45 (data not shown). Consistent with the observations in COS-7 cells, cross-linked species of actin are also only detected in the presence of the full-length ACD or ACD CΔ45 transgene (Figure 3-3A). Interestingly, expression of the ACD CΔ45, as well as some of the other constructs, is practically undetectable in HEp-2 cells by Western blot (Figure 3-3B) This result confirms that the actin cross-linking observed in COS-7 cells is not cell type specific or due to the over-expression of these constructs. In fact, the data obtained from HEp-2 cells suggests that very small amounts of the ACD protein are sufficient to mediate the actin cross-linking reaction.

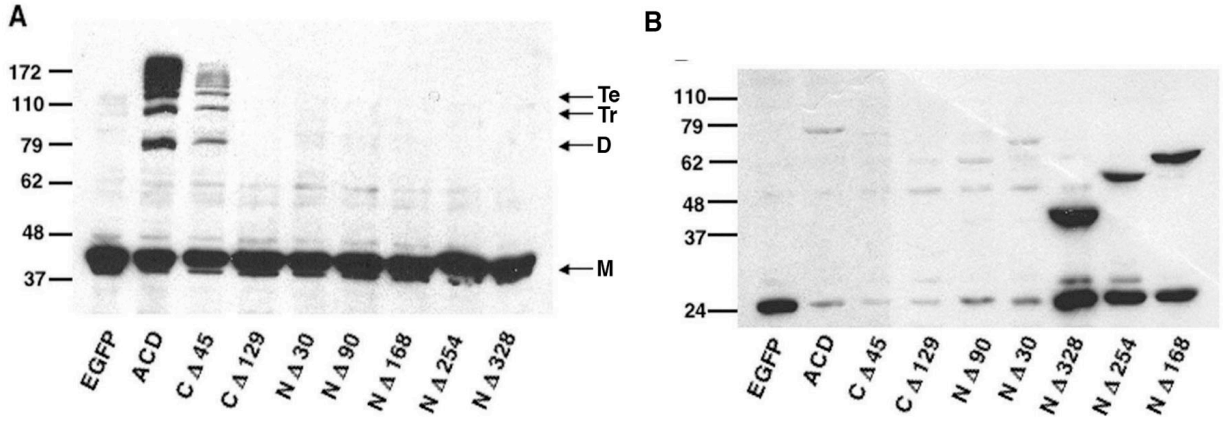

Figure 3-3: Actin cross-linking and EGFP expression of ACD constructs in HEp-2 cells.
HEp-2 cells transiently expressing EGFP (lane 1), ACD-EGFP (lane 2), and all of the truncated forms of ACD fused to EGFP (lanes 3-9) were harvested 24 hours after transfection. Collected cells were resuspended in SDS buffer, boiled, and subjected to SDS/PAGE. (A) Western blotting with an anti-actin antibody to measure actin cross-linking activity. Lines at right mark monomer (M), dimer (D), trimer (Tr), and Tetramer (Te) forms of actin. (B) Western blotting with an anti-GFP antibody to detect construct expression.

Deletion of the actin cross-linking domain of RTX

Next, the activity of RTX in the absence of the ACD was investigated. An in-frame deletion within the *rtxA* gene was constructed by Christina Cordero using double homologous recombination using the *sacB*-lethality counterselection method (Fullner and Mekalanos, 1999). Amino acids 1913-2441 of RTX were deleted to remove the novel domain ACD. The resulting strain CCO5 appears to produce normal levels of the RTX toxin in concentrated supernatant fluids; although, detection of toxin secretion is limited to the detection of low molecular weight breakdown products by Western blotting as previously observed for the full-length toxin (data not shown).

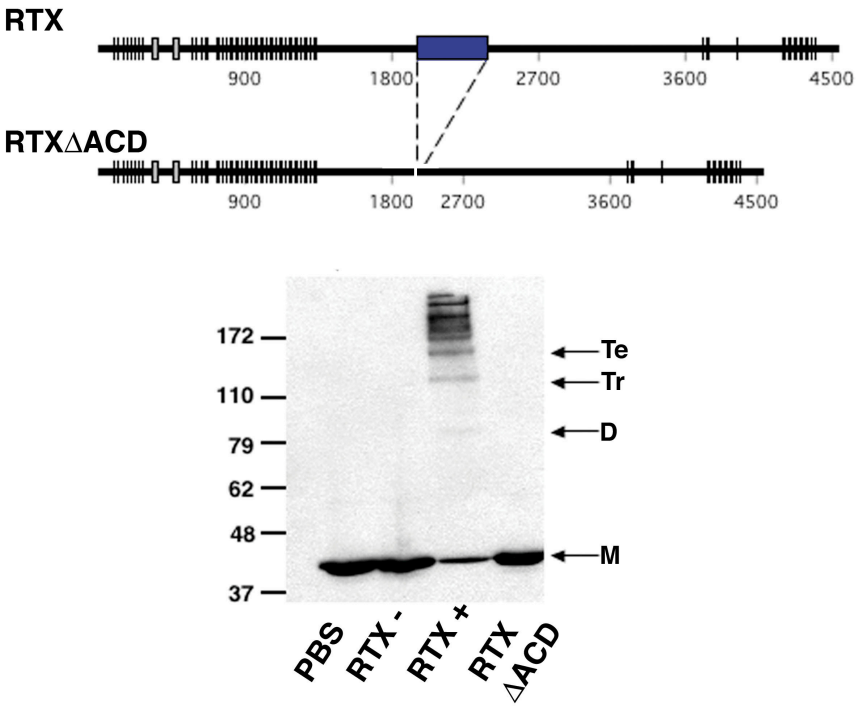

Figure 3-4: In-frame deletion of ACD within RTX eliminates cross-linking.
HEp-2 cells were incubated with PBS or *V. cholerae* strains with an intact *rtxA* gene (RTX+), a null mutation in *rtxA* (RTX-), or an *rtxA* gene with an in-frame deletion of the ACD (RTXΔACD). Cells were harvested after 90 minutes of incubation and actin cross-linking was measured by Western blotting with an anti-actin antibody. Lines at right mark monomer (M), dimer (D), trimer (Tr) and Tetramer (Te) forms of actin.

To test for actin cross-linking activity, *V. cholerae* strains KFV119, KFV92, or CCO5 were added to the culture media of HEp-2 cells at an MOI of 200. 90 minutes after addition, cells were collected and cell lysates were prepared for Western blotting with an anti-actin antibody. The actin within cells exposed to *V. cholerae* strain KFV119 expressing full length RTX is cross-linked (Figure 3-4), while only monomeric actin is detected in cells exposed to the isogenic *rtxA* null mutant, KFV92 (Figure 3-4). Cells exposed to *V. cholerae* strain CCO5 expressing RTX lacking the ACD also have no detectable cross-linked forms of actin (Figure 3-4). Therefore, the deletion of the ACD from RTX abolishes the catalytic activity of the toxin.

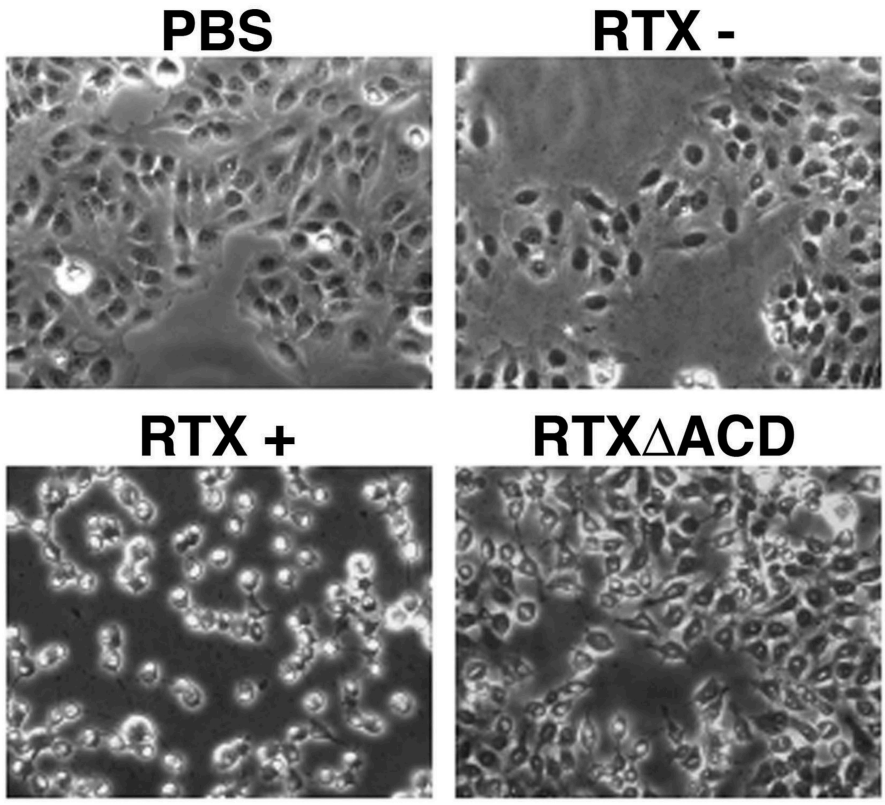

Figure 3-5: RTXΔACD still causes cell rounding.
HEp-2 cells were incubated with PBS or *V. cholerae* strains with an intact *rtxA* gene (RTX+), a null mutation in *rtxA* (RTX-), or an *rtxA* gene with an in-frame deletion of the ACD (RTXΔACD). Phase contrast images were acquired after 3 hours of incubation at 200x magnification.

Surprisingly, deletion of the ACD does not eliminate cell-rounding activity. Cell rounding observed in conjunction with actin cross-linking usually occurs between 60 and 90 minutes after addition of bacteria to cells. However, after 3 hours of incubation, cells incubated with the RTXΔACD strain of *V. cholerae* also round; although, the cells are less refractile than cells treated with the strain secreting the wild-type RTX (Figure 3-5). A Western blot for actin laddering at this time point does not suggest that this rounding is due to a delay of activity resulting from the deletion (data not shown). This rounding is also not associated with any slow cytotoxic pore forming activity characteristic of other RTX family members. HEp-2 cells rounded by incubation with either the RTX or the RTXΔACD strain of *V. cholerae* still retain their membrane integrity. There was no elevated release of lactate dehydrogenase into the culture medium as compared to controls at 3 and 6 hours post addition of bacteria (data not shown). In addition, cells incubated with either the RTX or the RTXΔACD strain of *V. cholerae* excluded the membrane impermeant dye DEAD-RED (Figure 3-6). These experiments further confirm the previous findings that the RTX toxin does not act as a pore forming toxin even at later time points.

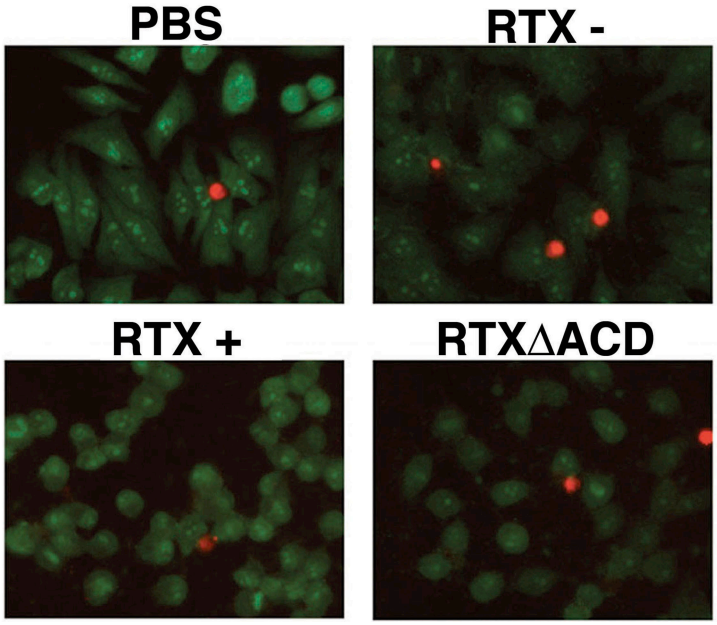

Figure 3-6: RTXΔACD does not disrupt membrane.
HEp-2 cells were incubated with PBS or *V. cholerae* strains with an intact *rtxA* gene (RTX+), a null mutation in *rtxA* (RTX-), or an *rtxA* gene with an in-frame deletion of the ACD (RTXΔACD). After 6 hours of incubation, cells were stained with SYTO10 (membrane permeant, green) and DEAD-RED (membrane impermeant, red) to determine membrane integrity. Images are an overlay of the fluorescence micrograph measured at 550-575 nm (green) and 610-675 nm (red) of a single field viewed at 200x magnification. Counting six random fields of >100 cells showed no difference in the viability of the cells incubated with PBS, RTX-, RTX+, and RTXΔACD.

Since this rounding occurs more slowly, is phenotypically distinct and is *rtxA* dependent, it can be concluded that this large toxin must contain additional catalytic activities unveiled by the deletion of the ACD. These data also confirm that the absence of cross-linking in Figure 3-4 is not due to a disruption of toxin secretion or cell membrane interaction, since activities other than actin cross-linking are maintained. Thus, these data further demonstrate that the ACD is responsible for the cross-linking activity of the RTX toxin.

Duplication of the ACD on Vibrio cholerae chromosome.

A PSI-BLAST search of the ACD revealed no sequence similarity to any other proteins of known function within the database (Altschul et al., 1997). However, this search did reveal that the ACD is 59% identical to the C-terminal portion of the *V. cholerae* hypothetical protein VC1416, also known as VgrG (E value of 1 x 10^{-153}) (Figure 3-7A). The N-terminal portion of VC1416 belongs to the family of proteins known as VgrG or Cog 3501 (www.ncbi.nlm.nih.gov/COG/new/release/cow.cgi?cog=COG3501).

Due to the overwhelming homology of the C-terminal domain of VC1416 to the ACD, it was hypothesized that this domain may also possess actin cross-linking activity and could have been duplicated on the chromosome and inserted into the RTX toxin during evolution. To test this hypothesis, pVC1416-EGFP was created to produce an EGFP fusion protein with amino acids 716-1161 of VC1416. Transient expression of this construct in COS-7 cells also produces cell rounding as determined by the visualization of VC1416-EGFP expressing cells as shown in Figure 3-7B. Actin cross-linking comparable to that generated with expression of ACD-EGFP is observed when pVC1416-EGFP is expressed in COS-7 cells (Figure 3-7C). Expression of VC1416-EGFP is detectable in COS-7 cells (Figure 3-7C), but not in HEp-2 cells (data not shown) by Western blotting with an anti-GFP antibody. This undetectable amount of VC1416-EGFP is still capable of covalently cross-linking actin in HEp-2 cells (data not shown). This result further confirms that very small amounts of this protein are necessary to generate the covalently modified actin. These data also demonstrate that *V. cholerae* has two copies of this unique actin cross-linking domain that is apparently not present in any other prokaryotic or eukaryotic organism. The discovery of a second ACD on the *V. cholerae* chromosome was a surprising result since cells incubated with a *V. cholerae* strain with a deletion of the *rtxA* gene

do not have cross-linked actin (Figure 3-4). However, microarray data observing gene expression for the *V. cholerae* El Tor strain N16961 in the stool of infected patients and in the rabbit ileal loop model revealed that the *VC1416* ranked 2783 and 3533, respectively, out of 3890 genes (Bina et al., 2003; Xu et al., 2003) suggesting that actin cross-linking is not observed in the absence of RTX due to low expression of VC1416.

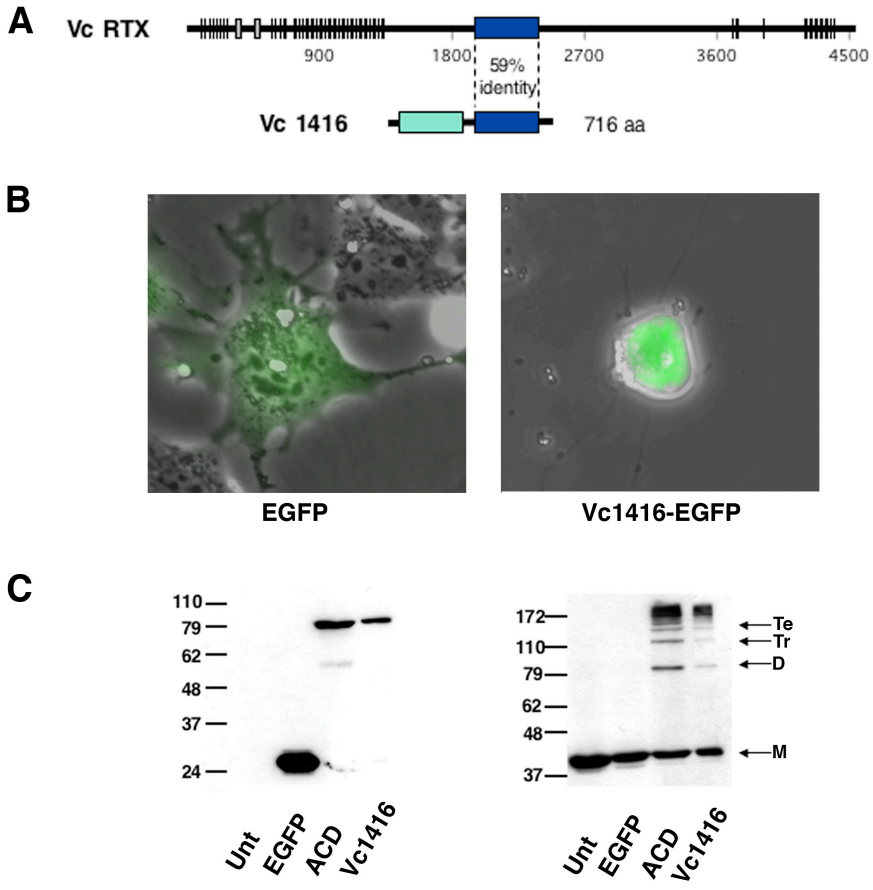

Figure 3-7: Expression of C-terminal domain of VC1416 also covalently cross-links actin.
(A)Schematic representing second copy of ACD within ORF VC1416. (B) Representative images of COS-7 cells transiently expressing EGFP and VC1416-EGFP displayed as an overlay of the phase contrast image with the fluorescence micrograph measured at 550-575 nm of a single field viewed at 400x magnification. (C) EGFP expression and actin cross-linking was detected from lysates of cells expressing EGFP, ACD-EGFP and VC1416-EGFP by Western blotting with either anti-GFP or anti-actin antibody. Lines at right mark monomer (M), dimer (D), trimer (Tr) and Tetramer (Te) forms of actin. Unt represents untransfected cells.

Inhibitors of endocytosis do not inhibit RTX actin cross-linking activity

Since transient expression of the ACD in eukaryotic cells mediated actin cross-linking, the toxin or at least this region must gain access to the cytosol. To investigate whether the RTX toxin utilizes receptor-mediated endocytosis to enter host cells, this pathway was blocked with various inhibitors to assess whether inhibition of endocytosis inhibited the actin cross-linking activity of RTX. Nocodazole and colchicine destabilize microtubules causing their depolymerization, which inhibits any endocytic vesicle trafficking within the cell (Bayer, 1998). Bafilomycin A1 specifically inhibits the vacuolar H^+-ATPase, thereby blocking the acidification of the endocytic vacuole to establish the lysosome (Bayer, 1998; Yoshimori, 1991). This step has been shown to be crucial for the intoxification of cells by other bacterial toxins that utilize receptor-mediated endocytosis to enter cells (Olnes, 2000). Chlorpromazine HCl blocks clathrin-mediated endocytosis through inhibition of the assembly and disassembly of the clathrin lattice. Lastly, Nystatin and Methyl-β-Cyclodextrin are sterol-binding drugs that deplete cholesterol disrupting lipid rafts and inhibiting endocytosis through caveolae (Sieczkarski and Whittaker, 2002).

Inhibition of endocytosis using the inhibitors Chlorpromazine HCl, Nystatin, and Methyl-β-Cyclodextrin has been well characterized and inhibitor concentrations for these studies were obtained from the literature (Akula et al., 2003; Rodal et al., 1999). To determine the concentration of Nocodazole and Colchicine required to depolymerize the microtubules, immunofluorescence staining was performed with anti-tubulin on HEp-2 cells after incubation with the inhibitors. The concentration of Bafilomycin A1 that inhibited the vacuolar H^+-ATPase in HEp-2 cells was identified using acridine orange staining.

HEp-2 cells were pre-incubated for 1 hour with the various inhibitors prior to incubation with *V. cholerae* secreting the wild-type RTX toxin. After 90 minutes of incubation with RTX,

cells were harvested and actin cross-linking was measured by Western blotting. As shown in Figure 3-8, inhibition of endocytosis by all of these inhibitors did not inhibit the actin cross-linking activity of the RTX toxin. This result indicates that blocking various aspects of the endocytic pathway does not inhibit the actin cross-linking activity of the RTX toxin. Therefore, RTX does not undergo receptor-mediated endocytosis and must utilize another mechanism to enter host cells.

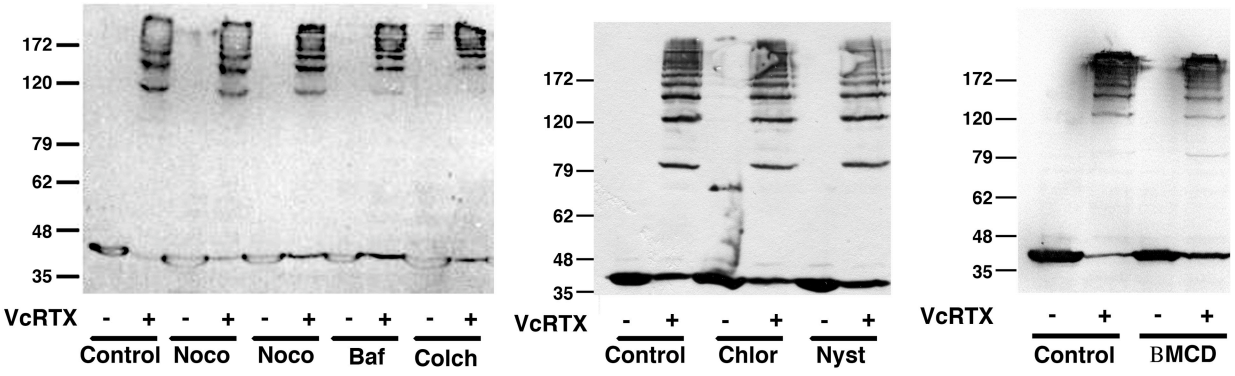

Figure 3-8: Inhibitors of endocytosis do not affect toxin activity.
Hep-2 cells were preincubated for 1 hour with the indicated inhibitors: Noco- Nocodazole (20 and 200 μM respectively), Baf- Bafilomycin A1 (50 nM), Colch- Colchicine (10 μM), Chlor-Chlorpromazine Hcl (10 µg/mL), Nys-Nystatin (100 µg/mL) and βMCD-Methyl-beta-Cyclodextrin (5 and 10 mM). The cells were then incubated with or without a *V. cholerae* strain secreting RTX for 90 minutes at 37°C before they were harvested and subjected to western blotting with an anti-actin antibody.

RTX disruption of T84 monolayer is dependent on ACD

Previous studies demonstrated that the RTX toxin disrupts the T84 epithelial monolayer as measured by a decrease in the transepithelial resistance (TER) (Fullner et al., 2001). To determine if the decrease in the TER caused by RTX is due to the actin-crosslinking activity, the TER of a T84 polarized monolayer was measured over 4 hours in the presence of *V. cholerae* strains with a null mutation in *rtxA* or secreting the wild-type RTX toxin or RTXΔACD. As

shown in Figure 3-9, the TER of the T84 monolayer decreased dramatically in the presence of the RTX toxin. However, in the presence of RTXΔACD there was no difference in the measured TER over the 4 hour time period as compared to the TER measured in the RTX- strain of *V. cholerae*. Therefore, the actin cross-linking activity of the RTX toxin was important for the disruption of the T84 monolayer. This result was unexpected since RTXΔACD was also associated with cell rounding. Since the cell rounding observed in the presence of RTXΔACD was slower, it could still cause a decrease in the TER of the monolayer at a later time point.

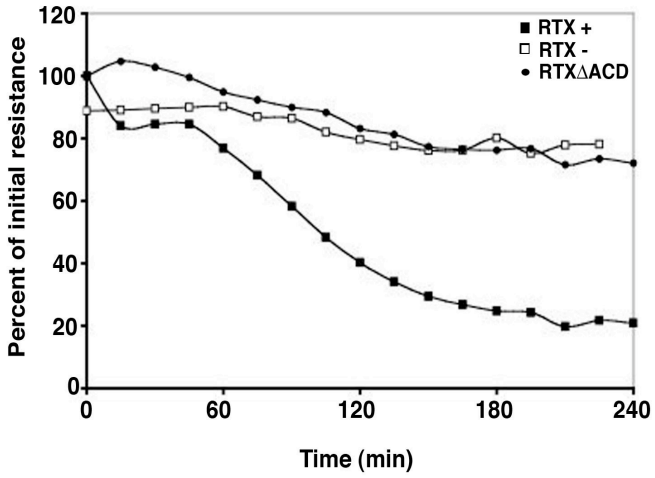

Figure 3-9: RTX disruption of T84 monolayer is dependent on ACD
TER was measured in T84 monolayer every 15 minutes after addition of *V. cholerae* strains with an intact *rtxA* gene (RTX+), a null mutation in *rtxA* (RTX-), or an *rtxA* gene with an in-frame deletion of the ACD (RTXΔACD). Values were derived by dividing the recorded resistance value by the mean of three initial resistance values recorded before addition of bacteria and are the means of triplicates of a single experiment.

Discussion

In this study, a unique 47.8 kDa domain was identified within the much larger full-length RTX toxin. This domain accounts for approximately one-tenth of the total toxin mass and is sufficient for the cross-linking of actin when expressed as a transgene. A structure/function analysis of the ACD reveals that a deletion of 45 amino acids from the C-terminus did not affect the catalytic

activity of the domain. The discovery of this domain will allow future studies to elucidate the precise catalytic mechanism of the ACD, as well as develop a mutagenesis screen to define the required catalytic residues.

The previously proposed model of the mechanism of RTX activity speculated whether the toxin was indirectly utilizing signaling pathways to activate endogenous cross-linking proteins or entering into host cells in order to catalyze the reaction directly (Fullner and Mekalanos, 2000). Since expression of the ACD within cells was found to generate the covalently modified actin species, the RTX toxin must gain entry into the cell when added exogenously. Preliminary studies using pharmacological inhibitors of endocytosis suggest that the toxin does not enter by receptor-mediated endocytosis. Therefore, I hypothesize that the *V. cholerae* RTX toxin inserts into the host cell plasma membrane similar to other members of the RTX toxin family and then, rather than forming a pore, translocates the ACD into the cell to either directly or indirectly catalyze the covalent cross-linking of actin. The RTX toxin *Bordetella pertussis* adenylate cyclase toxin (AC) uses this mechanism for insertion into the host cell membrane. AC then subsequently translocates the catalytic adenylate cyclase domain into the cell where it is held at the membrane to catalyze the transformation of ATP into cAMP (Welch, 2001). RTX could employ this same mechanism to anchor the ACD at the plasma membrane. Alternatively, a cellular protease or proteolytic activity within the RTX toxin could cleave and release the catalytic domain into the cytosol of the host cell.

The comparison of the RTX toxins from *V. cholerae* and *V. vulnificus* reveals new insight into the evolution of these two toxins. Although, the two toxins possess 80-90% identity over most of their sequence, they are associated with different cellular responses. The *V. vulnificus* RTX toxin does not cross-link actin and must cause cell rounding and lysis by an as yet

unidentified mechanism. These large bacterial toxins appear to have a capacity to carry multiple distinct toxic activities as demonstrated by the experimental evidence that the *V. cholerae* RTX toxin still causes cell rounding in the absence of actin cross-linking. It is possible that the cell rounding and cell lysis activities of the *V. vulnificus* RTX toxin could represent two independent activities of this toxin. Therefore, I hypothesize that these two highly conserved members of the RTX family of toxins share similar activities mediated through the conserved regions of these toxins, but through the acquisition of different genetic material, these two toxins acquired the unique activities of actin cross-linking and cell lysis that distinctly distinguish these toxins from each other.

The toxins may independently acquire these different catalytic activities by horizontal gene transfer. A search of the *V. vulnificus* genome did reveal the presence of an ORF that is similar to the N-terminal portion of VC1416, but this hypothetical protein lacks the C-terminal portion that contains the actin cross-linking activity. A second copy of the N-terminal portion of VC1416 is also present on the small chromosome of *V. cholerae*. Interestingly, the N-terminal portion of VC1416 belongs to the family of proteins, VgrG (Cog 3501), which consists of 45 different proteins in 10 different bacterial species (www.ncbi.nlm.nih.gov/COG/new/release/cow.cgi?cog=COG3501). This family of proteins is a component of *Rhs* elements from *E. coli* that recently has been proposed to be a mobile genetic element involved in the acquisition of novel genes, including virulence factors such as the *Pseudomonas aeruginosa* phospholipase D gene (Wang, 1998; Wilderman et al., 2001). The fact that VC1416 is located 36 ORFs upstream of RTX suggests that *V. cholerae* acquired this novel domain by horizontal gene transfer with the associated *Rhs* element and the ACD was subsequently duplicated and inserted within a ancestral *rtxA* gene closely related to the *V.*

vulnificus rtxA gene. It would be interesting to determine whether all strains of *V. cholerae* that express the RTX toxin also have the ability to cross-link actin, or if this activity was acquired by only a subset of *V. cholerae* serotypes. If the ACD was obtained through horizontal gene transfer, it is possible that other bacterial species contain this protein, but have yet to be identified.

Overall, discovery of the ACD has further advanced the study of the *V. cholerae* RTX toxin. Identification of the domain will greatly aid future investigations into the precise mechanism of the covalent modification of actin. The demonstration that RTX must gain entry into the host cell to mediate the cross-linking of actin and that deletion of the ACD unveils that this large 484 kDa RTX toxin does indeed have additional activities provides a strong foundation for future studies elucidating the mechanism of action of the RTX toxin.

Chapter 4

Identification and characterization of the inactivation of the Rho GTPases by the *Vibrio cholerae* RTX toxin

Abstract

Many bacterial toxins target small Rho GTPases in order to manipulate the actin cytoskeleton. The depolymerization of the actin cytoskeleton by the *Vibrio cholerae* RTX toxin was previously identified to be due to the unique mechanism of covalent actin cross-linking. However, identification and subsequent deletion of the actin cross-linking domain within the RTX toxin revealed that this toxin has an additional cell rounding activity. In this study, the multifunctional RTX toxin was identified to also disrupt the actin cytoskeleton by causing the inactivation of small Rho GTPases, Rho, Rac and Cdc42. Inactivation of Rho by RTX was reversible in the presence of cycloheximide and by treatment of cells with CNF1 to constitutively activate Rho. These data demonstrate that RTX targets Rho GTPase regulation rather than affecting Rho GTPase directly. A novel 548 amino acid region of RTX was identified to be responsible for the toxin-induced inactivation of the Rho GTPases. This domain did not carry GAP or phosphatase activities. Overall, these data show that the RTX toxin reversibly inactivates Rho GTPases by a mechanism distinct from other Rho modifying bacterial toxins.

Introduction

The large 484 kDa *Vibrio cholerae* RTX toxin was initially discovered due to its ability to cause cell rounding (Lin et al., 1999). Unlike other RTX toxins, the *V. cholerae* RTX toxin is not a pore-forming toxin, but rather causes cell rounding due to the depolymerization of actin stress fibers. This depolymerization of actin occurs by a mechanism unique to this toxin, resulting in the formation of covalently cross-linked actin dimers, trimers and higher order multimers (Fullner and Mekalanos, 2000).

In chapter 3, the actin cross-linking activity was mapped to a 47.8 kDa domain within the RTX toxin located at amino acids 1963-2419. This actin cross-linking domain (ACD) induced both cell rounding and the cross-linking of actin when expressed as a transgene in eukaryotic cells. An in-frame deletion of the coding region for the ACD within the *rtxA* gene (RTXΔACD) on the *V. cholerae* chromosome eliminated actin cross-linking activity, further confirming that the ACD carries the cross-linking activity. Unexpectedly, cells treated with *V. cholerae* expressing RTXΔACD still rounded. However, this RTXΔACD-induced rounding was slower, occurring after 3 hours of incubation as compared to the rounding typically observed after 75-90 minutes in the presence of actin cross-linking. These rounded cells were also phenotypically distinct from cells incubated with wild-type toxin in that the cells were not as spherical and were less refractive to light. These results revealed that RTX is a multi-functional toxin that causes cell rounding by at least two distinct mechanisms.

In this study, the mechanism of cell rounding in the absence of actin cross-linking was further investigated. Experiments uncovered that both in the presence and absence of actin cross-linking, the RTX toxin was able to induce the depolymerization of the actin cytoskeleton through the inactivation of Rho, Rac, and Cdc42. Due to the critical role of the Rho family

GTPases in many cellular processes, numerous bacterial toxins have adapted different mechanisms to target these signaling proteins. There are four general mechanisms utilized by bacterial toxins for inactivation of Rho family GTPases: 1) covalent modification by attachment of sugar moieties that block the ability of Rho, Rac, and Cdc42 to be activated by GEFs (Chardin et al., 1989; Just et al., 1995b; Sehr et al., 1998) ; 2) cleavage of C-terminal isoprenyl groups that facilitate interaction of Rho, Rac, and Cdc42 with the membrane (Shao *et al*., 2002); 3) mimicry of GAPs to stimulate the inherent GTPase activity of Rho, Rac, and Cdc42 (Black and Bliska, 2000; Goehring et al., 1999; Krall et al., 2000) ; and 4) dephosphorylation of focal adhesion proteins disrupting upstream signaling that could indirectly downregulating Rho GTPase activity (Persson *et al*., 1997; Schoenwaelder and Burridge, 1999). These studies, specifically focused on Rho, demonstrate that the RTX toxin does not use a mechanism similar to other bacterial toxins to inactivate Rho, suggesting it employs a novel mechanism for Rho GTPase inactivation.

Results

RTX depolymerizes actin in the absence of actin cross-linking activity

Previous studies showed that the *V. cholerae* RTX toxin can induce cell rounding both in the presence and absence of actin cross-linking. The cell rounding induced by RTXΔACD, as well as by wild-type toxin, is not a result of any pore forming activity of the toxin causing cell lysis. A mechanism by which numerous bacterial toxins round cells without directly affecting cell viability or membrane integrity is to induce depolymerization of actin stress fibers. To test if RTXΔACD affects the state of actin polymerization, human laryngeal epithelial cells (HEp-2) incubated with *V. cholerae* for 4 hours were fixed and stained with TRITC-labeled phalloidin to visualize F-actin by fluorescence microscopy. As shown in Figure 4-1, control cells incubated

with a *V. cholerae* strain with a null mutation in *rtxA* (RTX-) or mock treated with phosphate buffered saline (PBS) exhibited a normal cuboidal shape with stress fibers visibly crossing the cell, filopodia extending from the cells, and stress fibers and lamellipodia present at the edges. By contrast, cells incubated with *V. cholerae* secreting wild-type toxin (RTX+) were rounded with little or no staining of actin observed, which is consistent with 100% cross-linking of actin in these cells by 3 hours (Fullner and Mekalanos, 2000). Actin in cells treated with the RTXΔACD-expressing *V. cholerae* strain appeared clumped and condensed with no distinct actin structures, demonstrating that cell rounding in response to RTXΔACD was due to actin depolymerization.

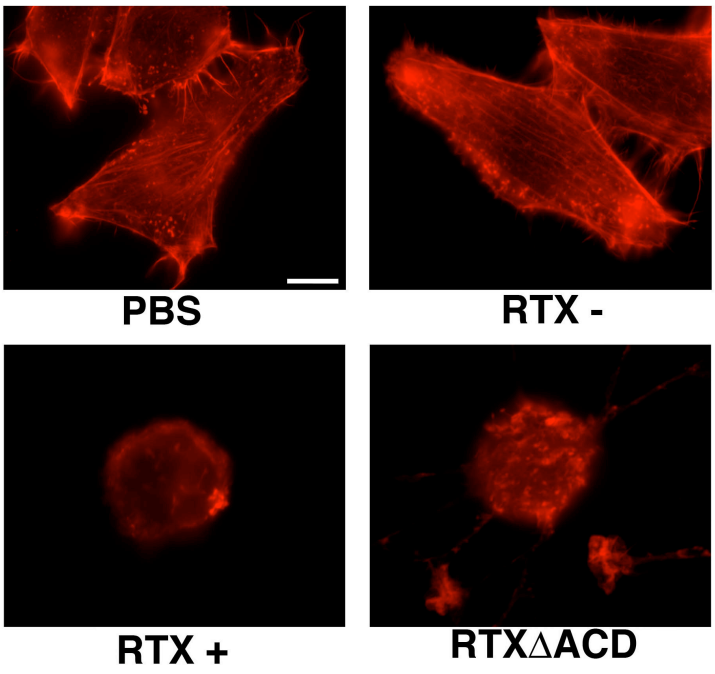

Figure 4-1: RTX causes depolymerization of actin in the absence of actin cross-linking.
HEp-2 cells were incubated with either PBS or *V. cholerae* strains with a null mutation in the *rtxA* gene (RTX-), a wild type *rtxA* gene (RTX+), or an *rtxA* gene with an in-frame deletion of the ACD (RTXΔACD) for 4 hours at 37°C. Cells were then fixed with 4% parafomaldehyde, permeabilized with 0.1% Triton X-100, and stained with TRITC-phalloidin. Representative images were acquired at 1000x. Scale bar represents 10 μm.

Constitutive activation of the Rho GTPases by CNF1 prevents RTXΔACD- induced cell rounding

Bacterial toxins that cause actin depolymerization either target actin assembly directly through modifications of actin or indirectly by targeting the small GTPase regulatory pathways (Aktories and Barbieri, 2005). Cytotoxic necrotizing factor (CNF1) from *E. coli* modifies the GTPase proteins Rho, Rac and Cdc42 by deamidation of Gln43 (Lerm et al., 1999; Schmidt et al., 1997). This modification causes constitutive activation of these proteins by inhibiting GTPase activity, even in the presence of GAPs, locking Rho GTPases in an active state (Aktories and Barbieri, 2005). Constitutive activation of the Rho GTPases can counteract the activity of most toxins that inhibit Rho GTPases, but has no effect on toxins that target actin directly (Fiorentini *et al*., 1995).

To investigate whether constitutive activation of the Rho GTPases could prevent RTXΔACD induced cell rounding, HEp-2 cells were pretreated with CNF1 for 1 hour followed by incubation with either the RTX- or RTXΔACD *V. cholerae* strains for 4 hours. Cells were then fixed and stained with TRITC-labeled phalloidin to observe the actin stress fibers. Constitutive activation of the Rho GTPases by CNF1 caused an increase in stress fiber formation as well as membrane ruffling in control cells (Figure 4-2). Pretreatment of HEp-2 cells with CNF1 prevented the cell rounding and actin depolymerization associated with RTXΔACD compared to cells incubated with RTXΔACD alone (Figure 4-2). These data indicated that RTXΔACD functions through the Rho GTPase signaling pathways and does not directly target actin.

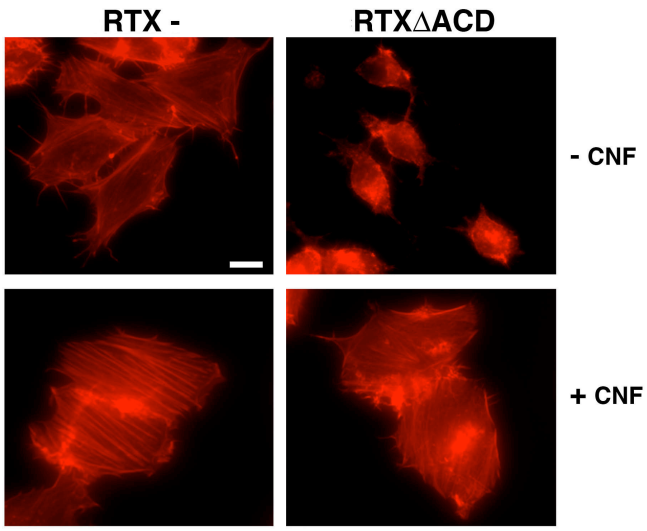

Figure 4-2: Constitutive activation of the Rho GTPases prevents RTXΔACD induced cell rounding.
HEp-2 cells were pretreated with 0.9 mg/mL CNF1 for 1 hour before incubation with the *V. cholerae* strains with an rtxA mutant (RTX-) or an rtxA gene with an in-frame deletion of the ACD (RTXΔACD) for 4 hours. All cells were fixed with 4% paraformaldehyde, permeabilized with 0.1% Triton, and stained with TRITC-phalloidin before observation by fluorescence microscopy. Scale bar represents 15 μm.

RTX inactivates the small GTPase Rho

To determine whether RTXΔACD-induced cell rounding is due to the inactivation of the Rho GTPases, an affinity precipitation assay was performed to assess whether the RTX toxin causes a decrease in the level of active Rho-GTP in cells (Ren *et al.*, 1999). HEp-2 cells were incubated with various *V. cholerae* strains as a source of RTX toxin at a multiplicity of infection of 200. Four hours following addition of bacteria, cells were collected and cell lysates were incubated with a glutathione-S-transferase fusion of the Rho binding domain (GST-RBD) from Rhotekin bound to glutathione agarose. GST-RBD specifically interacts with the active GTP-bound form of Rho in the cell lysate such that Rho-GTP, but not inactive Rho-GDP, is pelleted by centrifugation when bound to the GST-RBD agarose beads. Total Rho and Rho-GTP levels were then determined by Western blotting with an anti-RhoA antibody.

As shown in Figure 4-3, active Rho-GTP was precipitated by GST-RBD from lysates of HEp-2 cells that were incubated with either PBS or an *rtxA* null strain (RTX-) of *V. cholerae* indicating that active Rho-GTP is normally present in HEp-2 cells. However, GST-RBD added to lysates from HEp-2 cells incubated with either the *V. cholerae* strain secreting wild-type toxin (RTX+), or RTXΔACD did not precipitate any detectable Rho-GTP. Although exposure to the RTX toxin had an effect on the activation state of RhoA (Figure 4-3, upper panel), there was no effect on the amount of total RhoA within these cell lysates (Figure 4-3, lower panel). Similar studies were performed using a pan-specific Rho antibody that recognizes RhoA, RhoB, and RhoC, demonstrating that all forms of Rho were inactivated in toxin-treated cells (data not shown). From this experiment, I concluded that the RTX toxin inactivates Rho, and that this activity is independent of actin cross-linking catalyzed by the ACD.

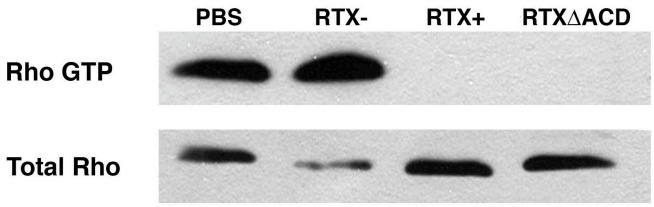

Figure 4-3: RTX inactivates the small GTPase Rho.
HEp-2 cells were incubated with either PBS, a *V. cholerae* strain with a wild type *rtxA* gene (RTX+), an *rtxA* mutant (RTX-), or an *rtxA* gene with an in-frame deletion in the ACD (RTXΔACD) for 4 hours. Cells were lysed and the active Rho was precipitated using GST-RBD coated agarose beads. Rho-GTP and total Rho levels were detected by Western blotting with an anti-RhoA antibody. Data represents a typical result from ≥ 3 independent experiments.

RTXΔACD causes the relocalization of Rho, Rac and Cdc42

Rho GTPases are localized at the membrane when in their active GTP-bound conformation, while inactive GDP-bound forms can be sequestered in the cytosol by Rho-GDI proteins (Krall *et al.*, 2002) . To further confirm that RTXΔACD inactivates Rho, subcellular fractionation experiments were performed to determine whether the toxin causes the relocalization of Rho to the cytosol. After incubation with *V. cholerae*, HEp-2 cells were collected and lysates were centrifuged at 100,000*g* to separate the membrane and cytosolic fractions. Western blotting with an anti-RhoA antibody revealed that RhoA was equally distributed between the membrane and cytosolic fractions of HEp-2 cells that were incubated with either PBS or an *rtxA* null strain of *V. cholerae* (RTX-) (Figure 4-4). However, exposure of HEp-2 cells to the RTXΔACD toxin relocalized the Rho GTPase such that 90% of RhoA is present in the cytosolic fraction (Figure 4), further demonstrating that Rho is inactivated in RTXΔACD treated cells.

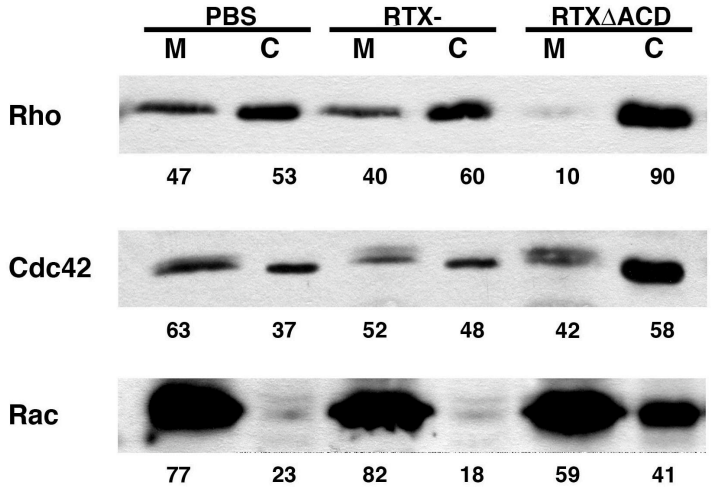

Figure 4-4: RTX inactivates Rho, Rac, and Cdc42.
HEp-2 cells were incubated with either PBS, a *V. cholerae* strain with an *rtxA* mutant (RTX-), or an *rtxA* gene with an in-frame deletion in the ACD (RTXΔACD) for 4 hours. Cells were lysed and fractionated. Equivalent membrane (M) and cytosolic (C) fractions were subjected to SDS-PAGE followed by Western blotting with anti-RhoA, anti-Cdc42, and anti-Rac antibodies. Numbers represent the percentage of each protein in the membrane verses cytosolic fractions determined by densitometric analysis. Data represents a typical result from ≥ 3 independent experiments.

Rac and Cdc42 are two other predominant members of the small Rho GTPase family that regulate actin dynamics. To determine if RTXΔACD specifically targets Rho or globally targets this family of small GTPases, the subcellular localization of Rac and Cdc42 was determined. Western blotting of membrane and cytosolic fractions with anti-Rac and anti-Cdc42 revealed that RTXΔACD redistributed approximately 20% of Rac from the membrane to the cytosol (Figure 4-4). A slight, but reproducible relocalization was detected for Cdc42 (Figure 4-4). From these experiments, it is evident that the RTXΔACD toxin causes the inactivation of Rho, Rac and Cdc42 with the most dramatic effect on Rho. Therefore, subsequent studies were focused on the mechanism of Rho inactivation.

RTXΔACD inactivation of Rho GTPase is reversible

Bacterial toxins have adapted many well-characterized mechanisms to target the Rho GTPases (Aktories and Barbieri, 2005). To identify the mechanism by which the RTX toxin inactivates the GTPase Rho, experiments were designed to determine whether RTX utilizes a known mechanism analogous to other bacterial toxins that target Rho. If the RTX toxin inactivates Rho in a similar manner to the Clostridial glucosyltransferase Toxins A (TcdA) and B (TcdB) or the cysteine protease YopT from *Yersinia spp.,* constitutive activation of the Rho GTPases should not reverse the cell rounding induced by the toxin (Fiorentini *et al.*, 1995; Sorg *et al.*, 2001). To test this hypothesis, HEp-2 cells were incubated with the RTX- or RTXΔACD strains of *V. cholerae* for 4 hours followed by the removal of the toxin and recovery in media supplemented with gentamicin in the presence or absence of CNF1. After 4 hours of recovery, cells were fixed and stained with TRITC-labeled phalloidin to visualize the actin stress fibers. As shown in Figure 4-5, cells exposed to RTXΔACD recovered in the absence of CNF1 are still round with clumped and condensed actin staining. However, the cell morphology and actin cytoskeleton of

cells incubated with RTXΔACD rapidly recovered in the presence of CNF1 resulting in more defined actin structures especially at the cell periphery (Figure 4-5). Control cells showed that the addition of CNF1 enhanced the actin stress fiber network (Figure 4-5). This experiment demonstrated that constitutive activation of the Rho GTPases with CNF1 enhanced the reversal of the cytotoxic effects by the RTXΔACD toxin. From this experiment, the conclusion was reached that the RTX toxin does not function similar to the Clostridial glucosyltransferase toxins that covalently modify Rho, since CNF1 can reverse the effects of RTXΔACD. In addition, since constitutively active Rho is equally susceptible to proteolysis as normal Rho, this experiment indicates that the RTX toxin does not proteolytically target the Rho GTPases in a mechanism similar to YopT.

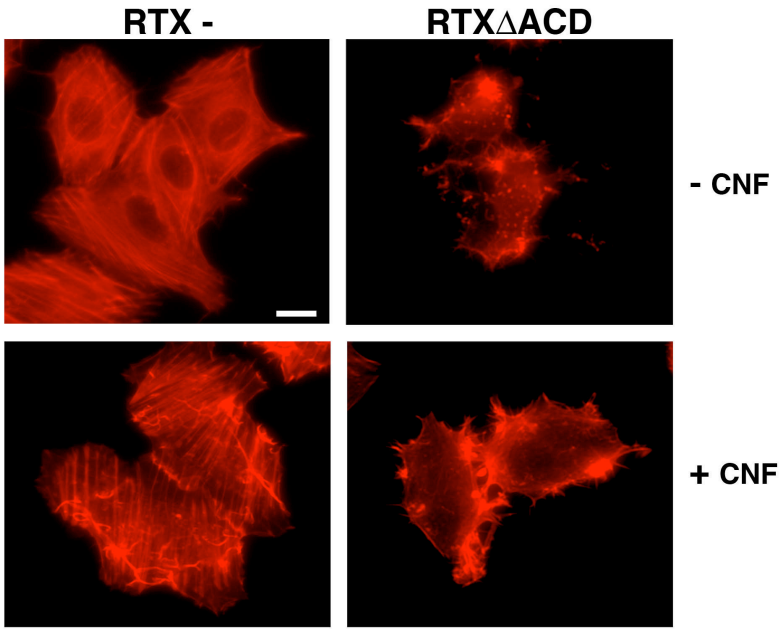

Figure 4-5 Constitutive activation of the Rho GTPases rapidly reverses RTXΔACD-induced cell rounding. HEp-2 cells were incubated for 4 hours with *V. cholerae* strains with an *rtxA* mutant (RTX-) or an *rtxA* gene with an in-frame deletion of the ACD (RTXΔACD), washed and then incubated with gentamicin in the presence or absence of CNF1 (1.5 mg/mL) for 4 hours. All cells were fixed with 4% paraformaldehyde, permeabilized with 0.1% Triton and stained with TRITC-phalloidin before observation by fluorescence microscopy. Scale bar represents 15 μm.

Constitutive activation of the Rho GTPases by CNF1 rapidly reverses the destruction of the actin cytoskeleton induced by ADP-ribosylation of Rho by the C3 exoenzyme from *Clostridia spp*. However, this covalent modification of the GTPase Rho is irreversible and requires re-synthesis of the protein to reverse the cytotoxic effects (Barth *et al*., 1999). To further investigate the mechanism of RTXΔACD inactivation of Rho, the reversibility of RTXΔACD inactivation of the Rho GTPase was determined upon removal of the toxin. HEp-2 cells were incubated with the RTX- or RTXΔACD strains of *V. cholerae* or PBS for 4 hours. Cells were then either collected (T=0) or the culture media was removed and the cells were washed to remove the toxin-secreting bacteria. Gentamicin was added to the culture media to eliminate any remaining bacteria, and the cells were collected after 2, 4, 6, and 24 hours of recovery. Collected cells were lysed and subjected to the GST-RBD affinity precipitation assay to detect the amount of Rho-GTP.

As shown in Figure 4-6A, active RhoA was detected within 2 hours following the removal of toxin-secreting bacteria. After 24 hours of recovery, the amount of Rho-GTP from cells previously incubated with RTXΔACD was equivalent to the amount of Rho-GTP detected from cells incubated with the PBS and RTX- controls. These cells exhibited a normal cell morphology, and phalloidin staining showed that actin stress fibers had regenerated by 24 hours (Figure 4-6C). The addition of cycloheximide (CHX) to the culture medium to inhibit eukaryotic cell protein synthesis did not affect the reversal of Rho-GTP levels within the cell after exposure to RTXΔACD (Figure 4-6B). However, cells recovered in the presence of CHX still appeared round under the microscope and had a depolymerized actin cytoskeleton after 24 hours of recovery (Figure 4-6C). Therefore, RTX toxin inactivation of Rho was concluded to be reversible, and that this reversibility does not require *de novo* protein synthesis. However,

synthesis of other cellular components is required for cells to regain a normal morphology. The reversibility of the reaction suggests that Rho is not covalently modified by RTXΔACD; or, if Rho is targeted directly, the host cell can reverse this modification on Rho.

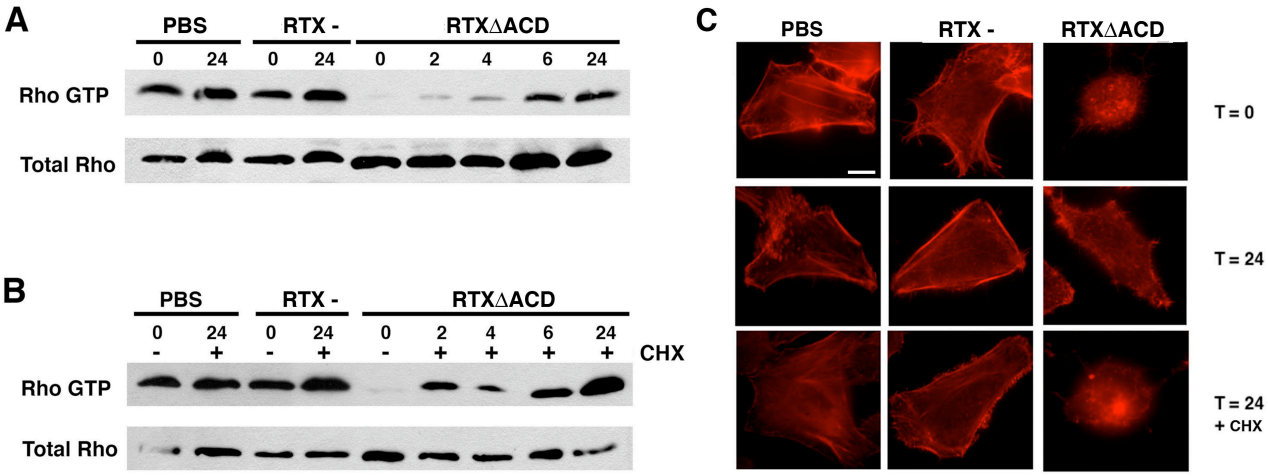

Figure 4-6: RTX inactivation of Rho is reversible.
HEp-2 cells were incubated for 4 hours with *V. cholerae* strains with an *rtxA* mutant (RTX-) or a *rtxA* gene with an in-frame deletion of the ACD (RTXΔACD). Cells were then washed to remove bacteria and allowed to recover in the presence of gentamicin (100 μg/mL) alone or with CHX (20 μM). (A,B) Cells were then harvested at the indicated time points and the active Rho was precipitated using GST-RBD agarose beads. Western blotting with an anti-RhoA was performed to detect active Rho and total Rho in cell lysates. Data represents a typical result from ≥ 3 independent experiments. (C) Cells were fixed at the indicated time points with 4% paraformaldehyde, permeabilized with 0.1% Triton and stained with TRITC-phalloidin before observation by fluorescence microscopy. Scale bar represents 10 μm.

Identification of a second cell rounding domain within RTX

Further characterization of the mechanism of RTX inactivation of the Rho GTPases required the identification of the region of the toxin responsible for this activity. To identify a second cell-rounding domain of RTX, the DNA corresponding to amino acids 2420-3443 of RTX representing the region between the ACD and CPD, another functional domain of RTX discussed in chapter 5, was cloned into the vector pEGFP-N1 for expression as a C-terminal fusion to

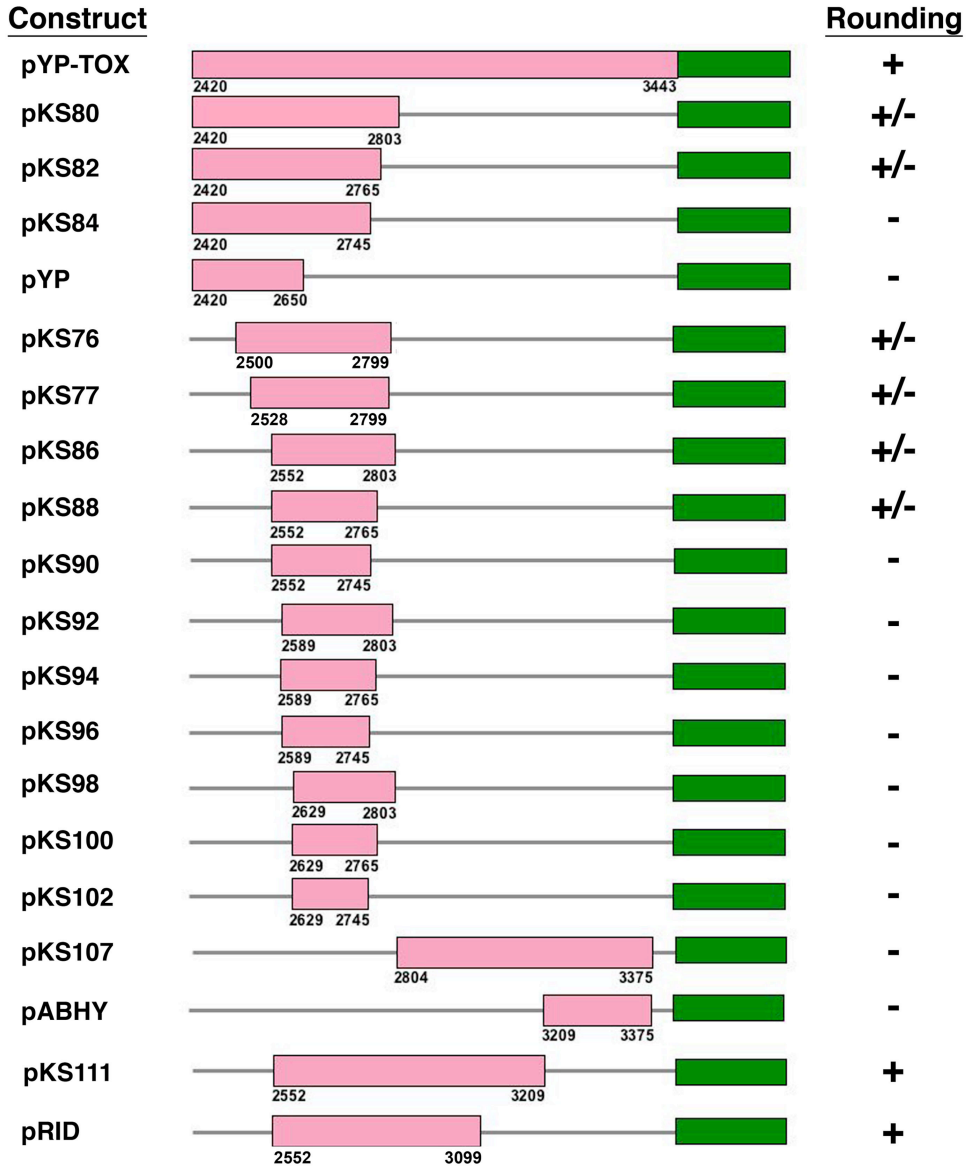

Figure 4-7: Structure/Function analysis of amino acids 2420-3443.
Schematic representation of plasmids constructed to identify second cell rounding domain. Plasmids were assessed for cell rounding by transient transfection and observing expression using fluorescence microscopy. Cloned regions corresponding to RTX are depicted by pink boxes and EGFP is depicted by green boxes. Constructs marked + =100% round, +/- exhibited a mixed phenotype with approximately 30-60% rounded cells and – = 0% rounded cells after transfectection.

EGFP. Transient transfection of this plasmid pYP-Tox in African green monkey kidney fibroblasts (COS-7) induced cell rounding in nearly all cells expressing this transgene (Figure 4-

8A). Since this region represents over 1000 amino acids of the RTX toxin, a structure/function analysis of this region was performed to determine the region essential for this cell rounding activity (Figure 4-7). Expression of amino acids 2804-3375 of RTX by the plasmid pKS108 in COS-7 cells did not cause rounding but rather these cells appeared similar to cells transiently expressing EGFP (Figure 4-8A). Interestingly, transient expression of the plasmid pKS80, which expresses amino acids 2420-2803 removing 640 amino acids from the C-terminus, resulted in a mixed phenotype where cells appeared normal, similar to cells transfected with pEGFP-N3 cells, as well as rounded. Additional analysis revealed that expression of amino acids 2552-2765 was sufficient to induce this mixed phenotype as shown by transient transfection of pKS88 (Figure 4-7).

The morphological phenotype of the cells appeared to be dependent on the level of expression of the plasmid pKS88 as estimated by the intensity of EGFP expression observed under fluorescence microscopy (Figure 4-8A). Cells rounded by transient transfection of pKS88 had a higher intensity of EGFP expression with a localized ring at the cell periphery (Figure 4-8A). Cells transiently transfected with pKS88 that were morphologically normal had a lower intensity of EGFP expression but still retained localization at the cell periphery, whereas cells transfected with pEGFP-N3 had diffuse localization of EGFP (Figure 4-8A). Closer examination of these cells revealed the fusion protein expressed by pKS88 also appeared to localize at the perinuclear region. Staining of these cells with TRITC-labelled phalloidin demonstrated an accumulation of actin in the perinuclear region as well. In fact the accumulation of actin in this region was also observed in phalloidin stained cells that were incubated with RTXΔACD. As shown in Figure 5-8B, the EGFP fusion protein expressed by pKS88 appeared to co-localize with the phalloidin stained actin at the cell periphery and the perinuclear region. However, these

are preliminary observations and further studies incorporating quantitation of EGFP expression and morphology by confocal or deconvolution microscopy need to be performed to confirm these findings.

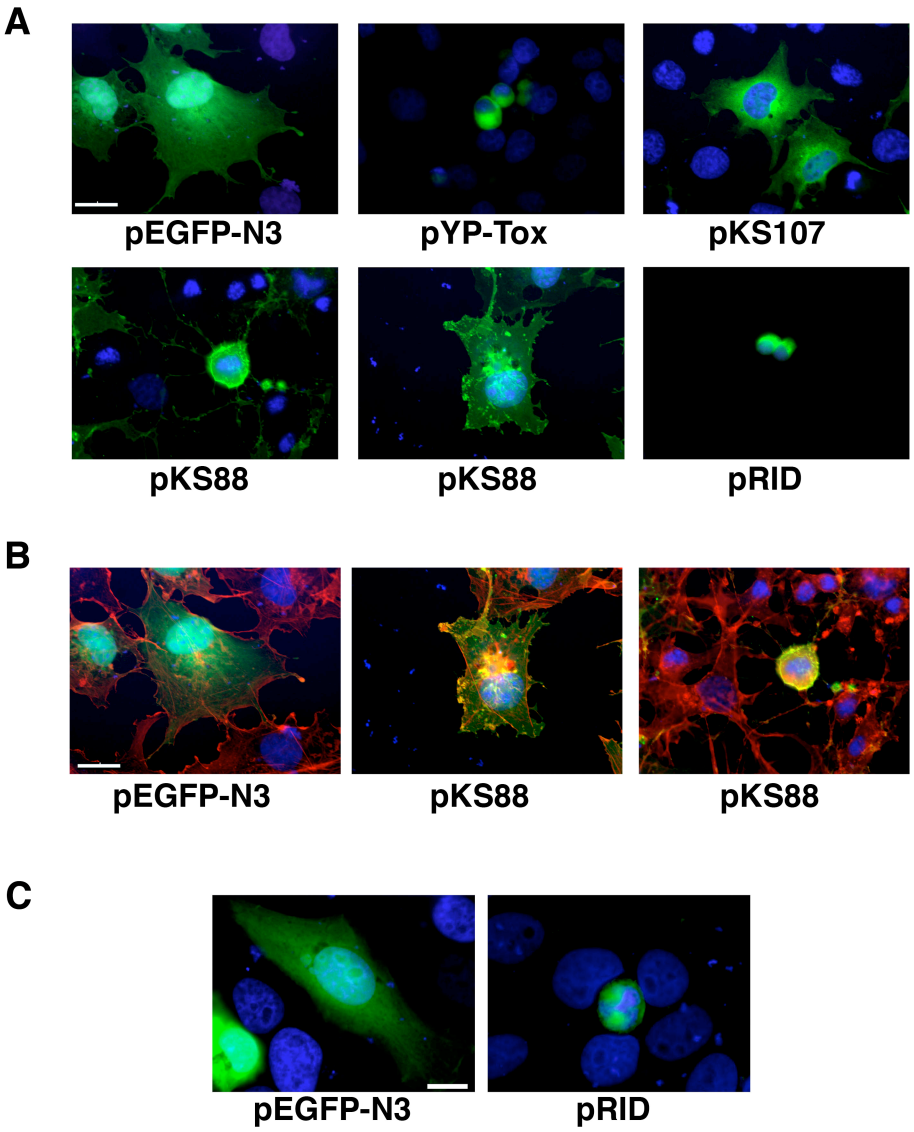

Figure 4-8: RTX amino acids 2552-3099 represent a second cell rounding domain.
Transfected cells were observed by fluorescence microscopy at 550-575 nm to detect GFP and 440-470 nm to detect Hoechst stain (A) COS-7 cells transiently transfected with pEGFP-N3, pYP-Tox, pKS107, pKS88 and pRID. Scale bar represents 20 μm. (B) Cells were stained with TRITC-phalloidin to observe actin stress fibers. Scale bar represents 20 μm. (C) HEp-2 cells transiently transfected with pEGFP-N3 or pRID. Scale bar represents 10 μm.

Since the cell rounding observed due to expression of RTX amino acids 2552-2765 was distinctly different than the rounding observed due to expression of the RTX amino acids 2420-2765 (Figure 4-8A), it was hypothesized that the C-terminal deletion in this construct was too severe. Therefore, the plasmids pRID and pKS111 were constructed extending the C-terminus by 334 or 534 amino acids. Transient transfection of pRID and pKS111 in COS-7 cells caused cell rounding in nearly all cells expressing these constructs similar to expression of the plasmid pYP-Tox (Figure 4-7 and Figure 4-8A). To address whether this cell rounding observed in COS-7 cells was cell type specific, HEp-2 cells were also transiently transfected with the plasmid pRID. As shown in Figure 4-8C, transient expression of the plasmid pRID also rounded HEp-2 cells. Interestingly, EGFP expression in these cells expressing RTX amino acids 2552-3099 was barely detectable upon microscopic analysis suggesting that low expression of this protein causes cell rounding. Since these data demonstrate that expression of RTX amino acids 2552-3099 caused cell rounding, this region was hypothesized to be responsible for the inactivation of the small Rho GTPases

Analysis of RTX amino acids 2552-3099 revealed that one of the two cysteines present in all of the 4545 amino acids of RTX is located in this region (Figure 4-9). To investigate whether this cysteine residue is important for the cell rounding activity of this region, the cysteine corresponding to Cys3022 was mutated to a Met on the plasmid encoding RTX amino acids 2552-3099. Transient expression of this plasmid pRID C-M in HEp-2 cells resulted in the same mixed phenotype observed above with expression of RTX amino acids 2552-2765. As observed above, cells transfected with pRID C-M morphologically appeared normal as well as rounded depending on the level of expression of the transgene (Figure 4-9). Cells expressing the plasmid pRID C-M also had localized EGFP expression at the cell periphery (Figure 4-9). These data

suggest that Cys3022 is important for the cell rounding activity of this domain since mutation of this residue caused a defect in the cell rounding activity associated with expression of RTX amino acids 2552-3099. However, higher expression of the plasmid pRID C-M lead to cell rounding suggesting that this mutation does not completely disrupt the activity of this domain. In the future, additional microscopic analysis and quantitation of these preliminary observations may provided insight into the role of Cys3022 in the cell rounding activity of this region.

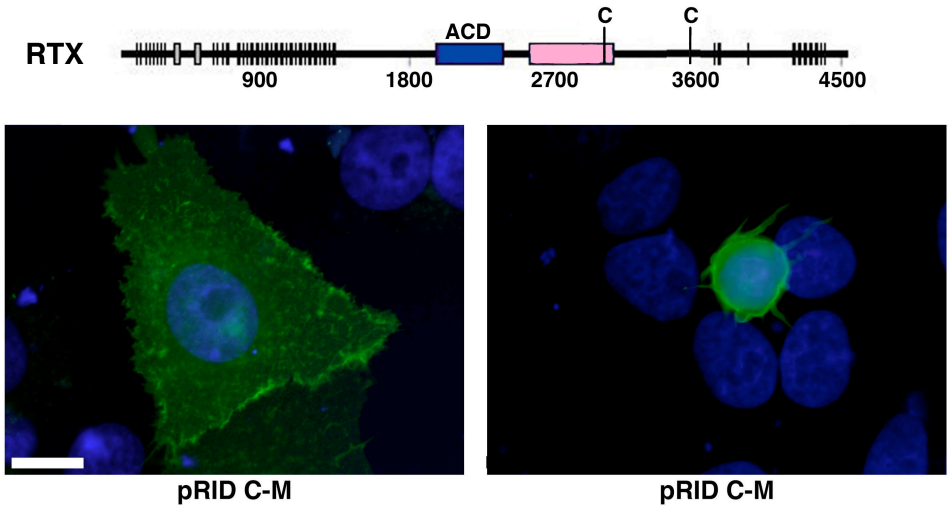

Figure 4-9: Cys 3022 from RTX is important for cell rounding.
Representative images of HEp-2 cells transiently transfected with pRID C-M observed by fluorescence microscopy at 550-575 nm to detect GFP and 440-470 nm to detect Hoechst stain. Scale bar represents 10 μm.

RTX amino acids 2552-3099 is the Rho Inactivation Domain (RID)

In order to associate this cell-rounding domain with Rho inactivation, the Rho-GTP affinity precipitation assay was performed. However, this assay is not sensitive enough to detect a change in the activation state of Rho in transiently transfected cells due to high level of Rho-GTP from untransfected cells. To address this issue, the well-characterized cellular entry mechanism of the Bacillus anthracis anthrax toxin was utilized to deliver this domain of RTX as a fusion to

the N-terminal 254 amino acids of lethal factor (LF_N) into the cell. Briefly, protective antigen (PA) binds to the anthrax toxin receptor, is cleaved by furin to its active form PA_{63} and undergoes oligomerization into a heptamer (Bradley et al., 2001; Milne et al., 1994; Molloy et al., 1992) . The LF_N fusion protein then binds to $[PA_{63}]_7$, the complex enters the cell through receptor-mediated endocytosis, and acidification of the vacuole triggers PA to form a pore and translocate the LF_N fusion protein into the cytosol (Elliott et al., 2000; Gordon et al., 1988; Koehler and Collier, 1991). This method has previously been used to facilitate the entry of enzymatic domains of the bacterial toxins C. difficile Toxin B, Corynebacterium diphtheriae diptheria toxin as well as the ACD from the RTX toxin (Cordero et al., 2006; Milne et al., 1995; Spyres et al., 2001). The DNA corresponding to RTX amino acids 2552-3099 was cloned into the pABII vector (Spyres et al., 2001) as an N-terminal fusion to LF_N and a 6x-His tag to create the plasmid pLF_NRID

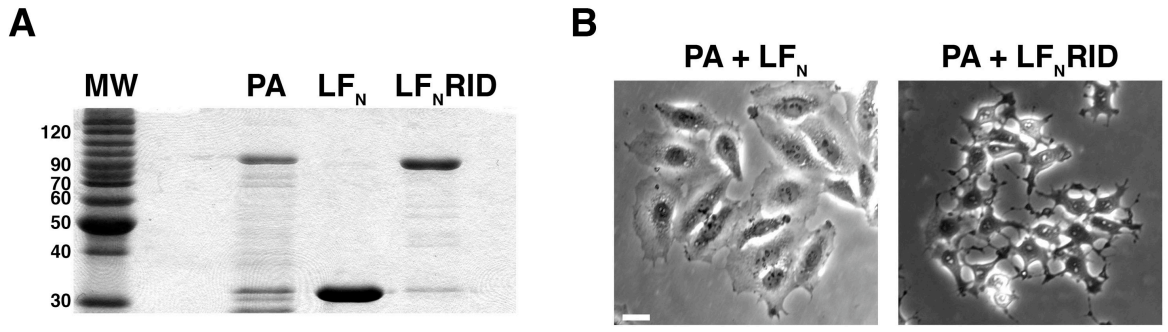

Figure 4-10: Cellular delivery of purified LF_NRID causes cell rounding.
(A) PA, LF_N and LF_NRID were purified by Ni^{2+} affinity chromatography and purity was assessed by SDS-PAGE and Coomasie Blue staining. MW represents molecular weight marker. (B) HEp-2 cells were incubated for 4 hours in the presence of PA (28 nm) with either LF_N (12 nM) or LF_NRID (12 nM). Phase contrast images were acquired at x200 magnification. Scale bar represents 30 μm.

After expression in *E. coli*, the proteins PA, LF_N, and LF_NRID were purified by Ni-affinity chromatography from the soluble fraction. The eluted proteins were analyzed by SDS-

PAGE to assess their purity (Figure 4-10A). HEp-2 cells were then incubated with LF_N or LF_NRID in either the presence or absence of PA at a 3:7 molar ratio, respectively (Mogridge *et al*., 2002). After 4 hours of incubation, cell rounding was observed with LF_NRID only in the presence of PA (Figure 4-10B). After extensive incubation, this cell rounding was reversed suggesting that degradation of LF_NRID allows the reversal of the cytotoxic effects (data not shown). This experiment indicated that this activity is similar to the rounding associated with the RTXΔACD inactivation of the Rho GTPases. Further analysis revealed that the cell rounding induced by the addition of PA and LF_NRID was correlative to a decrease in the amount of Rho-GTP in these cells as determined by the affinity precipitation assay (Figure 4-11). Based on these data, RTX amino acids 2552-3099 is the region of the RTX toxin responsible for the inactivation of the Rho GTPases, and this region was named the Rho GTPase inactivation domain (RID).

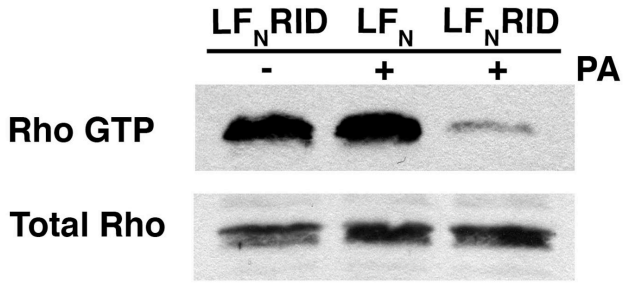

Figure 4-11: LF_NRID inactivates the small GTPase Rho.
HEp-2 cells were incubated for 4 hours in the presence of LF_NRID alone (12 nM), PA (28 nM) with LF_N (12 nM) or PA (28 nM) with LF_NRID (12 nM). Cells were harvested and the active Rho was pulled down in an affinity precipitation assay. Western blotting was performed to detect active Rho and total Rho in cell lysates. Data represents a typical result from ≥ 3 independent experiments.

RID is conserved in V. vulnificus

In chapter 3, the domain responsible for actin cross-linking was identified through a sequence alignment analysis with the putative RTX toxin from *V. vulnificus*, which does not cross-link

actin. Additional analysis of the *V. cholerae* RTX toxin and the putative RTX toxin from *V. vulnificus* revealed that RID is conserved between the two toxins with approximately 87% identity. In fact, Cys3022, identified above to be important for RID activity, is conserved between the two toxins. The *V. vulnificus* RTX toxin was previously reported to cause cell lysis (Gulig et al., 2005). Experiments presented in chapter 3 revealed that the *V. vulnificus* RTX toxin caused cell rounding (Figure 3-1). To determine whether this cell rounding was due to the depolymerization of actin, HEp-2 cells were incubated with either a *V. vulnificus* strain with a null mutation in the *rtxA* gene or a wild type *rtxA* gene, fixed and stained with TRITC-labeled phalloidin to observe the actin stress fibers. To circumvent the lysis of cells exposed to the *V. vulnificus* RTX toxin, cells were fixed after 90 minutes of incubation. As depicted in Figure 4-12A, the actin is depolymerized in cells exposed to the *V. vulnificus* RTX toxin exhibiting similar staining to cells exposed to the *V. cholerae* strain secreting the RTXΔACD toxin (Figure 4-1). The depolymerization of actin in cells observed in the presence of the *V. Vulnificus* RTX toxin correlated with inactivation of the GTPase Rho as determined by the affinity precipitation assay (Figure4-12B). These data indicated that the *V. cholerae* and the *V. vulnificus* RTX toxins, unlike actin cross-linking, both inactivate the Rho GTPases through a common domain.

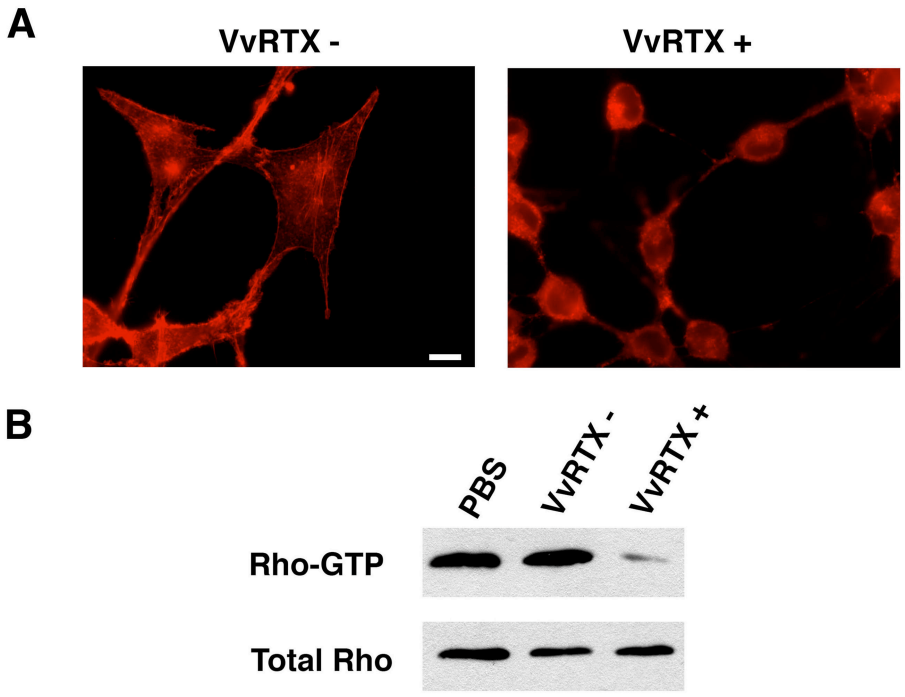

Figure 4-12: *V. vulnificus* also depolymerizes actin and inactivates the GTPase Rho.
HEp-2 cells were incubated with either PBS or *V. vulnificus* strains with a null mutation in the *rtxA* gene (RTX-) or a wild type *rtxA* gene (RTX+) for 90 minutes at 37°C. (A) Cells were then fixed with 4% parafomaldehyde, permeabilized with 0.1% Triton X-100, and stained with TRITC-phalloidin. Scale bar represents 15 μm. (B) Cells were harvested and the active Rho was pulled down in an affinity precipitation assay. Western blotting was performed to detect active Rho and total Rho in cell lysates.

RID does not function as a GAP or phosphatase

The Type III bacterial effectors ExoS and ExoT from *Pseudomonas aeruginosa*, YopE from *Yersinia spp.* and SptP from *Salmonella spp.* reversibly inactivate the Rho GTPases by mimicking eukaryotic GAP proteins (Black and Bliska, 2000; Fu and Galan, 1999; Goehring et al., 1999; Krall et al., 2000). Since the RTX toxin does not inactivate the Rho GTPases by covalent modification or proteolysis, it may modulate the activity of Rho by functioning as a GAP. Incubation of recombinant LF_NRID with RhoA loaded with [γ-^{32}P]GTP did not increase the intrinsic hydrolysis of GTP by RhoA as measured by a filter binding assay (Figure 4-13A).

These data revealed that recombinant LF_NRID does not have GAP activity, thus eliminating that the RTX toxin functions by stimulating the intrinsic GTPase activity of the Rho GTPases.

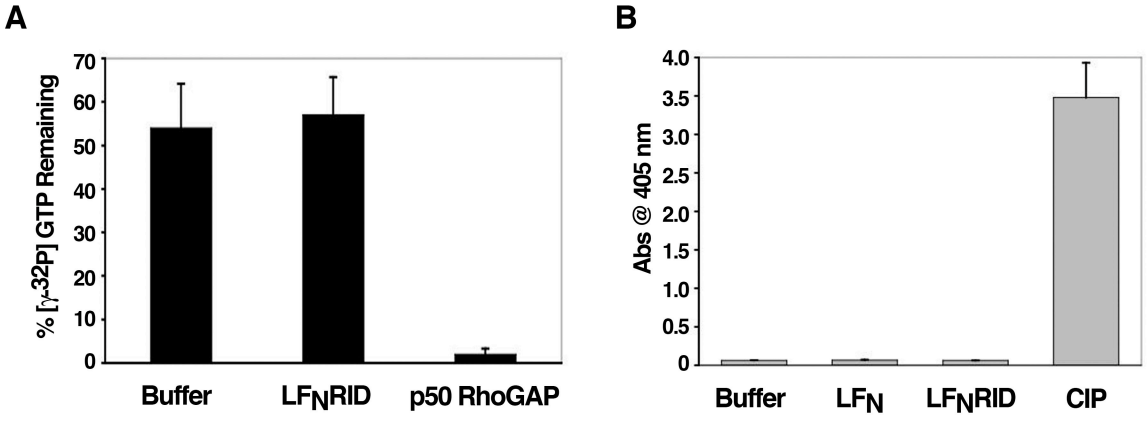

Figure 4-13: LF_NRID does not function as a GAP or phosphatase.
(A) 2 μM His-RhoA loaded with [γ-^{32}P]GTP was incubated with a buffer control, 100 nM LF_NRID or p50RhoGAP (positive control) for 10 minutes at 37°C and subjected to a filter binding assay to determine the %GTP bound to Rho. Data represents the average of duplicates from three independent experiments. (B) p-Nitrophenyl phosphate (120 μg) was incubated with buffer control, 1 μg of LF_N , LF_NRID or with 1 μl of calf intestinal alkaline phosphatase (CIP) for 15 minutes at 37°C. Absorbance was measured at 405 nm. Data represents the average of triplicates from three independent experiments.

Upstream signaling pathways of the Rho GTPases are regulated through phosphorylation events. Cellular GEFs and GAPs can also be activated and inactivated by phosphorylation (Moon and Zheng, 2003; Rossman *et al*., 2005)The type III effector from *Yersinia spp*. YopH is a phosphatase that has been shown to target members of the focal adhesions, disrupting the actin cytoskeleton and causing reversible cell rounding (Guan and Dixon, 1990; Persson *et al*., 1997). Interestingly, the critical residue of phosphatases is a cysteine and Cys3022 of RID was identified to be important for activity. However, experiments revealed that recombinant LF_NRID does not have phosphatase activity *in vitro* since it did not stimulate the hydrolysis of the substrate p-Nitrophenyl Phosphate (Figure 4-13B). Taken together, the experimental evidence

presented in this chapter suggests that the RTX toxin is utilizing a unique mechanism to target the Rho GTPases and disrupt the actin cytoskeleton.

Discussion

In this study, the cell rounding activity of the RTX toxin observed in the absence of actin cross-linking was demonstrated to be due to the inactivation of the small GTPase Rho. Additional experiments revealed that the toxin caused the dramatic relocalization of the GTPase Rho and Rac and to a lesser extent Cdc42, suggesting that the toxin affects all three GTPases. These results indicated that the multifunctional RTX toxin targets the actin cytoskeleton by two different mechanisms: actin cross-linking and inactivation of the small Rho GTPases.

Bacterial toxins utilize four general mechanisms to disrupt the Rho GTPases leading to the depolymerization of the actin cytoskeleton. These mechanisms include covalent modification, proteolytic cleavage, mimicry of host cell GAPs and dephosphorylation of proteins regulating upstream signaling pathways. Constitutive activation of the GTPases does not prevent or reverse the cell rounding elicited by YopT from *Yersinia spp*., which acts by cleaving the isoprenylated C-terminal cysteine releasing the GTPases from the membrane (Shao et al., 2002; Sorg et al., 2001). The cytotoxic effects of the glucosytransferase TcdB are prevented by constitutive activation of the Rho GTPases, but not reversed (Fiorentini *et al*., 1995). The experiments presented in this study revealed that RTXΔACD-induced cell rounding and actin depolymerization was prevented and rapidly reversed by CNF1-induced constitutive activation of the Rho GTPases. These results suggested that the RTX toxin is not inactivating the GTPases in a manner similar to YopT or TcdB. Therefore, these experiments established that the RTX

toxin does not inactivate the Rho GTPases through either proteolytic inactivation or glucosylation.

Previous studies of the C3 exoenzyme from *C. botulinum* demonstrated that *de novo* synthesis of Rho is required to reverse the cell rounding associated with ADP-ribosylation of Rho (Barth *et al*., 1999). RTXΔACD inactivation of the Rho GTPases was determined to be reversible. This reversibility did not require *de novo* protein synthesis, since the addition of CHX did not inhibit the restoration of active Rho-GTP in these cells. These data eliminated covalent modification of the Rho GTPase as the mechanism of RTX inactivation of Rho.

Cellular delivery of recombinant LF_NRID encoding amino acids 2552-3099 from RTX was able to inactivate the small GTPase Rho out of the context of the full-length RTX toxin. Identification of the domain responsible for RTX inactivation of Rho GTPases allowed further characterization of the mechanism utilizing purified protein. *In vitro* experiments revealed that recombinant LF_NRID does not have GAP or phosphatase activity (Figure 4-13). These experiments demonstrated that the RID of the RTX toxin is not inactivating the GTPase Rho by employing a mechanism similar to the type III effectors that either act as GAPs or phosphatases. However, the possibility that RID requires activation by a host cell factor cannot be ruled out. Based upon the experimental evidence presented in this study, I speculate that the RTX toxin is utilizing a unique mechanism to target the Rho GTPases and disrupt the actin cytoskeleton.

Therefore, this novel mechanism of RTX inactivation of the Rho GTPases is hypothesized to be acting (1) upon the regulation of the activation state of these GTPases, (2) through the activation of cellular GAPs or inactivation of cellular GEFs, or (3) possibly through the interference with the signaling pathways upstream of the GAPs and GEFs. Future studies to precisely determine the mechanism by which RTX inactivates the GTPases will focus on the

RID region of the toxin. RID is present in three other putative RTX toxins from *V. vulnificus* and the *Xenorhabdus* species *nematophila* and *bovinii* sharing 87, 56 and 54 percent identity, respectively. Experiments reveal that the *V. vulnificus* toxin also depolymerizes actin and inactivates the small GTPase Rho indicating that this is a common activity shared among these toxins. However, a PSI-BLAST search of this domain did not reveal homology to any other proteins of known function (Altschul *et al.*, 1997). Mutation of Cys3022 on the plasmid pRID results in a defect in the cell rounding activity of this domain. This cysteine residue is conserved among all four copies of this domain. Further studies need to be performed to determine the significance of this cysteine residue in RID induced cell rounding. In the future, additional mutational analysis of RID, as well as a broad screen to identify potential cellular targets will be performed to further investigate and define the mechanism by which the RID domain causes Rho GTPase inactivation.

Chapter 5

Autocleavage of the *Vibrio cholerae* RTX toxin is catalyzed by a novel cysteine protease domain

Abstract

Vibrio cholerae RTX is a large multifunctional bacterial toxin that causes cell rounding and actin cross-linking. Due to its size, it was predicted to undergo proteolytic cleavage during translocation into host cells to deliver activity domains to the cytosol. In this study, a domain within the RTX toxin was identified that is conserved in large clostridial glucosylating toxins TcdB, TcdA, TcnA, and TcsL; putative toxins from *V. vulnificus*, *Yersinia sp.*, *Photorhabdus sp.*, and *Xenorhabdus sp.*; and a filamentous/hemagglutinin-like protein FhaL from *Bordetella sp*. *In vivo* transfection studies and *in vitro* characterization of purified recombinant protein revealed that this domain from the *V. cholerae* RTX toxin is a GTP-stimulated cysteine protease responsible for autocleavage of the toxin. A cysteine point mutation within the RTX holotoxin attenuates actin cross-linking activity suggesting that processing of the toxin is an important step in toxin translocation. Overall, I hypothesize that autoprocessing by a cysteine protease domain is a new mechanism by which large bacterial toxins and proteins deliver catalytic activities to the eukaryotic cell cytosol by autoprocessing after translocation.

Introduction

Bacterial toxins utilize different mechanisms to facilitate entry into host cells. Type III and Type IV secretion effectors accomplish cytosolic delivery through direct injection of the cytotoxic protein from the bacterium to the eukaryotic cytosol (Henderson et al., 2004). Other bipartite toxins utilize a secreted B-subunit that binds to a eukaryotic membrane receptor and delivers a bound catalytic A-subunit to the cytosol through a pore or channel (Falnes and Sandvig, 2000). Some larger bacterial toxins such as the RTX toxin *Bordetella pertussis* adenylate cyclase (AC) utilize a poorly characterized self-translocation mechanism. AC self-inserts into the plasma membrane of host cells and then translocates the catalytic AC domain into the cell where it is held below the membrane to catalyze the transformation of ATP to cAMP (Rogel and Hanski, 1992). Similarly, the large clostridial glucosyltranseferase toxin TcdB gains entry into cells through receptor-mediated endocytosis followed by self-translocation across the endosomal membrane. However, TcdB then undergoes proteolytic processing through an unidentified mechanism releasing the N-terminal catalytic domain to the cytosol (Pfeifer et al., 2003).

The *Vibrio cholerae* RTX toxin is a large 484 kDa toxin proposed to enter target eukaryotic cells by a self-insertion/translocation mechanism similar to *B. pertussis* AC. The *V. cholerae* RTX toxin is a multifunctional toxin that was initially characterized for its ability to round epithelial cells (Lin et al., 1999). Further investigation revealed that the toxin causes depolymerization of the actin cytoskeleton through covalent actin cross-linking and Rho inactivation (Fullner and Mekalanos, 2000). Amino acids 1963-2419 of RTX were shown to be sufficient to mediate the cross-linking of actin when expressed as a transgene within eukaryotic cells thus demonstrating that this actin cross-linking domain (ACD) must access the cytosol to cross-link actin. Similarly, the Rho GTPase inactivation domain (RID) was mapped to amino

acids 2552-3099 of RTX and shown to function within the cytosol. Thus, the RTX toxin has two independent activity domains, suggesting that the toxin may undergo processing after translocation to release individual domains into the cytosol. In particular, the ACD and RID could be released to access actin and the Rho GTPases throughout the cell.

In this study, a domain was identified within RTX that is a cysteine protease responsible for autoproteolysis of the toxin. Activity of the protease requires binding of GTP indicating that processing would not occur until after translocation. Indeed, a conservative point mutation of the cysteine residue within the RTX holotoxin attenuates its actin cross-linking activity demonstrating that autoprocessing is important for cytopathic effects of this toxin. This domain is found in other known and putative large bacterial toxins suggesting that autoproteolysis by cysteine proteases is a conserved process for release and delivery of catalytic regions from large bacterial proteins.

Results

Identification of a conserved domain in large secreted bacterial proteins

Previously it was reported that amino acids 3376-3625 of *V. cholerae* RTX is 40% similar to a region of unknown function of *Clostridium difficile* TcdA (Fullner and Mekalanos, 2000). A BLAST search of GenBank (Altschul et al., 1997) identified 7 non-identical sequences of this domain that were subsequently used to perform a MEME analysis to define four motif consensus sequences to search the non-redundant protein database using MAST (Bailey and Elkan, 1994; Bailey and Gribskov, 1998). After each search, newly identified proteins that contained all four motifs in sequence were added to the MEME/MAST analysis. A total of 19 distinct copies of this

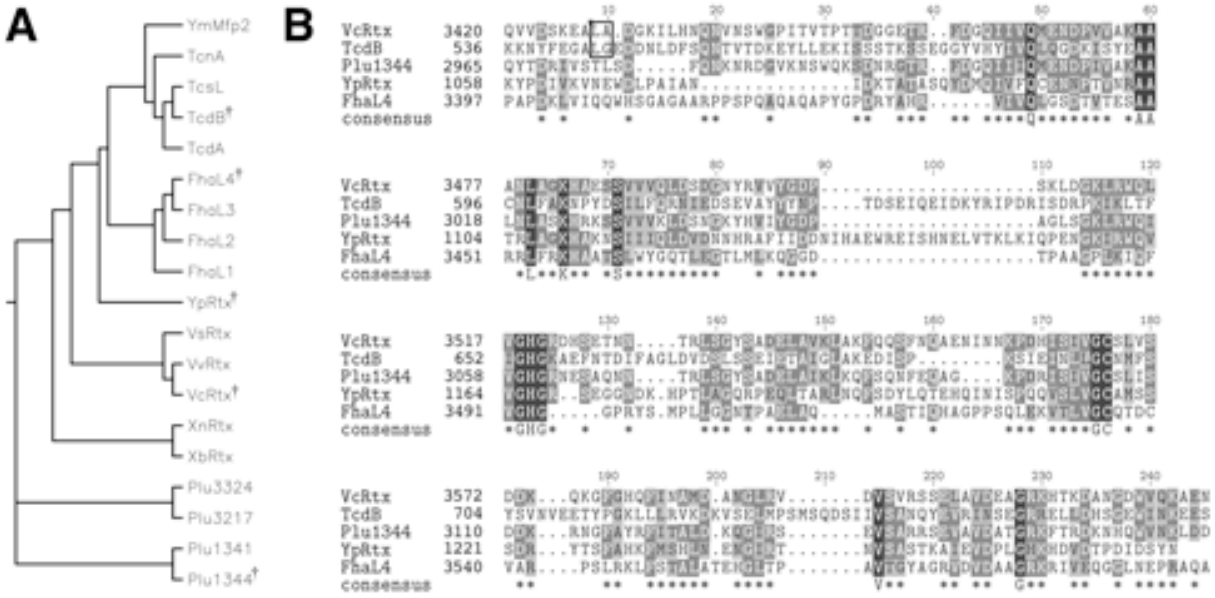

Figure 5-1: Alignment of putative cysteine protease domains.
(A) Phylogenetic tree of 19 putative CPDs and (B) CLUSTALW alignment of five diverse sequences. † symbol in phylogenetic tree indicates diverse sequences selected for alignment in panel B. In panel B, asterisks in consensus sequence represent conserved residues in 3/5 sequences and capital letters represent 100% identity. Outlined dipeptide sequence indicates cleavage sites determined experimentally. CPDs were identified within nine *Vibrio*-type RTX toxins from *V. cholerae* (VcRtx); *V. vulnificus* (VvRtx), *V. splendidus* (VsRtx), *Xenorhabdus nematophila* (XnRtx), *X. bovienii* (XbRtx), and *Photorhabdus luminescens* (Plu1344, Plu1341, Plu3217, and Plu3324); four clostridial toxins, specifically *Clostridium difficile* toxin A (TcdA), toxin B (TcdB), *C. sordellii* cytotoxin L (TcsL) and *C. noveyi* alpha toxin (TcnA); two putative *Yersinia* toxins *Y. pseudotuberculosis* YPTB3219 (YpRtx) and *Y. mollaretti* Mfp2 (YmMfp2); and four domains arranged in tandem in *B. pertussis* putative adhesin FhaL (FhaL1-4).

domain were identified (Figure 5-1A). 15 proteins, including 9 *Vibrio*-type RTX toxins, 4 clostridial glucosyltransferase toxins, and 2 putative toxins from *Yersinia* sp. carry one copy of the domain while the filamentous/hemagglutinin-like protein FhaL from *Bordetella* sp. has four copies appearing in tandem in the C-terminus. Alignment of 5 diverse sequences by CLUSTALW revealed 13 highly conserved residues (Figure 5-1B). A CLUSTALW alignment of all 19 sequences showed that (according to consensus sequence in Figure 5-1B) Q49, K66, GHG122-4, GC175-6, and G228 were conserved in all copies of the domain. Other highly conserved residues AA59-60, L63, S71, and V215 contained only conservative substitutions in

some copies (Appendix A). Thus, this domain originally identified in the *V. cholerae* RTX toxin appears to be a conserved domain of unknown function found in other large bacterial proteins that are predicted to be secreted and function either as toxins or adhesins.

Transient expression of amino acids 3376-3637 in COS-7 cells elicits cytotoxicity

In order to investigate the function of this domain, this region similar to TcdA corresponding to amino acids 3376-3637 of *V. cholerae* RTX was amplified by PCR from the *V. cholerae* chromosome and cloned into the eukaryotic expression vector pEGFP-N3 to create plasmid pCPDc. Transient transfection of this plasmid in African green monkey kidney fibroblasts (COS-7) elicited cell rounding that was quite distinct from the cell rounding observed after transient expression of the ACD (Figure 5-2A). While cells expressing ACD were spherical and refractory to light (Figure 3-2B), nearly all cells expressing this region of RTX appeared apoptotic exhibiting condensed nuclei revealed by Hoechst staining. This phenotype was specific for cells expressing the EGFP fusion protein and was not observed in neighboring untransfected cells or in cells transiently-expressing EGFP alone (Figure 5-2A). A Western blot of cell lysates with anti-GFP antibody revealed that the fusion protein runs aberrantly on SDS-PAGE with an apparent molecular weight of 48 kDa, approximately 9 kDa smaller than the predicted molecular weight 56.5 kDa (Figure 5-2B). These results initially suggested that this domain of the RTX toxin has cytotoxic activity and may undergo intracellular processing.

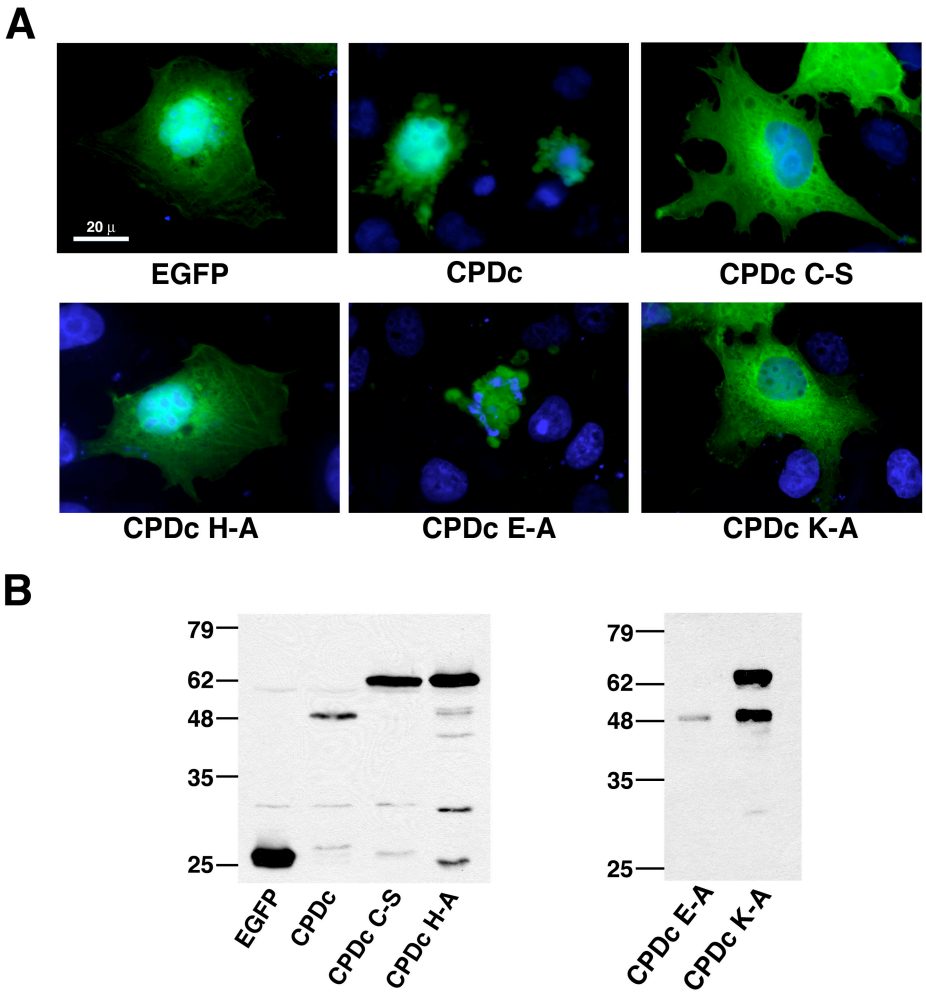

Figure 5-2: Expression of RTX amino acids 3376-3637 is cytotoxic to cells and the protein is processed intracellularly.
(A) COS-7 cells transiently expressing EGFP, CPDc, CPDc C-S, CPDc H-A, CPDc E-A, and CPDc K-A were observed by fluorescence microscopy. Representative images are displayed as an overlay of the fluorescence micrograph obtained at 550-575 nm to detect GFP and 440-470 nm to detect Hoechst staining. (B) 24 hours after transfection cells were resuspended in SDS buffer, boiled, and subjected to SDS-PAGE and Western blotting with an anti-GFP antibody. Data represents a typical result from ≥ 3 independent experiments.

Cys3568 and His3519 are essential for processing indicating the domain is an autoproteolytic cysteine protease

The CLUSTALW alignment showed that Cys3568 is conserved among all 19 copies of this domain (Figure 5-1B) and analysis of the entire RTX sequence revealed that there are only two Cys residues present in all 4545 amino acids of the toxin. In chapter four, mutagenesis of the

other cysteine, Cys3022, on the pRID plasmid resulted in a defect in cell rounding associated with transient expression of RID. Therefore, Cys3568 was hypothesized to be important for cytotoxicity observed with transient expression of CPDc. To test this hypothesis, the Cys3568 codon in pCPDc was altered to encode a Ser residue. When the resulting plasmid pCPDc C-S was transfected into COS-7 cells, cell rounding and nuclear condensation were not observed (Figure 5-2A). Western blotting with anti-GFP antibody revealed that CPD C-S fusion protein ran at the predicted molecular weight of 56.5 kDa (Figure 5-2B). Based on this observation, amino acids 3376-3637 of RTX was hypothesized to be a cysteine protease domain (CPD) that catalyzes autoprocessing of the toxin and the observed cytotoxic activity is an artifact of overexpression of a protease.

The catalytic dyad or triad of cysteine proteases generally requires a His residue (Rawlings and Barrett, 1994). His3519 was identified as a putative critical residue since it is conserved among all 19 proteins with this domain (Figure 5-1B). To determine if this residue is essential for proteolysis, pCPDc was mutagenized to convert the codon for His3519 to Ala. Transient expression of this plasmid in COS-7 cells also did not cause cytotoxicity (Figure 5-2A) and western blotting revealed that the fusion protein was expressed at its predicted molecular weight (Figure 5-2B). Some, but not all, cysteine proteases require a Glu to complete a catalytic triad. Glu3543 is conserved in 10 of the 19 copies of CPD. However, mutation of Glu3543 to an Ala on the pCPDc plasmid did not disrupt the cytotoxicity and autoprocessing activity associated with CPD (Figure 5-2). These data confirm that both Cys3568 and His3519 are critical for CPD activity and strengthen the hypothesis that this region of RTX is a cysteine protease domain required for autoprocessing.

CPD is autoprocessed in the N-terminus dependent upon C3568

Based on the above observations, it appeared that the CPDc is processed within the N-terminus since the detected processed protein maintained the C-terminal GFP epitope. To further address the site of autoprocessing, additional plasmids expressing EGFP fusion proteins were constructed. As depicted in Figure 5-3A, a longer gene fusion in pxlCPDc was constructed to express a C-terminal EGFP fusion that encodes amino acids 3101-3637 of RTX. This plasmid extended the expressed portion of RTX by 275 amino acids on the N-terminus and should encode a much longer fusion protein of 86.1 kDa. Transient transfection of pxlCPDc however yielded an EGFP fusion protein that resolved at the same apparent molecular weight as the protein expressed from pCPDc (Figure 5-3B).

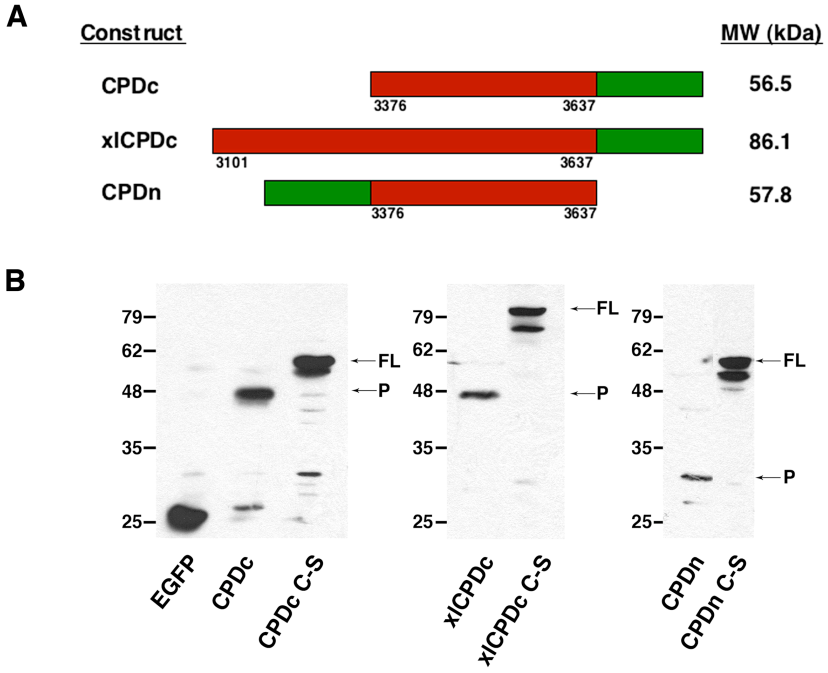

Figure 5-3: Transiently-expressed CPD in cells is autoprocessed within the N-terminus.
(A) Schematic representation of fusion proteins with the predicted molecular weight of each full-length (FL) fusion protein indicated at right. Numbers along the bottom correspond to the amino acid sequence of translated products according to the RTX toxin annotation of Lin et al. 1999 (GenBank accession no. gi|4455065). (B) Expression of the CPD and CPD C-S fusion proteins was detected in transiently transfected COS-7 cells by Western blotting for GFP. Arrows mark full-length (FL) and the processed (P) forms of CPD. Data represents a typical result from ≥ 3 independent experiments.

The plasmid pCPDn encodes amino acids 3376-3637 with an EGFP fusion on the N-terminus (Figure 5-3A) instead of the C-terminal EGFP fusion protein encoded by pCPDc. Expression of CPDn was observed at the apparent molecular weight of 32 kDa, which is smaller than the predicted 57.8 kDa (Figure 5-3B) and corresponds to the predicted molecular weight of GFP with only a small portion of the CPD construct attached. Mutant plasmids pxlCPDc C-S and pCPDn C-S were transfected to depict the correct size of these proteins upon Western blotting (Figure 5-3B). These experiments confirmed that the difference in size observed when CPDc and CPDc C-S were transiently expressed in COS-7 cells was due to the Cys3568 dependent cleavage of CPD within its N-terminus.

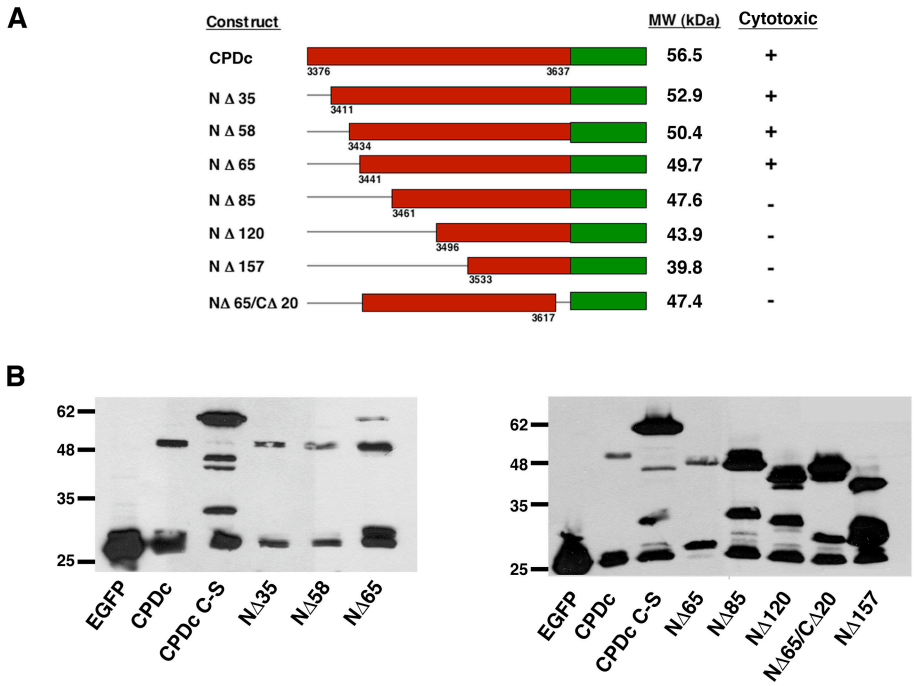

Figure 5-4: CPD cleavage occurs between amino acids 3411-3432 of RTX.
(A) Schematic representation of CPDc-EGFP full-length and truncated constructs with the predicted molecular weight of each fusion protein stated to the right. Numbers along the bottom correspond to the amino acid sequence of translated products according to the RTX toxin annotation of Lin et al. 1999 (GenBank accession no. gi|4455065). (B) Expression of the full-length and truncated CPDc fusion proteins was detected in transiently transfected COS-7 cells by Western blotting for GFP.

A structure/ function analysis of the CPD was performed to identify the region essential for CPD activity. Six N-terminal truncations were generated deleting 35 (NΔ35), 58 (NΔ58), 65 (NΔ65), 85 (NΔ85), 120 (NΔ120) and 157 (NΔ157) amino acids. Transfection of these constructs in COS-7 cells demonstrated that deletion of 85 amino acids from the N-terminus disrupts the cytotoxicity of associated with CPD (Figure 5-4A). A C-terminal truncation was also generated on the plasmid pCPDcNΔ65 deleting 20 amino acids to create the plasmid pCPDcNΔ65/CΔ20. This C-terminal deletion was not cytotoxic when transiently expressed in COS-7 cells (Figure 5-4A). Transfection of the plasmids pCPDcNΔ85, pCPDcNΔ120, pCPDcNΔ157, and pCPDcNΔ65/CΔ20 yielded EGFP fusion proteins at their predicted molecular weights (Figure 5-4B). Expression of CPDcNΔ35 and CPDcNΔ58 yielded fusion proteins at the same size as CPDc. However, experimental variability was observed for transient expression of CPDcNΔ65 which either resolved at the same apparent molecular weight of CPDc or slightly smaller. From this deletion analysis of the N-terminus of the CPD, autocleavage of CPD is hypothesized to occur within residues 3411-3441 of RTX.

Recombinant CPD (rCPD) requires a host factor for autoprocessing

In order to further characterize the CPD protease activity *in vitro*, the CPD was purified as a recombinant protein for biochemical analysis. Both the CPD and CPD C-S were cloned into the His-tag vector pMCSG7 (Stols et al., 2002) to encode amino acids 3378-3637 of RTX with 6xHis tag fusions on both the N- and C-termini (Figure 5-5A). After expression in *E. coli*, rCPD and rCPD C-S were purified by Ni-affinity chromatography from the soluble fraction. The proteins eluted from the column at the full length and were resolved on SDS-PAGE at the predicted molecular weight of 34 kDa demonstrating that rCPD was not cleaved in *E. coli* or

during purification. This observation suggested that a eukaryotic host factor is necessary to stimulate the autoproteolytic activity of CPD.

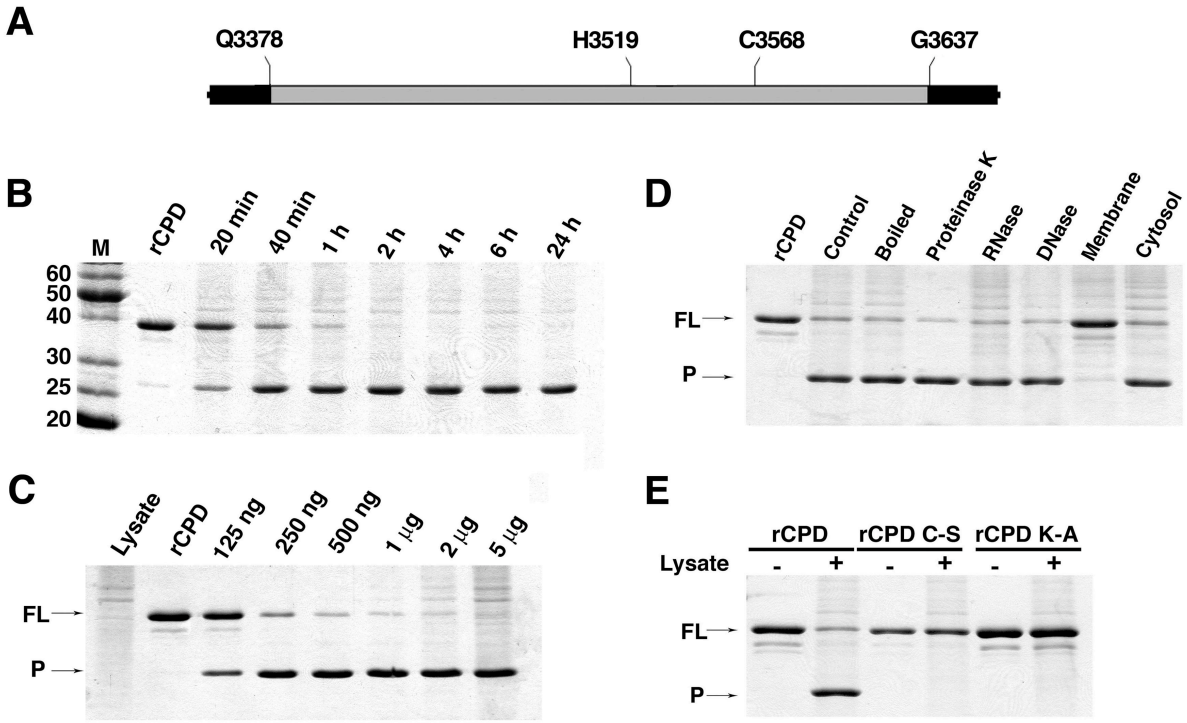

Figure 5-5: rCPD undergoes *in vitro* processing after addition of host cell lysate.
(A) Schematic representation of rCPD (grey shading) with N- and C-terminal 6xHis tag fusions (black shading). (B-E) *In vitro* processing reactions were performed with 2 μg rCPD incubated in the presence of lysate and samples were separated by SDS-PAGE and stained with Coomassie R250. (B) rCPD was incubated with 5 μg of total cell protein and the reaction was stopped at the indicated time points. (C) Overnight incubation of rCPD with increasing amounts of lysate as indicated. (D) rCPD was incubated with equivalent volumes of lysate, boiled lysate, or lysate pre-treated for 15 minutes with 200 μg/mL of Proteinase K, DNase, or RNase. rCPD was also incubated with membrane and cytosolic fractions (5 μg of total cell protein) obtained from subcellular fractionation of the lysate. (E) rCPD, rCPD C-S or rCPD K-A were incubated for 2 hours in the absence (lanes 1, 3 and 5) or presence of 5 μg of total cell protein (lanes 2, 4 and 6). Arrows mark full-length (FL) and the processed (P) forms of rCPD.

The CPD cleavage activity was indeed stimulated by the addition of a nuclear-free cell lysate confirming that a host factor is necessary. As depicted in Figure 5-5B, the addition of 5 μg of total cell protein to 2 μg of rCPD stimulated processing as rapidly as 20 minutes with

essentially all of the protein cleaved within 2 hours. Further analysis of the reaction revealed that as little as 125 ng of total cell protein was sufficient to stimulate the cleavage of 2 μg of rCPD after overnight incubation (Figure 5-5C). Increasing the ratio of cell lysate to rCPD was able to drive the cleavage of rCPD to completion demonstrating that the lysate contained a limiting component of the reaction. Cell lysate that was boiled for 5 minutes or incubated with Proteinase K, DNase or RNase prior to addition to rCPD also stimulated the processing activity (Figure 5-5D). Subcellular fractionation of the lysate revealed that the host cell factor stimulating cleavage of rCPD resides in the cytosolic fraction (Figure 5-5D). Thus, the autoprocessing activity of RTX requires a heat-stable cytosolic host cell factor that is not a protein, DNA or RNA. The addition of cell lysate to the rCPD C-S protein did not produce the processed protein confirming that the cysteine is necessary for activity and processing did not depend on a protease in the cell lysate (Figure 5-5E).

Co-incubation of rCPD C-S with rCPD in the presence of lysate inhibits the processing of rCPD (Figure 5-6). This experiment suggests that autoprocessing of rCPD could occur as a *trans*-acting processing event. Alternatively, rCPD C-S could interact with the host factor required to stimulate rCPD processing therefore blocking the interaction of the host factor with rCPD and inhibiting processing. To further investigate whether rCPD autoprocessing occurs in *trans*, co-transfection studies of the plasmids pCPDnC-S and pxlCPDc were performed in COS-7 cells. As a control the plasmids pCPDn, pxlCPDc and pCPDnC-S were co-transfected with pEGFP-N3 to visualize the size of these fusion proteins when expressed in COS-7 cells. Co-expression of CPDnC-S and xlCPDc reveals that the inactive CPDnC-S fusion protein could be cleaved by the active xlCPDc resulting in a band resolving at the same molecular weight of

CPDn. These data suggest that while a *trans*-acting processing event can occur, CPD predominantly undergoes a *cis*-acting proteolytic event.

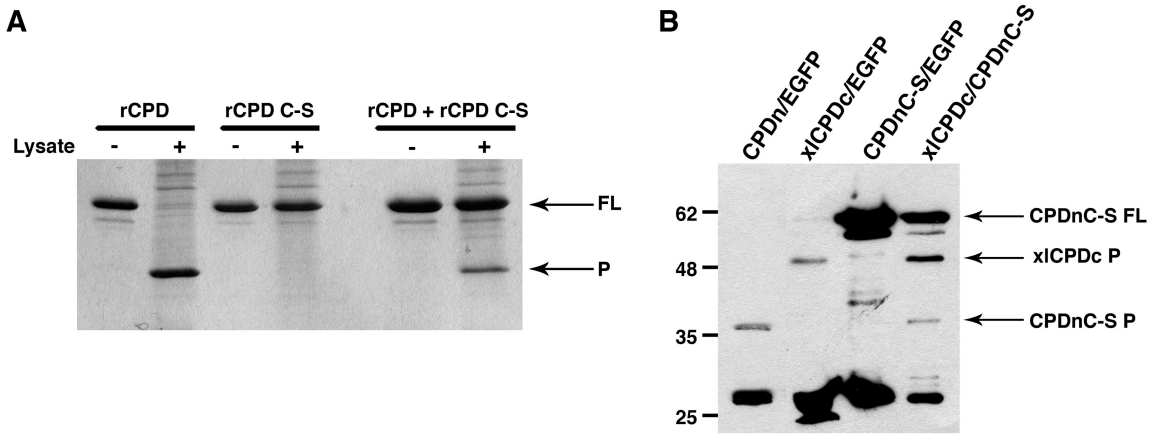

Figure 5-6: *In trans* cleavage of CPD.
(A) 2 µg rCPD and rCPD C-S were incubated separately or together with 5 µg of total cell protein for 2 hours at 37°C. Samples were separated by SDS-PAGE and stained with Coomassie R250. Arrows mark full-length (FL) and the processed (P) forms of rCPD. (B) COS-7 cells co-transfected with 0.5 μg of pCPDn, pxlCPDc, and pCPDnC-S with pEGFP-N3 (lanes 1-3) or pxlCPDc with pCPDnC-S (lane 4). 24 hours post transfection, cell lysates were subjected to SDS-PAGE and Western blotting with anti-GFP antibody. Arrows mark full-length CPDnC-S and the processed forms of xlCPDc and CPDnC-S.

Autoprocessing of CPD is inhibited by N-ethylmaleimide but not other protease inhibitors

To further define the proteolytic mechanism of the CPD cleavage reaction, rCPD was pre-incubated with various protease inhibitors for 30 minutes, followed by the addition of cell lysate and continued incubation overnight to stimulate *in vitro* cleavage. Only *N*-ethylmaleimide (NEM) completely inhibited *in vitro* cleavage of rCPD (Figure 5-7). This inhibitor irreversibly alkylates the thiol group of cysteine and is a potent inhibitor of all cysteine protease families further confirming that this protein is a cysteine protease (Anderson and Vasini, 1970).

The small molecule E64, an inhibitor of the CA clan of cysteine proteases, and calpeptin, an inhibitor of the calpain family within the CA clan (Hanada, 1978; Sasaki et al., 1990), did not inhibit cleavage of rCPD consistent with the His-Cys arrangement of the catalytic dyad of rCPD

(Figure 5-1B) rather than the Cys-His arrangement found in clan CA cysteine proteases. Phenylmethylsulphonylfluoride (PMSF), which is predominantly a serine protease inhibitor but has also been shown to inhibit some cysteine proteases (Whitaker and Perez-Villase nor, 1968), partially inhibited cleavage and this inhibition was not due to the addition of isopropanol used to solubilize PMSF (data not shown). Other protease inhibitors including aspartate protease inhibitor pepstatin and serine protease inhibitor leupeptin did not inhibit cleavage of rCPD. Altogether, these inhibitor studies confirm that rCPD is an autoprocessing cysteine protease unrelated to the Clan CA proteases.

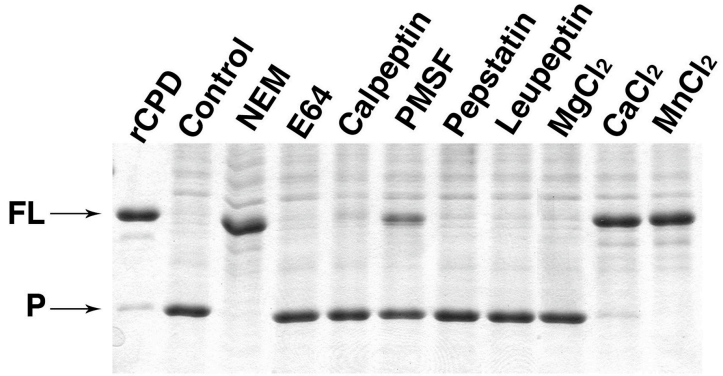

Figure 5-7: Autoprocessing of rCPD is inhibited by NEM, $CaCl_2$, or $MnCl_2$.
2 µg rCPD was pre-incubated for 30 minutes with 1 mM NEM, E-64, Calpeptin, or PMSF, 100 μM Pepstatin, 200 μM Leupeptin, or 2 mM $MgCl_2$, $CaCl_2$, or $MnCl_2$. 5 μg of total cell protein was then added to stimulate processing followed by overnight incubation. Proteins were separated by SDS-PAGE and stained with Coomasie R250. Arrows mark full-length (FL) and the processed (P) forms of rCPD.

GTP binding activates rCPD

Further inhibition studies revealed that a 30 minute pre-incubation of rCPD with $CaCl_2$ and $MnCl_2$, but not $MgCl_2$, inhibited cell lysate-stimulated processing. This result suggested that Ca^{2+} and Mn^{2+} cations are blocking the binding of Mg^{2+}, which might be essential for the processing reaction. In the absence of cell lysate, 5 mM $MgCl_2$ was not sufficient to stimulate processing

(Figure 5-8A) indicating that either Mg^{2+} is not required or that an additional stimulatory factor is needed. Common small molecule enzymatic co-factors present in the cytosol that require Mg^{2+} include ATP and GTP. As depicted in Figure 5-8A, 5 mM GTP was able to stimulate the processing of rCPD and activity was enhanced in the presence of 5 mM $MgCl_2$. Experimental variability was observed in the amount of rCPD processed in the presence of 5mM GTP plus 5 mM $MgCl_2$, possibly due to the hydrolysis of GTP in aqueous solution. To address this concern, GTP was substituted with the non-hydrolyzable analog GTPγS in the *in vitro* reaction. GTPγS stimulation of the processing of rCPD in 2 hours was equivalent to processing observed in the presence of cell lysate and the presence of $MgCl_2$ appeared to slightly enhance processing, but was not essential (Figure 5-8A).

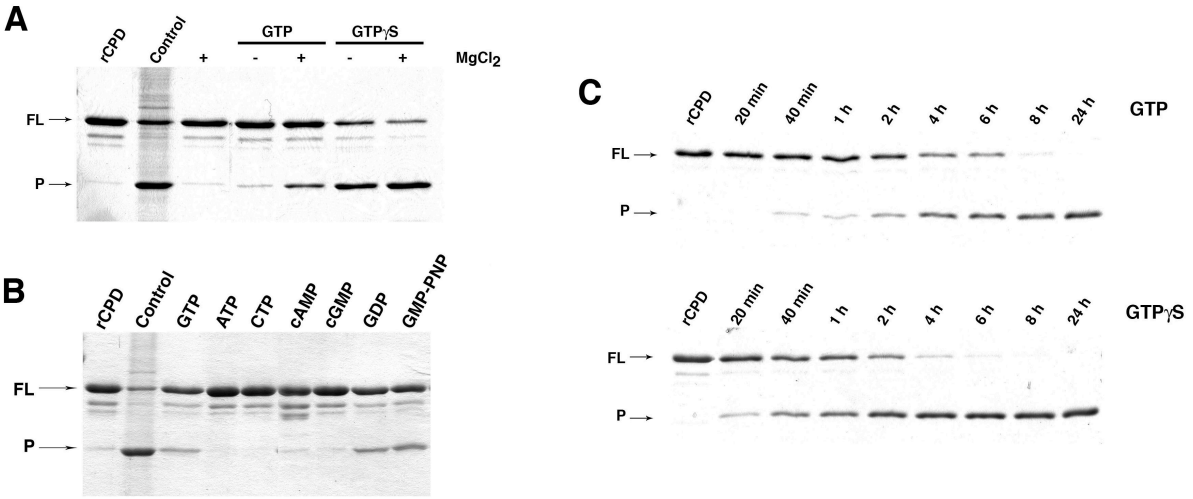

Figure 5-8: rCPD processing is stimulated by GTP.
(A) 2 μg rCPD was incubated for 2 hours alone (rCPD), with 5 μg of total cell protein (Control), with 5 mM $MgCl_2$ (+) or with GTP and GTPγS in the presence or absence of 5 mM $MgCl_2$ as indicated. (B) Incubation of 2 μg rCPD with 5 mM of either GTP or GTPγS in the presence of 5 mM $MgCl_2$ for the indicated time points. (C) rCPD (2 μg) was incubated alone (rCPD), with lysate (control), or with 5 mM of the indicated nucleotide in the presence of 5 mM $MgCl_2$ at 37° C for 2 hours. Proteins were separated by SDS-PAGE and stained with Coomasie R250. Arrows mark full-length (FL) and the processed (P) forms of rCPD

In the presence of GTP and $MgCl_2$, processing of rCPD was observed as early as 40 minutes and was complete in 8 hours (Figure 5-8B). rCPD processing stimulated by GTPγS and $MgCl_2$ progressed more quickly with detection of processed product as early as 20 minutes and complete by 4 hours (Figure 5-8B). rCPD processing was not observed in the presence of $MgCl_2$ with other nucleotides including ATP, CTP, cAMP and cGMP at 2 hours (Figure 5-8C). GDP and the non-hydrolyzable GTP analog guanosine 5'-[β,γ-imido]triphosphate (GMP-PNP) substituted for GTP in the reaction (Figure 5-8C). These experiments indicate that processing of rCPD is stimulated in the presence of GTP and the activity is enhanced by addition of $MgCl_2$. GTPγS stimulation of rCPD processing was more efficient than GTP demonstrating that binding and not hydrolysis of GTP is important for stimulation.

To further investigate GTP stimulation of CPD, the fluorophore-labeled nucleotide analog N-methylanthraniloyl-guanosine-triphosphate (mant-GTP) was utilized to demonstrate that rCPD binds GTP. mant-GTP fluoresces at 440 nm when excited at 350 nm. However when mant-GTP binds to a protein, there is a detectable increase in florescence due to the stabilization of the fluorophore. As depicted in Figure 5-9A, upon excitation at 350 nm the emission spectra revealed that the addition of rCPD to mant-GTP resulted in an increase in the fluorescence intensity by 38% in the absence of $MgCl_2$. Based on the rCPD processing assay (Figure 5-8), we expected that addition of $MgCl_2$ would enhance mant-GTP binding to rCPD. By contrast, the addition of $MgCl_2$ inhibited binding of rCPD to mant-GTP as detected by only a 5% increase in fluorescence intensity (Figure 5-9B).

Incubation of rCPD with mant-GDP increased the intensity of fluorescence by approximately 24% in the absence of $MgCl_2$ and 10% in the presence of $MgCl_2$ (Figure 5-9B). These data indicate that rCPD does bind GTP as well as GDP and this binding does not require,

and indeed is inhibited, by Mg^{2+}. However, experimental evidence suggests that Mg^{2+} enhances (Figure 5-8A), and does not inhibit (Figure 5-7), processing of rCPD. Thus, the role of Mg^{2+} in protease activity appears to be independent of GTP binding. However, the inhibition of GTP binding by Mg^{2+} likely explains the strong inhibition of processing by other divalent cations (Figure 5-7). In fact, the addition of $CaCl_2$ resulted in a 4-fold decrease in GTP binding to rCPD (Figure 5-9C). Hence, after translocation, the entry of the holotoxin into the high GTP, low calcium eukaryotic environment under the membrane would be favorable for CPD activation enabling release of the activity domains from the C-terminus of the toxin.

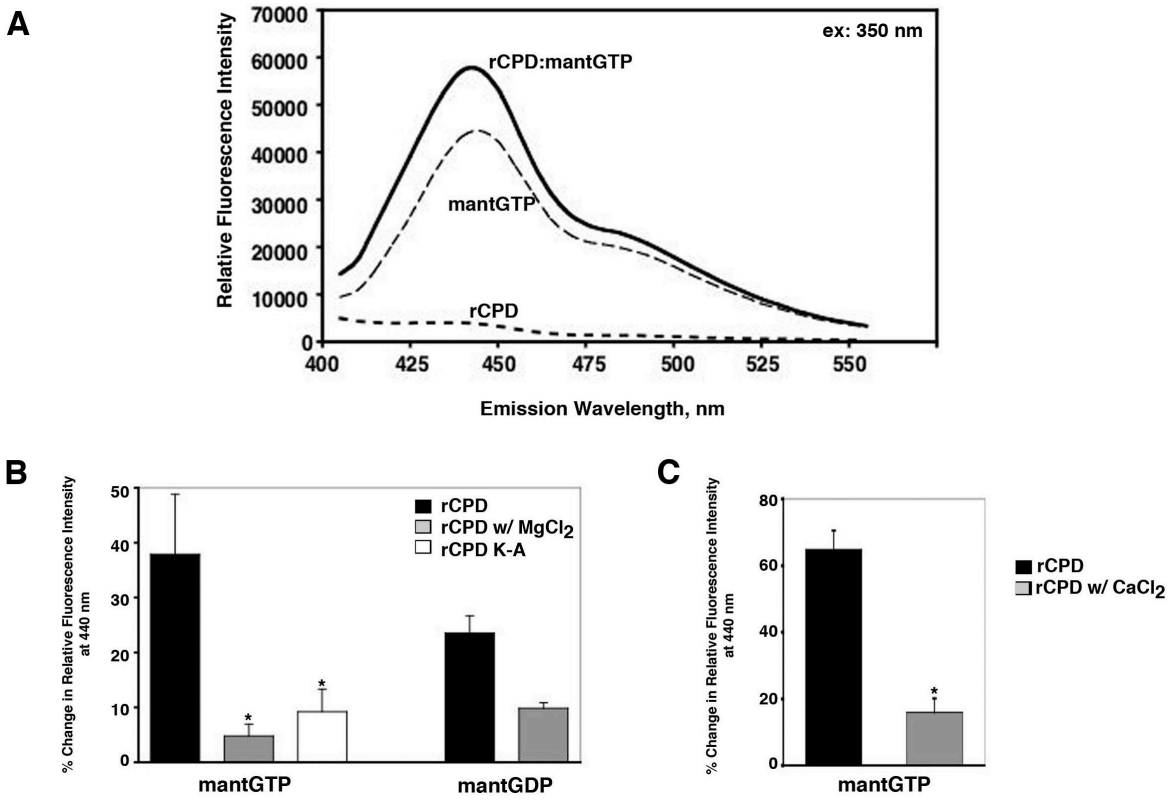

Figure 5-9: rCPD binds mant-GTP.
Fluorescence spectra were obtained of rCPD (200 μM) and mant-GTP or mant-GDP (0.5 μM) incubated alone or together in the presence and absence of 2 mM $MgCl_2$ or 5 mM $CaCl_2$ as indicated. rCPD K-A (200 μM) was incubated with mant-GTP (0.5 μM) in the absence of $MgCl_2$. (A) Representative emission scan after excitation at 350 nm of rCPD alone, mant-GTP alone or rCPD with mant-GTP. (B, C) Calculated change in fluorescent intensity observed at 440 nm compared to mant-GTP or mant-GDP alone. All data are expressed as mean ± SEM. n≥3. *$p < 0.05$ compared to rCPD:mant-GTP.

Lys3482 is important for GTP binding and rCPD processing

Analysis of the sequence of the CPD revealed a putative ATP/GTP binding site according to the consensus sequence (A/G)-X_4-GK(S/T) where the Lys is important for the binding of the nucleotide (Saraste et al., 1990). The peptide sequence **A**ANLA**GK**HAES**S** located at amino acids 3475-3487 was identified as a potential site for GTP binding. Analysis of all 19 copies of this conserved domain revealed high sequence conservation in this region. In fact the Lys is conserved among all 19 copies (Appendix A). The pCPDc plasmid was mutagenized to convert Lys3482 codon to an Ala. Transient expression of CPDc K-A in COS-7 cells did not cause cytotoxicity but Western blotting revealed that CPDc K-A resolved at the predicted molecular weight of 56.5 kDa as well as at the processed molecular weight indicating a partial defect in processing *in vivo* (Figure 5-2). *In vitro* analysis of rCPD K-A revealed that the addition of cell lysate did not stimulate autoprocessing confirming that Lys3482 is important for activity (Figure 5-5E). In addition, incubation of rCPD K-A with mant-GTP only increased the fluorescent intensity by approximately 9% indicating that this protein had a defect in binding to mant-GTP compared to rCPD (Figure 5-9B). These data indicate that mutation of Lys3482 affects GTP binding decreasing the overall efficiency of CPD autoprocessing.

CPD cleaves between L3428 and A3429 of the RTX toxin

Fourier Transform Mass Spectrometry (FT-MS) is an analytical method that can determine the molecular weight of proteins under 30,000 Da to within 0.1 mass units. Since the molecular weight of rCPD is known to be 34157.2 Da, the exact cleavage site can be deduced from the FT-MS determined molecular weight of the peptides obtained after stimulation of the protease. After overnight incubation, the rCPD cleavage reaction was directly injected onto a C-8 reverse phase

column and peptides eluted in two peaks at 10.56 and 10.88 minutes. The samples were then analyzed by LTQ-FT and the mass of the proteins in the two peaks was measured as 25854.08 Da and 8320.86 Da (Figure 5-10). Calculation of the predicted masses using PROTPARAM for all potential N-terminal and C-terminal rCPD cleavage products indicated that the observed molecular weight would correspond to a cleavage between Leu3428 and Ala3429 resulting in predicted fragments of 25854.4 Da and 8320.8 Da (Figure 5-10). This cleavage site falls within the region between residues 3411 and 3432 identified by deletion analysis using the transfection assay.

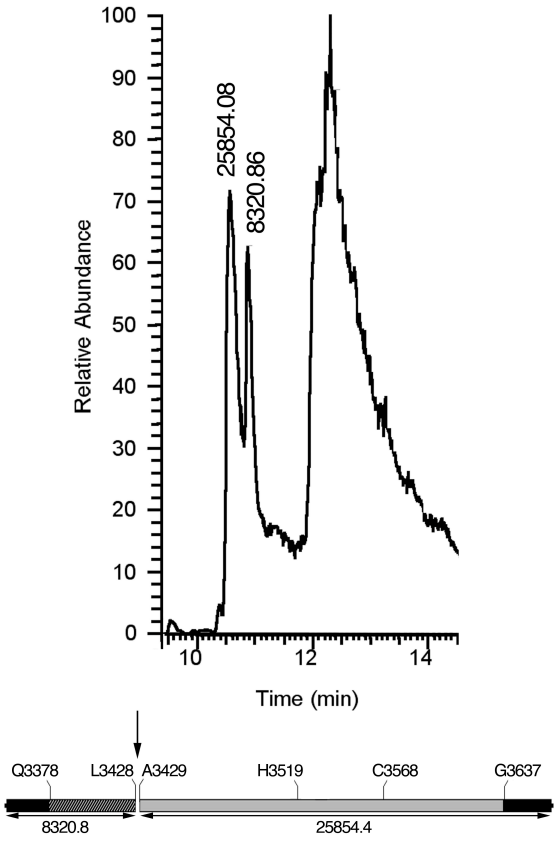

Figure 5-10: rCPD is cleaved between L3428 and A3429.
FT-MS was performed at Chicago Biomedical Consortium Proteomic Facility at the University of Illinois at Chicago.Processed rCPD eluted from C8 reverse phase column in two peaks at 10.56 and 10.88 minutes. The third peak at 12.31 minutes consists of poorly resolved materials such a polymers, small molecules and peptides. The mass of the proteins contained within the peptide fragment peaks was determined by LTQ-FT analysis and the results are shown above the peak. Schematic representation of rCPD shows the determined cleavage site as well as the computer predicted mass of the two fragments.

A C3568S mutation in the RTX holotoxin is defective for actin cross-linking

In order to investigate whether the autocleavage of the RTX toxin was important to the overall function of the toxin, a point mutation of the catalytic Cys codon was introduced onto the bacterial chromosome by double homologous recombination using the *sacB*-lethality counterselection method (Metcalf et al., 1996). The resulting mutant strain, KSV10, carried a Ser residue in place of Cys3568 in the *rtxA* gene. To assess the effect of the C3568S point mutation on RTX toxin function, actin cross-linking activity was measured. As expected, the actin from cells exposed to the *V. cholerae* strain KFV119 expressing the wild type RTX toxin appeared as a ladder of covalently cross-linked actin at 90 minutes with the actin progressing to only higher multimers at 180 minutes, while exposure to the *rtxA* null isogenic *V. cholerae* strain KFV92 did not generate cross-linked forms of actin (Figure 5-11) By contrast, cells incubated with KSV10 expressing the C3568S mutant RTX protein had a defect in actin cross-linking activity. As shown in Figure 5-11, cross-linked dimer was barely detectable after 90 minutes and the normal actin laddering pattern usually observed after exposure to the RTX toxin was not generated even after 180 minutes. It is unlikely that this defect was due to a disruption of the actin cross-linking activity of the toxin since the ACD is a distinct domain that can cross-link actin independent of the remainder of the toxin both *in vivo* when expressed as a transgene. Thus, these results suggest a model wherein this defect in the actin cross-linking activity of the RTX toxin is due to the inability of the toxin to access substrate in the absence of autocleavage. Overall, I speculate that the autocleavage activity of the CPD within the RTX toxin plays an important role in the delivery of activity domains as part of the mechanism of action of this toxin.

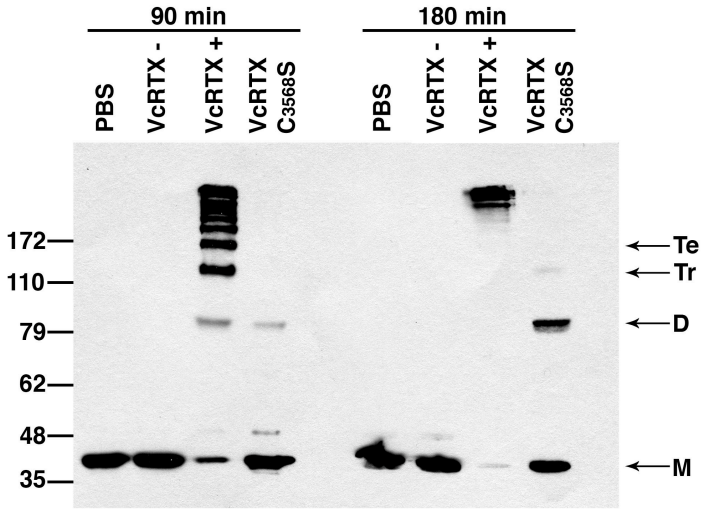

Figure 5-11: Cys3568 is important for RTX toxin actin cross-linking activity.
COS-7 cells were incubated with PBS or *V. cholerae* strains with an intact *rtxA* gene (RTX+), a null mutation in *rtxA* (RTX-), or an *rtxA* gene with a C3568S point mutation (RTX C3568S). Cells were harvested after 90 and 180 minutes of incubation, and actin cross-linking was measured by Western blotting with an anti-actin antibody. Lines at right mark monomer (M), dimer (D), trimer (Tr), and tetramer (Te) forms of actin.

Discussion

In this study, a domain of unknown function was identified within the RTX toxin that is conserved among many large secreted bacterial proteins. Characterization of this domain both *in vivo* and *in vitro* revealed that it is a cysteine protease responsible for autoprocessing of the *V. cholerae* RTX between L3428 and A3429. Mutation of the catalytic cysteine on the *V. cholerae* chromosome inhibited the actin cross-linking activity of RTX suggesting that cleavage of the toxin is important for activity. *In vitro* studies demonstrated that the rCPD cleavage was stimulated upon exposure to host cell factors. Additional experiments established that GTP binding stimulated the cleavage of CPD. The addition of Mg^{2+} appeared to enhance GTP stimulation of CPD autoprocessing but the role of Mg^{2+} is not to facilitate GTP binding.

Since GTP stimulated the processing of CPD, it was surprising that full-length rCPD was purified from *E. coli*. It is possible that the intracellular concentration of GTP in prokaryotes is too low to stimulate the processing of rCPD as compared to eukaryotes. Alternatively, if rCPD is processed in *E. coli*, the processed protein may not be purified from the bacterium. rCPD was constructed to have an N-terminal and C-terminal 6xHis tag but Western blotting with a anti-His antibody did not detect the larger cleavage product fused to the C-terminal 6xHis tag. These data suggest that purification of rCPD is primarily mediated by the N-terminal 6xHis tag and processed rCPD would not be purified from *E. coli*. However, since I did not observe a difference in the yield of rCPD verses the inactive rCPD C-S upon purification, rCPD is probably not processed in *E. coli*.

Addition of Ca^{2+}, on the other hand, inhibited both processing and GTP binding. Therefore, processing of *V. cholerae* RTX toxin could be stimulated after transitioning from the high calcium extracellular environment to the low calcium, high GTP intracellular environment of the eukaryotic cytosol. Premature cleavage of the toxin in the bacterial cytoplasm would be prevented since the *V. cholerae* RTX toxin remains unfolded until after secretion by the type I secretion system (Boardman and Satchell, 2004).

As depicted in Figure 5-12, the CPDs of the *V. cholerae* RTX toxin and another putative RTX toxin from *P. luminescens* (Duchaud et al., 2003) lie adjacent to the internal portions of the toxin that are hypothesized to contain the catalytic activity domains. In chapter 3, a model of toxin entry was proposed suggesting that the *V. cholerae* RTX toxin self-inserts into the host cell plasma membrane and translocates its catalytic region into the cytosol of the cell similarly to the *B. pertussis* AC toxin. Once inside the cell, the toxin would either remain anchored to the plasma membrane like the AC toxin or undergo proteolytic processing to release the catalytic region into

the cytosol. This study provides evidence that the *V. cholerae* RTX toxin is potentially autoprocessed between L3428 and A3429. Since even after processing at this location, the ACD and RID would be contained within a >350 kDa protein, the CPD possibly cleaves the RTX toxin at multiple sites releasing the previously identified activity domains into the cytosol.

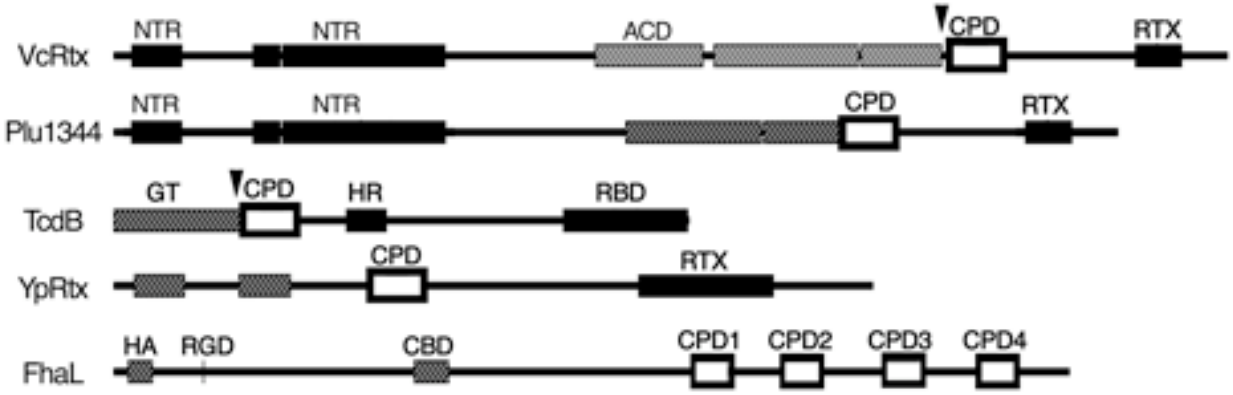

Figure 5-12: Autoprocessing by CPD is a common mechanism for processing large bacterial toxins.
Schematic representation of CPD location within large bacterial proteins. CPD is marked as an outlined open box. Black boxes represent regions predicted to be critical for toxin entry (NTR- N-terminal repeats, RTX- RTX repeats, HR- hydrophobic region, RBD- receptor binding domain). Grey hatched boxes represent known or predicted functional regions (ACD-actin cross-linking domain, GT-glucosyltransferase, HA-hemagglutinin, CBD-carbohydrate binding domain, RGD-integrin binding). Arrowheads mark cleavage sites determined experimentally.

Unfortunately, characterization of RTX holotoxin processing after translocation is hindered due to a lack of purified toxin for *in vitro* study. However, processing *in vivo* and *in vitro* has been demonstrated for a different bacterial toxin that was identified in this study to carry a CPD. *C. difficile* TcdB is known to be proteolytically processed at a Leu-Gly pair to the N-terminal side of the TcdB CPD (Figure 5-1B) after translocation across the endosomal membrane. Cleavage then releases the N-terminal glucosyltransferase domain to the cytosol where it can UDP-glucosylate the target Rho (Pfeifer et al., 2003; Rupnik et al., 2005). This process is consistent with the model hypothesized for RTX that autoprocessing by CPDs after translocation releases activity domains to the cytosol. Indeed, in 16 identified large bacterial

proteins, the CPDs are always located between putative translocation regions and catalytic or adherence regions, and are thus appropriately positioned to release activity domains from large bacterial proteins after translocation (Figure 5-12).

This model contrasts with the previous model proposed for processing of TcdB. *In vitro* studies on TcdB demonstrated that processing was stimulated by a host cell lysate and inhibited by Ca^{2+} leading the authors to conclude that TcdB processing is due to a cellular protease (Rupnik et al., 2005). However, a boiled or proteinase K treated lysate preparation was not tested to confirm that the protease was present within the lysate. Since TcdB has a CPD and previous mutagenesis studies revealed that the putative catalytic Cys and His residues within the CPD were important for TcdB cytotoxicity (Barroso et al., 1994), it seems reasonable to suggest that TcdB also undergoes GTP-stimulated autoprocessing after translocation rather than processing by a cellular protease. The CPDs in other clostridial toxins and putative *Yersinia* toxins could function in a similar manner. Therefore, GTP-stimulated autoprocessing may be a newly recognized common mechanism by which large bacterial toxins deliver catalytic domains to the cytosol of host eukaryotic cells.

In addition to the CPD-mediated cleavage representing a new mechanism for bacterial toxin delivery, the CPDs are apparently a novel cysteine protease family. The characterization of the CPD as a cysteine protease was surprising since alignment programs, including a search of the MEROPS peptidase database (Rawlings et al., 2006), did not reveal sequence similarity to known cysteine proteases. The closest relative of the CPD may be NS2 from Hepatitis C virus, a cysteine protease that remains unclassified in the MEROPS database (Rawlings and Barrett, 1997). Both CPD and NS2 catalyze autocleavage of their respective proteins. Indeed, NS2 also

cleaves between a Leu-Ala pair although the site of cleavage is to the C-terminal side of NS2 (Grakoui et al., 1993).

Comparison of CPD and NS2 revealed that the orientation and particularly the spacing of the catalytic residues are very similar suggesting a similar mechanism of catalysis. Although there are similarities between these two proteins, a mutation of Glu972 between the catalytic His952 and Cys993 within NS2 had a defect in processing of the HCV polyprotein suggesting that this residue may be required to form a catalytic triad (Grakoui et al., 1993; Hijikata et al., 1993; Wu et al., 1998). The studies of CPD determined that His3519 and Cys3568 comprise a catalytic dyad of the CPD but mutation of the putative third catalytic Glu3543 residue of RTX did not disrupt CPD activity.

Additionally, activation of CPD was achieved by addition of GTP. By contrast, the NS2/3 cleavage required ATP for *in trans* processing although ATP hydrolysis is more likely needed for activity of host cofactor Hsp90 and not for stimulation of protease activity (Waxman et al., 2001). Hsp90 is not likely involved in autoprocessing of the CPD, since addition of Hsp90 inhibitor geldanamycin had no effect on *in vitro* CPD processing (data not shown) and previous experiments have also shown that geldanamycin did not inhibit TcdB activity (Schirmer and Aktories, 2004).

In total, the inability to assign CPD to any known family and the requirement of GTP binding for CPD activity indicates that this is a novel cysteine protease that could share a mechanism of catalysis with the unclassified NS2 cysteine proteases. This common enzymatic domain is proposed to autoprocess large bacterial toxins allowing release of activity domains into the cytosol.

Chapter 6

Discussion

The goal of this study was to further characterize the mechanism of the *Vibrio cholerae* RTX toxin. In this study, three functional domains were identified and characterized within the multifunctional RTX toxin (Figure 6-1). Expression of a 47.8 kDa domain from RTX mediated the cross-linking of actin when transfected in eukaryotic cells. In chapter 4, RTX was discovered to have a second actin depolymerizing activity – inactivation of the Rho GTPases. In chapter 5, a novel cysteine protease autoprocessing domain was identified within the RTX toxin suggesting the toxin undergoes autocleavage. This domain was found to be a common domain of large bacterial toxins indicating that the autoprocessing activity observed in RTX is common among large bacterial toxins. Furthermore both cysteine residues within the RTX toxin, located in RID and CPD, were determined to be important for the activity of these domains. Overall, these studies have further advanced the characterization of the RTX mechanism of action.

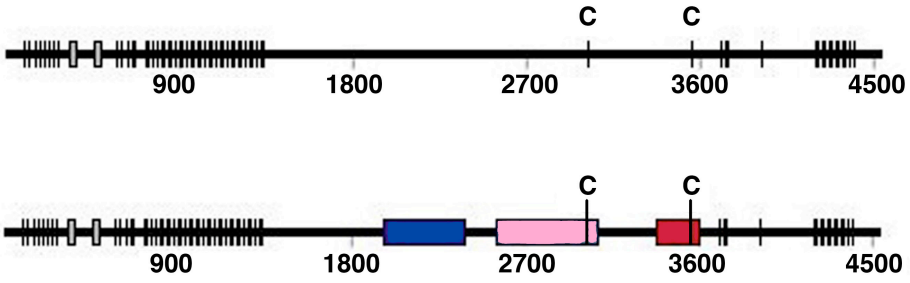

Figure 6-1: Schematic of *V. cholerae* RTX Toxin Before and After.
Three identified domains are depicted in blue – ACD, pink - RID, and red – CPD.

Identification of the Actin Cross-linking Domain (ACD) within RTX

Discovery of the ACD was a major breakthrough for the characterization of the RTX toxin. This result for the first time provided evidence that the RTX or at least a portion of the RTX needs to access the cytosol as observed by transient expression of this domain causing the covalent cross-linking of actin in the cell. The identification of this domain provided a foundation for other members of the laboratory to study this unique protein. Purification of this domain by Christina Cordero allowed the development of an *in vitro* assay to further study the cross-linking reaction. This assay revealed that the ACD does directly cross-link actin and does not activate a cellular protein to cross-link actin. Characterization of the reaction identified that the ACD required the co-factors Mg^{2+} and ATP to catalyze the cross-linking reaction. *In vivo* inhibitor studies demonstrated that G-actin, not F-actin, is the substrate of ACD (Cordero et al., 2006). Additional *in vitro* studies confirmed this data (C. Cordero, unpublished data).

A linker scanning mutagenesis project has identified regions of the ACD that are essential for cross-linking activity. Currently individual point mutations are being constructed to strengthen this data as well as identify the important catalytic residues in these regions. Further characterization of ACD will also focus on the interaction of this domain with actin and whether any of the above mutants have a defect in actin binding. Lastly, studies are currently ongoing to crystallize the ACD. Solving the crystal structure of ACD may reveal insight into the mechanism of ACD catalysis.

ACD is a novel protein that only has homology to a second copy of the domain on the *V. cholerae* chromosome contained within the ORF VC1416. An analysis of the entire genomic region surrounding VC1416 suggests this gene has been recently acquired, possibly as a mobile element similar to *E. coli Rhs* (rearrangement hot spot) elements (Lin et al., 1984). A

comparative genome alignment reveals that while homologues of thermostable carboxypeptidase I gene VC1414 and conserved hypothetical gene VC1421 are adjacent in the same relative genomic structure within *V. parahemolyticus* and *V. vulnificus*, these genes are separated in *V. cholerae* by a >10,000 bp insertion flanked by AT-rich sequences. This insertion contains 6 ORFs including the hemolysin-coregulated protein (*hcp*) gene VC1415 followed by VC1416, a fusion of genes that encode VgrG and the second copy of the ACD. Both *hcp* and *vgrG* are genes of unknown function that are components of *Rhs* elements (Wang, 1998). However, instead of a high GC% *Rhs* core gene, the remainder of the insertion encodes four hypothetical proteins and has a low GC% content (<45% G+C) compared to the flanking genomic DNA that includes other horizontally acquired elements including the CTX phage, pTLC1 and pTLC2.

Although *Rhs* elements were originally characterized by the presence of the *Rhs* core, recent evidence suggests that the more ubiquitous *vgrG* is a mobile genetic element that can lead to the acquisition of novel genes, including virulence factors such as the *Pseudomonas aeruginosa* phospholipase D gene (Wilderman et al., 2001). The VgrG family currently consists of 45 genes identified in 10 Gram-negative bacteria with putative Vgr-like genes identified in 5 more bacterial species (www.ncbi.nlm.nih.gov/COG/new/release/cow.cgi?cog=COG3501). The sequenced *V. cholerae* strain N16961 has 3 copies of *vgrG*. Previously, Wilderman *et al.* speculated on the functional significance of the genes adjacent to these *vgrG* genes and their potential involvement in horizontal transfer (Wilderman et al., 2001). Indeed, the ORF VC1416 contains a *vgrG* gene fused to the second copy of ACD. VCA0018 is 86% identical to the VgrG domain of VC1416 and is linked to the *hcp* gene VCA0017 suggesting a possible gene duplication event that did not include the ACD domain of VC1416. The third copy of VgrG,

VCA0123, is only 45% identical to the other VgrG proteins and is not linked to an *hcp* gene. Taken together, these observations suggest the RTX toxin of *V. cholerae* may have acquired the ACD by horizontal gene transfer via acquisition of VC1416 as part of an *Rhs*-like element.

After these initial observations, a recent study to identify virulence factors of non-O1/non-O139 strains associated with mild cholerae disease identified a cluster of genes on the small chromosome important for *V. cholerae* cytotoxicity towards *Dictyostelium discoideum* (Pukatzki et al., 2006). This gene cluster was previously characterized through bioinformatic analysis to be highly conserved in Gram-negative bacteria. Due to the observed homology of these genes to *Legionella pneumophila icmF,* these genes were designated the IcmF-associated homologous protein (IAHP) gene cluster (Das and Chaudhuri, 2003). Further studies of the IAHP gene cluster in the *V. cholerae* strain V52 indicated that these genes encode a secretion system distinct from type III and type IV secretion. Therefore, the authors proposed that this is a type VI secretion system. Four proteins were detected in the culture supernatant of the V52 *V. cholerae* strain dependent upon this IAHP gene cluster. These proteins included the Hcp, encoded by the ORFs VC1415 and VCA0017, VgrG-1 (VC1416), VgrG-2 (VCA0018), and VgrG-3 (VCA0123) (Pukatzki et al., 2006). Characterization of the IAHP gene cluster in *Pseudomonas aeruginosa* confirmed that these genes are a secretion apparatus. In this study, the crystal structure of Hcp revealed that 3 Hcp monomers formed a hexameric ring. The authors proposed that following secretion Hcp oligomerizes to form this ring, associates with proteins and builds a channel to transport macromolecules (Mougous et al., 2006). Therefore, Hcp may then insert into a host cell membrane to facilitate the transport of the VgrG proteins into the cell.

In the study by Pukatzki et al., the *V. cholerae* strain V52 was also cytotoxic to J774 macrophages and a deletion of the RTX and HlyA toxins did not disrupt this cytotoxicity

suggesting that VgrG-1 is responsible for the observed cytotoxicity. The authors also demonstrated that the *V. cholerae* strain N16961, the strain used in the studies presented in this thesis, was not cytotoxic to *D. discoideum* even though this strain contains the IAHP gene cluster. Since experiments indicated that these genes were tightly regulated, the authors suggested that the genes are not expressed in the N16961 strain of *V. cholerae* (Pukatzki et al., 2006). This conclusion was in agreement with the results obtained in chapter 3 reporting that a deletion of RTX and HlyA in the N16961 strain was not cytotoxic to HEp-2 cells (Figure 3-1). Even though the second copy of ACD encoded by VC1416 did not contribute to the cytotoxicity observed with the *V. cholerae* O1 strain N16961, VC1416 contributed to the observed sytotoxicity in a non-O1/non-O139 strain of *V. cholerae.*

RTX Inactivation of the Rho GTPases

The deletion of the ACD within RTX unveiled a second cell rounding activity due to depolymerization of the actin cytoskeleton. Actin depolymerization by the RTX toxin with an in-frame deletion of ACD was prevented and rapidly reversed by the constitutive activation of the Rho GTPases by the Cytotoxic Necrotizing Factor 1 (CNF1) from *E. coli*. Further characterization revealed that RTX causes the inactivation of the small Rho GTPases, Rho, Rac and Cdc42. Inactivation of the GTPase Rho by RTXΔACD was determined to be reversible and *de novo* synthesis of Rho was not required for this reversibility.

Many bacterial toxins either reversibly or irreversibly target the Rho GTPase signaling pathway through a variety of mechanisms. However, the data presented in chapter 4 suggests that RTX does not inactivate the Rho GTPases in a manner similar to other previously described common bacterial toxins. Experiments indicate that RTX does not covalently modify Rho,

proteolytically cleave Rho, or have GTPase activation activity or phosphatase activity. Due to the reversibility of this activity, I speculate that RTX is targeting the regulation of the GTPases not the GTPases directly. RTX could either be activating cellular GTPase activating proteins (GAPs) or inactivating cellular guanine exchange factors (GEFs). It is also possible that RTX does not target the Rho GTPases but rather targets the signaling pathways upstream of the Rho GTPases resulting in the inactivation of the Rho GTPases.

Phosphorylation of Rho on the Ser188 residue downregulates Rho activity and increases the association of Rho with the Rho-guanine dissociation inhibitor (Rho-GDI) (Ellerbroek et al., 2003). RTX could be functioning as a kinase to directly phosphorylate Rho. Future experiments should assess whether there is an increase in phosphorylated Rho after exposure to the RTX toxin. Also, the bacterial type III effector YopO also known as YpkA from *Yersinia spp*. is a kinase whose *in vivo* target is unknown but *in vitro* can phosphorylate actin (Juris et al., 2000). *In vivo* YopO is hypothesized to target proteins that regulate the actin cytoskeleton. Experiments have shown that YopO binds actin as well as Rho and Rac (Barz et al., 2000; Dukuzumuremyi et al., 2000; Juris et al., 2000). YopO also causes cell rounding and studies have shown that this toxin decreases the Rho-GTP levels but not to the degree observed in the presence of RTX (Dukuzumuremyi et al., 2000; Hakansson et al., 1996). Also cells exposed to YopO do not appear to have the dramatic disruption of the actin cytoskeleton and the cell morphology observed in the presence of RTX. Since the exact mechanism by which YopO causes the deploymerization of actin is not clear, I cannot rule out that RTX does not function like YopO. There is no sequence homology between RID and YopO and the observed cytotoxic effects of YopO were distinct from RTX. So I do not believe that RTX functions similarly to YopO.

However, RTX could have kinase activity either to directly phosphorylate Rho or a protein that regulates Rho.

Identification of the Rho inactivation domain (RID) was critical for future studies investigating the mechanism of GTPase inactivation. The extensive structure/function analysis of the region of RTX between the ACD and the cysteine protease domain (CPD) revealed that amino acids 2552-3099 of RTX caused cell rounding when expressed as a transgene in the cell as well as when delivered to the cell as a recombinant protein. This cell rounding corresponded to inactivation of the GTPase Rho. However, expression of amino acids 2552-2765 yielded an interesting mixed phenotype. Preliminary experiments revealed that this shorter region of RTX appears to cause cell rounding dependent upon the level of expression. Analysis of the amino acid sequence of RID revealed that one of the two cysteines residues among all of the 4545 amino acids of RTX was present. Mutation of Cys3022 on the pRID plasmid disrupted the cell rounding activity observed due to expression of RID and resulted in the mixed phenotype observed with expression of RTX amino acids 2552-2765.

Future experiments need to address whether the cell rounding observed with this mixed phenotype correlates with a decrease in the Rho-GTP levels in the cell. Expression of amino acids 2552-2765 or RID C-M could just have a defect in the ability to inactivate Rho. This defect requires increased expression of the fusion proteins to produce a similar phenotype observed with expression of RID. An alternative interpretation of this result is that RID could have two independent activities that cause cell rounding. Except expression of RTX amino acids 2804-3375 does not cause cell rounding so I do not expect that RID contains two cell rounding activities. Another interpretation is that a region of RID is responsible for localization of the domain while another is important for activity. This N-terminal portion of RID generating the

mixed phenotype could be lacking proper localization yielding a defect in activity. However, preliminary observations reveal that cells expressing amino acids 2552-2765 appear to have localization at the cell periphery as well as at the perinuclear region that co-localizes with actin. The mixed phenotype observed due to the mutation of Cys3022 within RID suggests this residue is important for activity. Cys3022 could either be important for localization or activity of RID. A third possibility is that mutation of Cys3022 is effecting the proper folding of the protein but this hypothesis is unlikely since this is a conservative mutation changing the cysteine residue to a methionine.

To further investigate the mechanism by which RID inactivates the Rho GTPases, a broad based screen will be employed in the future. A screen to identify potential binding partners of RID will provide information to design additional experiments to aid in discovery of the mechanism of this domain. Additional studies of the truncated RID constructs may also provide insight into the mechanism by which RID leads to the inactivation of the Rho GTPases. Further microscopic analysis investigating the localization of RID within the cell may identify key pathways in the cell to focus studies on.

The presence of RID in three other putative RTX toxins from *V. vulnificus, Xenorhabdus nematophila* and *bovienii* indicates these three toxins share this same activity. In fact, experiments reveal that the putative *V. vulnificus* RTX toxin also inactivates the GTPase Rho. The cysteine residue identified to be important for function is conserved in all four copies of this domain. This domain is highly conserved between the RTX toxins from *V. cholerae* and *V. vulnificus* exhibiting 87% identity. However, the conservation of this region between *V. cholerae* and *X. nematophila* and *bovienii* has 56% and 54% identity, respectively. Analysis of the sequence of the domains from *X. nematophila* and *bovienii* with RID from *V. cholerae* may

reveal regions that are highly conserved and could be important for activity assuming that all four of these domains cause the inactivation of the Rho GTPases. Since RID is conserved within these other three putative toxins, it is possible that more toxins in the future may be discovered to have this domain. Thus the *V. cholerae* RTX toxin RID may represent a novel mechanism for bacterial toxins to inactivate the Rho GTPases.

Actin Cross-linking and Rho Inactivation

As reported in chapter 4, RTX inactivation of the Rho GTPases is independent from actin cross-linking activity. However, future experiments need to focus on whether Rho GTPase inactivation is necessary for efficient RTX cross-linking of actin. As stated above, *in vivo* and *in vitro* studies have shown that G-actin is the preferred substrate for actin cross-linking (Cordero et al., 2006);C. Cordero, unpublished data). It is thus possible that RTX-induced inactivation of the Rho GTPases increases the intracellular pool of G-actin to serve as the substrate for the ACD to enhance the rate of actin cross-linking. Experiments in chapter 3 show that transient transfection of ACD can adequately cross-link actin, generating an actin ladder similar to cells incubated with the RTX toxin. Overexpression of the ACD in this experiment could possibly overcome any requirement for toxin inactivation of Rho for efficient actin cross-linking. Also the amount of RTX toxin *in vivo* is probably substantially less than the overexpressed ACD, so it may require GTPase inactivation in order to help drive the cross-linking reaction.

There is also the possibility that the RTX toxin may simply have two independent activities to disrupt the cytoskeleton and cause cell rounding reversibly and irreversibly. The RTX toxin is not the first toxin reported to have dual cell rounding activities. For example, the type III effectors ExoS and ExoT from *P. aeruginosa* have bifunctional activity: GAP and ADP-

ribosylation. These two activities act independently from each other and target different substrates (Aktories and Barbieri, 2005). In the future, studies need to investigate whether the two cell rounding activities from the RTX toxin act together or independently from each other in the context of the full-length toxin.

Discovery of a Novel Cysteine Protease Domain within RTX

Cysteine proteases are classified into seven clans representing common ancestral lineages that are further separated into over 40 different families. These proteases are organized into clans based upon similar structure, function and orientation of their catalytic dyads (Rawlings et al., 2006). The characterization of this domain as a cysteine protease was surprising since sequence alignment programs did not reveal sequence similarity to any known cysteine proteases. Furthermore, a search of the MEROPS database (http://merops.sanger.ac.uk/) did not assign the sequence of the CPD to any known cysteine protease families suggesting the *V. cholerae* RTX toxin CPD represents a new family of cysteine proteases (Rawlings et al., 2006).

In chapter 5, I determined that His3519 and Cys3568 comprise the catalytic dyad of this cysteine protease. Analysis of the seven clans of cysteine proteases revealed that the catalytic residues are generally in a Cys-His or His-Cys orientation. Since the CPD has a His-Cys orientation and is resistant to inhibition by E64, this protease could classify it among the CD, CE, or PA(C) clans (Barrett and Rawlings, 2001). However, the CPD family does not fit within the CE clan typified by the human adenovirus protease adenain since a conserved glutamine generally located 5-6 residues up from catalytic cysteine (Rawlings et al., 2006) is not found in the *V. cholerae* RTX toxin CPD or any of the other 18 members. Inclusion within the CD family typified by the caspases is also unlikely since the identified target cleavage site was a Leu-Ala

pair, not an aspartate residue (Rawlings et al., 2006). The CPD could classify within the PA(C) subclan of proteases since conserved aspartate and glutamate residues are found between the His and Cys; however the spacing between the His and Cys residues in this clan are between 77 and 131 residues (Rawlings et al., 2006), much longer than the 48 residues that separate the His and Cys in the CPD family (Figure 5-1B). As discussed in chapter 5, CPD does have some similarities to another unclassified cysteine protease NS2 from the Hepatitis C virus. Although determination of the structure would be required to fully demonstrate if CPD is related to any known protease families, information based on sequence analysis indicates that the CPD family does not classify within any of the known families of cysteine proteases.

Autoprocessing Represents a New Mechanism for Large Bacterial Toxins

This novel cysteine protease domain hypothesized to be responsible for autoprocessing of RTX was identified in 15 other large bacterial proteins. Analysis of all the copies of CPD reveal conservation of the lysine, histidine and cysteine, as shown in Appendix A, that were demonstrated in chapter 5 to be essential for the cleavage of the CPD from RTX. Therefore, I speculate that autoprocessing is a common mechanism for processing large bacterial proteins. It is interesting to note that nine of these proteins, including the *V. cholerae* RTX, are putative *Vibrio*-type RTX toxins as discussed in chapter 1 indicating this could be a conserved function of these toxins. Other toxins that contain this domain are the large clostridial glucosylating toxins, which includes the *Clostridium difficile* Toxin B (TcdB). As discussed in chapter 5, this toxin is processed in the cell releasing the N-terminal catalytic region into the cytosol of the cell. In fact, mutagenesis of the conserved cysteine and histidine decreases the cytotoxicity observed with this toxin suggesting that processing of this toxin affects the catalytic activity as hypothesized for

RTX. Future studies need to be performed to determine whether the CPD located in these toxins are responsible for autoprocessing of these large bacterial proteins.

GTP Binding Stimulates CPD Processing of RTX

The identification that GTP stimulated the CPD cleavage was not expected. The physiological concentration of GTP in a eukaryotic cell is predicted to be in the millimolar range, but I could not find the exact concentration in the literature. Due to the abundance of GTP signaling proteins at the plasma membrane of the cell, I would assume that the concentration is high in this area of the cell. Since RTX is hypothesized to enter through a self-insertion membrane translocation event, I expect CPD contained within the holotoxin will interact with GTP at this location. The experimental variability of GTP stimulated processing of CPD could indicate that another co-factor is required for efficient processing. However, GTP hydrolysis in solution could also account for the observed variability in processing. In fact, GTPγS was able to stimulate CPD processing as efficiently as lysate indicating that hydrolysis of the GTP in solution was responsible for the experimental variability. However, it is still possible that another co-factor is involved. Future studies fractionating the cell lysate would be able to identify any other potential co-factors.

Experiments indicated that Mg^{2+} enhanced processing by GTP but unexpectedly inhibited the binding of GTP. Currently, the role of Mg^{2+} in CPD processing is not understood. The inhibition experiments revealed that Mg^{2+} is not inhibiting processing like other divalent cations Ca^{2+} and Mn^{2+}. In the binding assay, it is possible that the inhibition of GTP binding observed in the presence of Mg^{2+} is because the protein was processed under these conditions. After processing, the protein could subsequently release the GTP. To investigate this hypothesis, GTP

binding studies could be performed using the CPD C-S mutation, which should be defective in processing of CPD but not GTP binding. If this experiment demonstrates no observed difference in GTP binding in the presence or absence of Mg^{2+} then GTP may be released after CPD processing explaining the unexpected result with Mg^{2+}.

Overall Model of RTX Toxin

Based upon the data presented in this study, a new speculative model for the mechanism of action of the *V. cholerae* RTX toxin can be proposed (Figure 6-2). The unfolded RTX toxin is secreted by its atypical Type I secretion system into the extracellular milieu. In this environment, it is hypothesized that the GTP stimulated processing of the RTX toxin is inhibited due to the high concentration of calcium. Experimental evidence suggests that the RTX does not enter through receptor-mediated endocytosis (Figure 3-8). Therefore, I speculate that RTX binds to an unidentified receptor on the cell surface, self-inserts into the host cell plasma membrane, and translocates the internal catalytic region of the toxin, containing the ACD and RID, into the cytosol similarly to the *Bordetella pertussis* Adenylate Cyclase toxin (Rogel and Hanski, 1992).

After translocation into the low calcium environment of the cytosol, GTP may then bind to the CPD domain of the RTX toxin to possibly stimulate the autoprocessing of the toxin. CPD potentially cleaves the toxin just once between the experimentally determined L3428 and A3429 or at multiple sites releasing individual activity domains into the cytosol to access their respective substrates. After the processing of the RTX toxin by the CPD, the RID can then interact with its unknown target to cause the reversible inactivation of the Rho GTPases and depolymerization of the actin cytoskeleton. The depolymerization of actin increases the

intracellular pool of G-actin. The ACD can then irreversibly catalyze the covalent cross-linking of this G-actin.

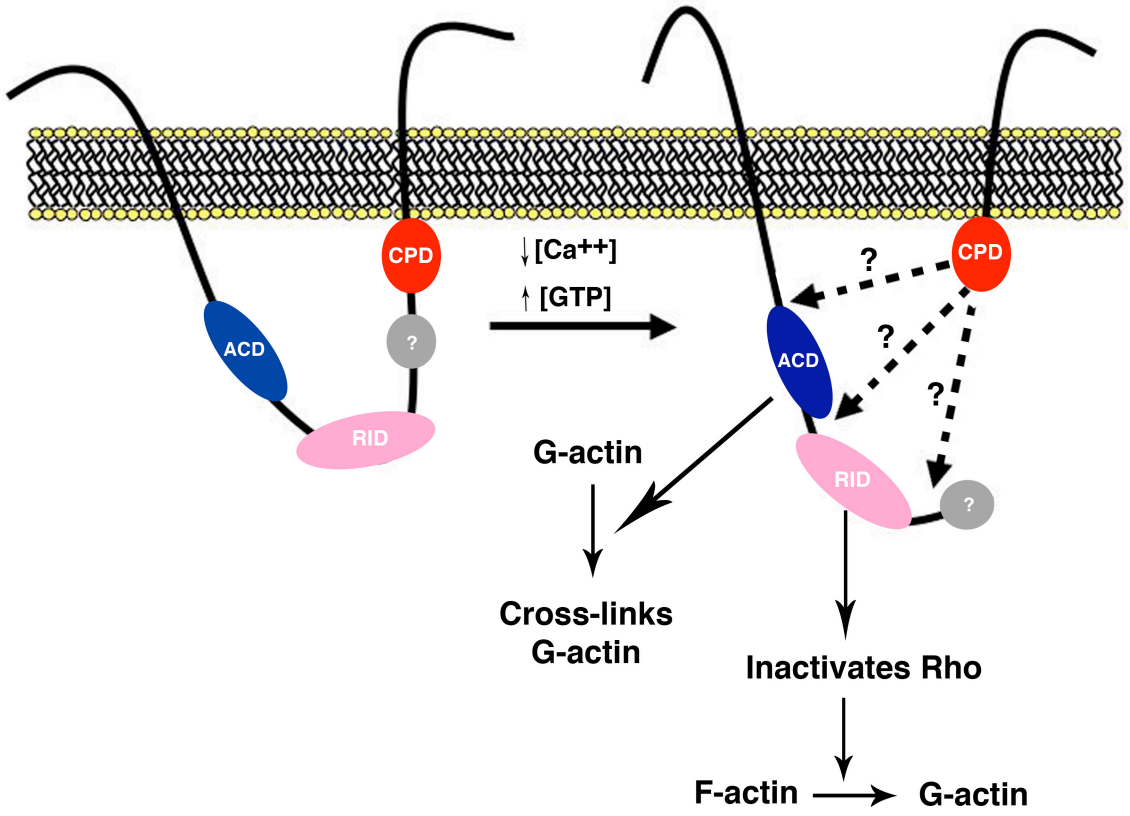

Figure 6-2: Hypothesized model of the mechanism of action of the RTX toxin.
RTX self-inserts into the host cell membrane and translocates the catalytic portion of the toxin into the cell. The low [Ca^{2+}] and high [GTP] stimulates the cleavage of RTX by the CPD. RID then inactivates the Rho GTPases to increase the intracellular pool of G-actin. The ACD then cross-links G-actin. Dashed arrows with question marks indicate other possible processing sites.

Many aspects of this proposed model for the RTX toxin need further investigation. Due to the lack of purified RTX toxin and the limitations in detecting this large toxin, experiments to determine whether the RTX does self-insert into the membrane were unsuccessful. Future efforts

need to focus on developing reagents that will help determine whether the toxin does gain entry into the cells by this mechanism.

These reagents would also allow further experiments on RTX toxin processing. Characterization of toxin processing was performed using CPD. The conclusions are based on the assumption that CPD functions in the same manner in the context of the holotoxin. At this point, processing has not been demonstrated for the full-length RTX toxin. Mutation of the catalytic cysteine within RTX does attenuate actin cross-linking activity, which I speculate was due to the lack of processing of the holotoxin. However, it is possible that this cysteine mutation affects the stability or folding of the full-length toxin leading to the observed decrease in activity. To further investigate whether full-length RTX is processed, the experiments presented in this study should be repeated using purified toxin. These experiments would also reveal whether RTX is processed once or at multiple sites within the toxin. Since even after RTX cleavage by the CPD between Leu3428 and Ala3429, the ACD and RID would still be contained within a nearly 350,000 Da protein, it seems reasonable that the CPD could cleave the RTX toxin at multiple sites releasing the activity domains independently to the cytosol. In fact, there are putative substrate recognition sequences found within the unstructured junction regions between the ACD and RID activity domains of the *V. cholerae* RTX toxin. Alternatively, additional processing could occur by signal peptidase, other host proteases, or by another currently unidentified protease activity carried within the RTX toxin following the model of cleavage of the HCV polyprotein by multiple types of proteases (Hijikata et al., 1993).

The catalytic cysteine of the CPD was shown to be required for efficient actin cross-linking activity in the context of the holotoxin. However, future studies need to investigate whether the hypothesized processing of the RTX toxin is necessary for inactivation of the Rho

GTPases. Lastly, the contribution of the Rho GTPase activity on actin cross-linking activity in the context of the holotoxin needs to be determined whether these two activities are synergistic or independent.

RTX Toxin Contribution to Pathogenesis

Although I did not present studies regarding the RTX toxin in pathogenesis, the cytotoxic activities associated with this toxin could possibly contribute to the pathogenesis of *V. cholerae* especially in the absence of cholera toxin. Previous studies demonstrated that the RTX toxin disrupts the epithelial monolayer measured *in vitro* using T84 intestinal epithelial cells. In chapter three, a preliminary experiment revealed that the deletion of the ACD within RTX abrogates the ability of the toxin to disrupt the epithelial monolayer. This result was surprising since RTX also inactivated the Rho GTPases and I expected that this activity should also disrupt the epithelial monolayer. However, this cell rounding activity appeared to be slower than actin cross-linking so therefore the disruption of the monolayer in the presence of RTXΔACD may occur at a later time point but this hypothesis needs further investigation. Overall this experiment demonstrated that RTX could lead to the disruption of the monolayer *in vivo* leading to the dissemination of the bacteria. As stated in chapter one, non-O1/non-O139 and cholera toxin negative strains of *V. cholerae* have been shown to cause bacteremia, therefore the RTX toxin could be contributing to the invasiveness of the bacteria (Crump et al., 2003; Ninin et al., 2000).

Alternatively, the *in vivo* target of RTX could be cells of the immune system. RTX has been shown previously to cause cytotoxicity in macrophages (Fullner and Mekalanos, 2000). The actin cross-linking and Rho inactivation activities of RTX would severely hinder the activity of these innate immune cells. The toxin could prevent the motility of these immune cells to the

site of infection. Also RTX would prevent phagocytosis of *V. cholerae* by these cells. The role of RTX in infection may be to dampen the immune cell response. Currently studies in the laboratory are investigating the role of RTX as well as the other two accessory toxins hemagglutinin protease and hemolysin.

Summary

Overall the results presented in this thesis have significantly contributed to the knowledge of the mechanism of the RTX toxin. Three functional domains were identified and characterized though a combination of molecular biological, cell biological and biochemical techniques. These three domains do not even represent one-third of this very large toxin indicating that the toxin may have other activities that have yet to be identified. These studies were able to circumvent the obstacle that purified RTX toxin does not exist. However, characterization of this toxin is still extremely hindered by unavailability of purified toxin. Hopefully, the future will provide the means to rectify this current problem. Purified toxin will help answer two big aspects left unanswered in our current hypothesized model – if the toxin does enter through insertion into the plasma membrane and whether it undergoes processing at multiple sites.

References

Abrami, L., Reig, N. and van der Goot, F.G. (2005) Anthrax toxin: the long and winding road that leads to the kill Trends Microbiol, 13, 72-78.

Aktories, K. and Barbieri, J.T. (2005) Bacterial cytotoxins: targeting eukaryotic switches Nat Rev Microbiol, 3, 397-410.

Akula, S.M., Naranatt, P.P., Walia, N.S., Wang, F.Z., Fegley, B. and Chandran, B. (2003) Kaposi's sarcoma-associated herpesvirus (human herpesvirus 8) infection of human fibroblast cells occurs through endocytosis J Virol, 77, 7978-7990.

Altschul, S.F., Madden, T.L., Schaffer, A.A., Zhang, J., Zhang, Z., Miller, W. and Lipman, D.J. (1997) Gapped BLAST and PSI-BLAST: a new generation of protein database search programs Nucleic Acids Res, 25, 3389-3402.

Andersen, C., Hughes, C. and Koronakis, V. (2000) Chunnel vision. Export and efflux through bacterial channel-tunnels EMBO Rep, 1, 313-318.

Anderson, B.M. and Vasini, E.C. (1970) Nonpolar effects in reactions of the sulfhydryl group of papain Biochemistry, 9, 3348-3352.

Arora, N. and Leppla, S.H. (1993) Residues 1-254 of anthrax toxin lethal factor are sufficient to cause cellular uptake of fused polypeptides J Biol Chem, 268, 3334-3341.

Arora, N. and Leppla, S.H. (1994) Fusions of anthrax toxin lethal factor with shiga toxin and diphtheria toxin enzymatic domains are toxic to mammalian cells Infect Immun, 62, 4955-4961.

Bailey, T.L. and Elkan, C. (1994) Fitting a mixture model by expectation maximization to discover motifs in bioploymers Proceedings of the Second International Conference on Intelligent Systems for Molecular Biology AAAI Press, Menlo Park, California, pp. pp. 28-36.

Bailey, T.L. and Gribskov, M. (1998) Combining evidence using p-values: application to sequence homology searches Bioinformatics, 14, 48-54.

Barrett, A.J. and Rawlings, N.D. (2001) Evolutionary lines of cysteine peptidases Biol Chem, 382, 727-733.

Barroso, L.A., Moncrief, J.S., Lyerly, D.M. and Wilkins, T.D. (1994) Mutagenesis of the Clostridium difficile toxin B gene and effect on cytotoxic activity Microb Pathog, 16, 297-303.

Barth, H., Olenik, C., Sehr, P., Schmidt, G., Aktories, K. and Meyer, D.K. (1999) Neosynthesis and activation of Rho by Escherichia coli cytotoxic necrotizing factor (CNF1) reverse cytopathic effects of ADP-ribosylated Rho J Biol Chem, 274, 27407-27414.

Barth, H., Pfeifer, G., Hofmann, F., Maier, E., Benz, R. and Aktories, K. (2001) Low pH-induced formation of ion channels by clostridium difficile toxin B in target cells J Biol Chem, 276, 10670-10676.

Barz, C., Abahji, T.N., Trulzsch, K. and Heesemann, J. (2000) The Yersinia Ser/Thr protein kinase YpkA/YopO directly interacts with the small GTPases RhoA and Rac-1 FEBS Lett, 482, 139-143.

Bayer, N., Schober, D, Prchla, E, Murphy, R, Blaas, D, Fuchs, R. (1998) Effect of Bafilomycin A1 and Nocodazole on Endocytic Transport in HeLa Cells: Implications for Viral Uncoating and Infection. J. Virol., 72, 9645-9655.

Beitz, E. (2000) TEXshade: shading and labeling of multiple sequence alignments using LATEX2 epsilon Bioinformatics, 16, 135-139.

Bhattacharya, M.K., Dutta, D., Bhattacharya, S.K., Deb, A., Mukhopadhyay, A.K., Nair, G.B., Shimada, T., Takeda, Y., Chowdhury, A. and Mahalanabis, D. (1998) Association of a disease approximating cholera caused by Vibrio cholerae of serogroups other than O1 and O139 Epidemiol Infect, 120, 1-5.

Bina, J., Zhu, J., Dziejman, M., Faruque, S., Calderwood, S. and Mekalanos, J. (2003) ToxR regulon of Vibrio cholerae and its expression in vibrios shed by cholera patients Proc Natl Acad Sci U S A, 100, 2801-2806.

Black, D.S. and Bliska, J.B. (2000) The RhoGAP activity of the Yersinia pseudotuberculosis cytotoxin YopE is required for antiphagocytic function and virulence Mol Microbiol, 37, 515-527.

Boardman, B.K. and Satchell, K.J. (2004) Vibrio cholerae strains with mutations in an atypical type I secretion system accumulate RTX toxin intracellularly J Bacteriol, 186, 8137-8143.

Bradley, K.A., Mogridge, J., Mourez, M., Collier, R.J. and Young, J.A. (2001) Identification of the cellular receptor for anthrax toxin Nature, 414, 225-229.

Braga, V.M., Machesky, L.M., Hall, A. and Hotchin, N.A. (1997) The small GTPases Rho and Rac are required for the establishment of cadherin-dependent cell-cell contacts J Cell Biol, 137, 1421-1431.

Cassel, D. and Selinger, Z. (1977) Mechanism of adenylate cyclase activation by cholera toxin: inhibition of GTP hydrolysis at the regulatory site Proc Natl Acad Sci U S A, 74, 3307-3311.

CDC (2005) Vibrio Illnesses After Hurricane Katrina---Multiple States, August-September 2005 MMWR US Department of Health and Human Services, Atlanta, GA.

Chardin, P., Boquet, P., Madaule, P., Popoff, M.R., Rubin, E.J. and Gill, D.M. (1989) The mammalian G protein rhoC is ADP-ribosylated by Clostridium botulinum exoenzyme C3 and affects actin microfilaments in Vero cells Embo J, 8, 1087-1092.

Chow, K.H., Ng, T.K., Yuen, K.Y. and Yam, W.C. (2001) Detection of RTX toxin gene in Vibrio cholerae by PCR J Clin Microbiol, 39, 2594-2597.

Coelho, A., Andrade, J.R., Vicente, A.C. and Dirita, V.J. (2000) Cytotoxic cell vacuolating activity from Vibrio cholerae hemolysin Infect Immun, 68, 1700-1705.

Cordero, C.L., Kudryashov, D.S., Reisler, E. and and Satchell, K.J. (2006) The Actin Cross-linking Domain of the Vibrio cholerae RTX Toxin Directly Catalyzes the Covalent Cross-linking of Actin J. Biol. Chem., 281, 32366-32374.

Crump, J.A., Bopp, C.A., Greene, K.D., Kubota, K.A., Middendorf, R.L., Wells, J.G. and Mintz, E.D. (2003) Toxigenic Vibrio cholerae serogroup O141-associated cholera-like diarrhea and bloodstream infection in the United States J Infect Dis, 187, 866-868.

Dalsgaard, A., Serichantalergs, O., Forslund, A., Lin, W., Mekalanos, J., Mintz, E., Shimada, T. and Wells, J.G. (2001) Clinical and environmental isolates of Vibrio cholerae serogroup O141 carry the CTX phage and the genes encoding the toxin-coregulated pili J Clin Microbiol, 39, 4086-4092.

Das, S. and Chaudhuri, K. (2003) Identification of a unique IAHP (IcmF associated homologous proteins) cluster in Vibrio cholerae and other proteobacteria through in silico analysis In Silico Biol, 3, 287-300.

Dhakal, B.K., Lee, W., Kim, Y.R., Choy, H.E., Ahnn, J. and Rhee, J.H. (2006) Caenorhabditis elegans as a simple model host for Vibrio vulnificus infection Biochem Biophys Res Commun, 346, 751-757.

Duchaud, E., et al. (2003) The genome sequence of the entomopathogenic bacterium Photorhabdus luminescens Nat Biotechnol, 21, 1307-1313.

Dukuzumuremyi, J.M., Rosqvist, R., Hallberg, B., Akerstrom, B., Wolf-Watz, H. and Schesser, K. (2000) The Yersinia protein kinase A is a host factor inducible RhoA/Rac-binding virulence factor J Biol Chem, 275, 35281-35290.

Ellerbroek, S.M., Wennerberg, K. and Burridge, K. (2003) Serine phosphorylation negatively regulates RhoA in vivo J Biol Chem, 278, 19023-19031.

Elliott, J.L., Mogridge, J. and Collier, R.J. (2000) A quantitative study of the interactions of Bacillus anthracis edema factor and lethal factor with activated protective antigen Biochemistry, 39, 6706-6713.

Etienne-Manneville, S. and Hall, A. (2002) Rho GTPases in cell biology Nature, 420, 629-635.

Falnes, P.O. and Sandvig, K. (2000) Penetration of protein toxins into cells Curr Opin Cell Biol, 12, 407-413.

Faruque, S.M., Chowdhury, N., Kamruzzaman, M., Dziejman, M., Rahman, M.H., Sack, D.A., Nair, G.B. and Mekalanos, J.J. (2004) Genetic diversity and virulence potential of environmental Vibrio cholerae population in a cholera-endemic area Proc Natl Acad Sci U S A, 101, 2123-2128.

Faruque, S.M. and Mekalanos, J.J. (2003) Pathogenicity islands and phages in Vibrio cholerae evolution Trends Microbiol, 11, 505-510.

Felsenstein, J. (1989) PHYLIP -- Phylogeny Inference Package.

Field, M., Fromm, D., al-Awqati, Q. and Greenough, W.B., 3rd (1972) Effect of cholera enterotoxin on ion transport across isolated ileal mucosa J Clin Invest, 51, 796-804.

Figueroa-Arredondo, P., Heuser, J.E., Akopyants, N.S., Morisaki, J.H., Giono-Cerezo, S., Enriquez-Rincon, F. and Berg, D.E. (2001) Cell vacuolation caused by Vibrio cholerae hemolysin Infect Immun, 69, 1613-1624.

Fiorentini, C., Donelli, G., Matarrese, P., Fabbri, A., Paradisi, S. and Boquet, P. (1995) Escherichia coli cytotoxic necrotizing factor 1: evidence for induction of actin assembly by constitutive activation of the p21 Rho GTPase Infect Immun, 63, 3936-3944.

Fiorentini, C., Fabbri, A., Flatau, G., Donelli, G., Matarrese, P., Lemichez, E., Falzano, L. and Boquet, P. (1997) Escherichia coli cytotoxic necrotizing factor 1 (CNF1), a toxin that activates the Rho GTPase J Biol Chem, 272, 19532-19537.

Florin, I. and Thelestam, M. (1983) Internalization of Clostridium difficile cytotoxin into cultured human lung fibroblasts Biochim Biophys Acta, 763, 383-392.

Florin, I. and Thelestam, M. (1986) Lysosomal involvement in cellular intoxication with Clostridium difficile toxin B Microb Pathog, 1, 373-385.

Fu, Y. and Galan, J.E. (1999) A salmonella protein antagonizes Rac-1 and Cdc42 to mediate host-cell recovery after bacterial invasion Nature, 401, 293-297.

Fullner, K.J., Boucher, J.C., Hanes, M.A., Haines, G.K., 3rd, Meehan, B.M., Walchle, C., Sansonetti, P.J. and Mekalanos, J.J. (2002) The contribution of accessory toxins of Vibrio cholerae O1 El Tor to the proinflammatory response in a murine pulmonary cholera model J Exp Med, 195, 1455-1462.

Fullner, K.J., Lencer, W.I. and Mekalanos, J.J. (2001) Vibrio cholerae-induced cellular responses of polarized T84 intestinal epithelial cells are dependent on production of cholera toxin and the RTX toxin Infect Immun, 69, 6310-6317.

Fullner, K.J. and Mekalanos, J.J. (1999) Genetic characterization of a new type IV-A pilus gene cluster found in both classical and El Tor biotypes of Vibrio cholerae Infect Immun, 67, 1393-1404.

Fullner, K.J. and Mekalanos, J.J. (2000) In vivo covalent cross-linking of cellular actin by the Vibrio cholerae RTX toxin Embo J, 19, 5315-5323.

Gasteiger, E., Hoogland, C., Gattiker, A., Duvaud, S., Wilkins, M.R., Appel, R.D. and Bairoch, A. (2005) Protein Identification and Analysis Tools on the ExPASy Server In Walker, J.M. (ed.), The Proteomics Protocols Handbook Humana Press, pp. pp. 571-607.

Goehring, U.M., Schmidt, G., Pederson, K.J., Aktories, K. and Barbieri, J.T. (1999) The N-terminal domain of Pseudomonas aeruginosa exoenzyme S is a GTPase-activating protein for Rho GTPases J Biol Chem, 274, 36369-36372.

Gordon, V.M., Leppla, S.H. and Hewlett, E.L. (1988) Inhibitors of receptor-mediated endocytosis block the entry of Bacillus anthracis adenylate cyclase toxin but not that of Bordetella pertussis adenylate cyclase toxin Infect Immun, 56, 1066-1069.

Grakoui, A., McCourt, D.W., Wychowski, C., Feinstone, S.M. and Rice, C.M. (1993) A second hepatitis C virus-encoded proteinase Proc Natl Acad Sci U S A, 90, 10583-10587.

Guan, K.L. and Dixon, J.E. (1990) Protein tyrosine phosphatase activity of an essential virulence determinant in Yersinia Science, 249, 553-556.

Gulig, P.A., Bourdage, K.L. and Starks, A.M. (2005) Molecular Pathogenesis of Vibrio vulnificus J Microbiol, 43 Spec No, 118-131.

Hakansson, S., Galyov, E.E., Rosqvist, R. and Wolf-Watz, H. (1996) The Yersinia YpkA Ser/Thr kinase is translocated and subsequently targeted to the inner surface of the HeLa cell plasma membrane Mol Microbiol, 20, 593-603.

Hall, A. and Nobes, C.D. (2000) Rho GTPases: molecular switches that control the organization and dynamics of the actin cytoskeleton Philos Trans R Soc Lond B Biol Sci, 355, 965-970.

Hanada, K., Tamai,M., Yamagishi,M., Ohmura,S., Sawada,J. and Tanaka,I. (1978) Isolation and chracterization of E-64, a new thiol protease inhibitor. Agric. Biol. Chem., 42, 523-528.

Hardt, W.D., Chen, L.M., Schuebel, K.E., Bustelo, X.R. and Galan, J.E. (1998) S. typhimurium encodes an activator of Rho GTPases that induces membrane ruffling and nuclear responses in host cells Cell, 93, 815-826.

Hase, C.C. and Finkelstein, R.A. (1993) Bacterial extracellular zinc-containing metalloproteases Microbiol Rev, 57, 823-837.

Henderson, I.R., Navarro-Garcia, F., Desvaux, M., Fernandez, R.C. and Ala'Aldeen, D. (2004) Type V protein secretion pathway: the autotransporter story Microbiol Mol Biol Rev, 68, 692-744.

Herrington, D.A., Hall, R.H., Losonsky, G., Mekalanos, J.J., Taylor, R.K. and Levine, M.M. (1988) Toxin, toxin-coregulated pili, and the toxR regulon are essential for Vibrio cholerae pathogenesis in humans J Exp Med, 168, 1487-1492.

Hijikata, M., Mizushima, H., Akagi, T., Mori, S., Kakiuchi, N., Kato, N., Tanaka, T., Kimura, K. and Shimotohno, K. (1993) Two distinct proteinase activities required for the processing of a putative nonstructural precursor protein of hepatitis C virus J Virol, 67, 4665-4675.

Hirst, T. (1999) Cholera Toxin and Escherichia coli heat-labile enterotoxin In Alouf JE, F., JH (ed.), The comprehensive sourcebook of bacterial protein toxins, 2nd edition Academic Press, London, pp. 104-129.

Hisatsune, K., Kondo, S., Isshiki, Y., Iguchi, T., Kawamata, Y. and Shimada, T. (1993) O-antigenic lipopolysaccharide of Vibrio cholerae O139 Bengal, a new epidemic strain for recent cholera in the Indian subcontinent Biochem Biophys Res Commun, 196, 1309-1315.

Hlady, W.G. and Klontz, K.C. (1996) The epidemiology of Vibrio infections in Florida, 1981-1993 J Infect Dis, 173, 1176-1183.

Hofmann, F., Busch, C., Prepens, U., Just, I. and Aktories, K. (1997) Localization of the glucosyltransferase activity of Clostridium difficile toxin B to the N-terminal part of the holotoxin J Biol Chem, 272, 11074-11078.

Horiguchi, Y., Inoue, N., Masuda, M., Kashimoto, T., Katahira, J., Sugimoto, N. and Matsuda, M. (1997) Bordetella bronchiseptica dermonecrotizing toxin induces reorganization of actin stress fibers through deamidation of Gln-63 of the GTP-binding protein Rho Proc Natl Acad Sci U S A, 94, 11623-11626.

Juris, S.J., Rudolph, A.E., Huddler, D., Orth, K. and Dixon, J.E. (2000) A distinctive role for the Yersinia protein kinase: actin binding, kinase activation, and cytoskeleton disruption Proc Natl Acad Sci U S A, 97, 9431-9436.

Just, I., Selzer, J., Wilm, M., von Eichel-Streiber, C., Mann, M. and Aktories, K. (1995a) Glucosylation of Rho proteins by Clostridium difficile toxin B Nature, 375, 500-503.

Just, I., Wilm, M., Selzer, J., Rex, G., von Eichel-Streiber, C., Mann, M. and Aktories, K. (1995b) The enterotoxin from Clostridium difficile (ToxA) monoglucosylates the Rho proteins J Biol Chem, 270, 13932-13936.

Kaper , J., Morris, JG, Levine, MM (1995) Cholera Clinical Microbiology Reviews, 8, 48-86.

Kirn, T.J., Bose, N. and Taylor, R.K. (2003) Secretion of a soluble colonization factor by the TCP type 4 pilus biogenesis pathway in Vibrio cholerae Mol Microbiol, 49, 81-92.

Kirn, T.J., Lafferty, M.J., Sandoe, C.M. and Taylor, R.K. (2000) Delineation of pilin domains required for bacterial association into microcolonies and intestinal colonization by Vibrio cholerae Mol Microbiol, 35, 896-910.

Koehler, T.M. and Collier, R.J. (1991) Anthrax toxin protective antigen: low-pH-induced hydrophobicity and channel formation in liposomes Mol Microbiol, 5, 1501-1506.

Kovach, M.E., Shaffer, M.D. and Peterson, K.M. (1996) A putative integrase gene defines the distal end of a large cluster of ToxR-regulated colonization genes in Vibrio cholerae Microbiology, 142 (Pt 8), 2165-2174.

Krall, R., Schmidt, G., Aktories, K. and Barbieri, J.T. (2000) Pseudomonas aeruginosa ExoT is a Rho GTPase-activating protein Infect Immun, 68, 6066-6068.

Krall, R., Sun, J., Pederson, K.J. and Barbieri, J.T. (2002) In vivo rho GTPase-activating protein activity of Pseudomonas aeruginosa cytotoxin ExoS Infect Immun, 70, 360-367.

Lerm, M., Selzer, J., Hoffmeyer, A., Rapp, U.R., Aktories, K. and Schmidt, G. (1999) Deamidation of Cdc42 and Rac by Escherichia coli cytotoxic necrotizing factor 1: activation of c-Jun N-terminal kinase in HeLa cells Infect Immun, 67, 496-503.

Levine, M.M., Black, R.E., Clements, M.L., Cisneros, L., Nalin, D.R. and Young, C.R. (1981) Duration of infection-derived immunity to cholera J Infect Dis, 143, 818-820.

Levine, M.M., Kaper, J.B., Herrington, D., Losonsky, G., Morris, J.G., Clements, M.L., Black, R.E., Tall, B. and Hall, R. (1988) Volunteer studies of deletion mutants of Vibrio cholerae O1 prepared by recombinant techniques Infect Immun, 56, 161-167.

Levine, M.M., Nalin, D.R., Craig, J.P., Hoover, D., Bergquist, E.J., Waterman, D., Holley, H.P., Hornick, R.B., Pierce, N.P. and Libonati, J.P. (1979) Immunity of cholera in man: relative role of antibacterial versus antitoxic immunity Trans R Soc Trop Med Hyg, 73, 3-9.

Lin, R.J., Capage, M. and Hill, C.W. (1984) A repetitive DNA sequence, rhs, responsible for duplications within the Escherichia coli K-12 chromosome J Mol Biol, 177, 1-18.

Lin, W., Fullner, K.J., Clayton, R., Sexton, J.A., Rogers, M.B., Calia, K.E., Calderwood, S.B., Fraser, C. and Mekalanos, J.J. (1999) Identification of a vibrio cholerae RTX toxin gene cluster that is tightly linked to the cholera toxin prophage Proc Natl Acad Sci U S A, 96, 1071-1076.

Mekalanos, J.J. (1983) Duplication and amplification of toxin genes in Vibrio cholerae Cell, 35, 253-263.

Metcalf, W.W., Jiang, W., Daniels, L.L., Kim, S.K., Haldimann, A. and Wanner, B.L. (1996) Conditionally replicative and conjugative plasmids carrying lacZ alpha for cloning, mutagenesis, and allele replacement in bacteria Plasmid, 35, 1-13.

Mills, M., Meysick, K.C. and O'Brien, A.D. (2000) Cytotoxic necrotizing factor type 1 of uropathogenic Escherichia coli kills cultured human uroepithelial 5637 cells by an apoptotic mechanism Infect Immun, 68, 5869-5880.

Milne, J.C., Blanke, S.R., Hanna, P.C. and Collier, R.J. (1995) Protective antigen-binding domain of anthrax lethal factor mediates translocation of a heterologous protein fused to its amino- or carboxy-terminus Mol Microbiol, 15, 661-666.

Milne, J.C., Furlong, D., Hanna, P.C., Wall, J.S. and Collier, R.J. (1994) Anthrax protective antigen forms oligomers during intoxication of mammalian cells J Biol Chem, 269, 20607-20612.

Mitra, R., Figueroa, P., Mukhopadhyay, A.K., Shimada, T., Takeda, Y., Berg, D.E. and Nair, G.B. (2000) Cell vacuolation, a manifestation of the El tor hemolysin of Vibrio cholerae Infect Immun, 68, 1928-1933.

Mogridge, J., Cunningham, K. and Collier, R.J. (2002) Stoichiometry of anthrax toxin complexes Biochemistry, 41, 1079-1082.

Molloy, S.S., Bresnahan, P.A., Leppla, S.H., Klimpel, K.R. and Thomas, G. (1992) Human furin is a calcium-dependent serine endoprotease that recognizes the sequence Arg-X-X-Arg and efficiently cleaves anthrax toxin protective antigen J Biol Chem, 267, 16396-16402.

Moon, S.Y. and Zheng, Y. (2003) Rho GTPase-activating proteins in cell regulation Trends Cell Biol, 13, 13-22.

Morris, J.G., Jr. (2003) Cholera and other types of vibriosis: a story of human pandemics and oysters on the half shell Clin Infect Dis, 37, 272-280.

Mosley, W.H., Aziz, K.M., Mizanur Rahman, A.S., Alauddin Chowdhury, A.K., Ahmed, A. and Fahimuddin, M. (1972) Report of the 1966-67 cholera vaccine trial in rural East Pakistan Bull World Health Organ, 47, 229-238.

Moss, J. and Vaughan, M. (1977) Mechanism of action of choleragen. Evidence for ADP-ribosyltransferase activity with arginine as an acceptor J Biol Chem, 252, 2455-2457.

Mougous, J.D., Cuff, M.E., Raunser, S., Shen, A., Zhou, M., Gifford, C.A., Goodman, A.L., Joachimiak, G., Ordonez, C.L., Lory, S., Walz, T., Joachimiak, A. and Mekalanos, J.J. (2006) A virulence locus of Pseudomonas aeruginosa encodes a protein secretion apparatus Science, 312, 1526-1530.

Musher, D.M. (1989) Cutaneous manifestations of bacterial sepsis Hosp Pract (Off Ed), 24, 71-75, 80-72, 92 passim.

Ninin, E., Caroff, N., El Kouri, D., Espaze, E., Richet, H., Quilici, M.L. and Fournier, J.M. (2000) Nontoxigenic vibrio Cholerae O1 bacteremia: case report and review Eur J Clin Microbiol Infect Dis, 19, 489-491.

Nobes, C.D. and Hall, A. (1995) Rho, rac, and cdc42 GTPases regulate the assembly of multimolecular focal complexes associated with actin stress fibers, lamellipodia, and filopodia Cell, 81, 53-62.

Nusrat, A., Giry, M., Turner, J.R., Colgan, S.P., Parkos, C.A., Carnes, D., Lemichez, E., Boquet, P. and Madara, J.L. (1995) Rho protein regulates tight junctions and perijunctional actin organization in polarized epithelia Proc Natl Acad Sci U S A, 92, 10629-10633.

Olnes, S., Wesche, J , Falnes, PO (2000) Uptake of protein toxins acting inside cells. In K Aktories, I.J. (ed.), Bacterial Protein Toxins. Volume 145, Handbook of Experimental Pharmacology. Springer-Verlag, New York, pp. 45-66.

Persson, C., Carballeira, N., Wolf-Watz, H. and Fallman, M. (1997) The PTPase YopH inhibits uptake of Yersinia, tyrosine phosphorylation of p130Cas and FAK, and the associated accumulation of these proteins in peripheral focal adhesions Embo J, 16, 2307-2318.

Pfeifer, G., Schirmer, J., Leemhuis, J., Busch, C., Meyer, D.K., Aktories, K. and Barth, H. (2003) Cellular uptake of Clostridium difficile toxin B. Translocation of the N-terminal catalytic domain into the cytosol of eukaryotic cells J Biol Chem, 278, 44535-44541.

Pukatzki, S., Ma, A.T., Sturtevant, D., Krastins, B., Sarracino, D., Nelson, W.C., Heidelberg, J.F. and Mekalanos, J.J. (2006) Identification of a conserved bacterial protein secretion system in Vibrio cholerae using the Dictyostelium host model system Proc Natl Acad Sci U S A, 103, 1528-1533.

Ramamurthy, T., Garg, S., Sharma, R., Bhattacharya, S.K., Nair, G.B., Shimada, T., Takeda, T., Karasawa, T., Kurazano, H., Pal, A. and et al. (1993) Emergence of novel strain of Vibrio cholerae with epidemic potential in southern and eastern India Lancet, 341, 703-704.

Rawlings, N.D. and Barrett, A.J. (1994) Families of cysteine peptidases Methods Enzymol, 244, 461-486.

Rawlings, N.D. and Barrett, A.J. (1997) In Hopsuhavu, V.K., Jarvinen, M. and Kirschke, H. (ed.), Proteolysis in Cell Functions IOS Press, pp. 13-21.

Rawlings, N.D., Morton, F.R. and Barrett, A.J. (2006) MEROPS: the peptidase database Nucleic Acids Res, 34, D270-272.

Ren, X.D., Kiosses, W.B. and Schwartz, M.A. (1999) Regulation of the small GTP-binding protein Rho by cell adhesion and the cytoskeleton Embo J, 18, 578-585.

Ridley, A.J. and Hall, A. (1992) The small GTP-binding protein rho regulates the assembly of focal adhesions and actin stress fibers in response to growth factors Cell, 70, 389-399.

Ridley, A.J., Paterson, H.F., Johnston, C.L., Diekmann, D. and Hall, A. (1992) The small GTP-binding protein rac regulates growth factor-induced membrane ruffling Cell, 70, 401-410.

Rodal, S.K., Skretting, G., Garred, O., Vilhardt, F., van Deurs, B. and Sandvig, K. (1999) Extraction of cholesterol with methyl-beta-cyclodextrin perturbs formation of clathrin-coated endocytic vesicles Mol Biol Cell, 10, 961-974.

Rogel, A. and Hanski, E. (1992) Distinct steps in the penetration of adenylate cyclase toxin of Bordetella pertussis into sheep erythrocytes. Translocation of the toxin across the membrane J Biol Chem, 267, 22599-22605.

Rossman, K.L., Der, C.J. and Sondek, J. (2005) GEF means go: turning on RHO GTPases with guanine nucleotide-exchange factors Nat Rev Mol Cell Biol, 6, 167-180.

Rupnik, M., Pabst, S., von Eichel-Streiber, C., Urlaub, H. and Soling, H.D. (2005) Characterization of the cleavage site and function of resulting cleavage fragments after limited proteolysis of Clostridium difficile toxin B (TcdB) by host cells Microbiology, 151, 199-208.

Sack, D.A., Sack, R.B., Nair, G.B. and Siddique, A.K. (2004) Cholera Lancet, 363, 223-233.

Saraste, M., Sibbald, P.R. and Wittinghofer, A. (1990) The P-loop--a common motif in ATP- and GTP-binding proteins Trends Biochem Sci, 15, 430-434.

Sasaki, T., Kishi, M., Saito, M., Tanaka, T., Higuchi, N., Kominami, E., Katunuma, N. and Murachi, T. (1990) Inhibitory effect of di- and tripeptidyl aldehydes on calpains and cathepsins J Enzyme Inhib, 3, 195-201.

Schirmer, J. and Aktories, K. (2004) Large clostridial cytotoxins: cellular biology of Rho/Ras-glucosylating toxins Biochim Biophys Acta, 1673, 66-74.

Schmidt, G., Sehr, P., Wilm, M., Selzer, J., Mann, M. and Aktories, K. (1997) Gln 63 of Rho is deamidated by Escherichia coli cytotoxic necrotizing factor-1 Nature, 387, 725-729.

Schoenwaelder, S.M. and Burridge, K. (1999) Bidirectional signaling between the cytoskeleton and integrins Curr Opin Cell Biol, 11, 274-286.

Sehr, P., Joseph, G., Genth, H., Just, I., Pick, E. and Aktories, K. (1998) Glucosylation and ADP ribosylation of rho proteins: effects on nucleotide binding, GTPase activity, and effector coupling Biochemistry, 37, 5296-5304.

Self, A.J. and Hall, A. (1995) Measurement of intrinsic nucleotide exchange and GTP hydrolysis rates Methods Enzymol, 256, 67-76.

Shao, F., Merritt, P.M., Bao, Z., Innes, R.W. and Dixon, J.E. (2002) A Yersinia effector and a Pseudomonas avirulence protein define a family of cysteine proteases functioning in bacterial pathogenesis Cell, 109, 575-588.

Sharma, C., Thungapathra, M., Ghosh, A., Mukhopadhyay, A.K., Basu, A., Mitra, R., Basu, I., Bhattacharya, S.K., Shimada, T., Ramamurthy, T., Takeda, T., Yamasaki, S., Takeda, Y. and Nair, G.B. (1998) Molecular analysis of non-O1, non-O139 Vibrio cholerae associated with an unusual upsurge in the incidence of cholera-like disease in Calcutta, India J Clin Microbiol, 36, 756-763.

Sieczkarski, S.B. and Whittaker, G.R. (2002) Dissecting virus entry via endocytosis J Gen Virol, 83, 1535-1545.

Silva, T.M., Schleupner, M.A., Tacket, C.O., Steiner, T.S., Kaper, J.B., Edelman, R. and Guerrant, R. (1996) New evidence for an inflammatory component in diarrhea caused by selected new, live attenuated cholera vaccines and by El Tor and Q139 Vibrio cholerae Infect Immun, 64, 2362-2364.

Sorg, I., Goehring, U.M., Aktories, K. and Schmidt, G. (2001) Recombinant Yersinia YopT leads to uncoupling of RhoA-effector interaction Infect Immun, 69, 7535-7543.

Speelman, P., Butler, T., Kabir, I., Ali, A. and Banwell, J. (1986) Colonic dysfunction during cholera infection Gastroenterology, 91, 1164-1170.

Spyres, L.M., Qa'Dan, M., Meader, A., Tomasek, J.J., Howard, E.W. and Ballard, J.D. (2001) Cytosolic delivery and characterization of the TcdB glucosylating domain by using a heterologous protein fusion Infect Immun, 69, 599-601.

Stender, S., Friebel, A., Linder, S., Rohde, M., Mirold, S. and Hardt, W.D. (2000) Identification of SopE2 from Salmonella typhimurium, a conserved guanine nucleotide exchange factor for Cdc42 of the host cell Mol Microbiol, 36, 1206-1221.

Stols, L., Gu, M., Dieckman, L., Raffen, R., Collart, F.R. and Donnelly, M.I. (2002) A new vector for high-throughput, ligation-independent cloning encoding a tobacco etch virus protease cleavage site Protein Expr Purif, 25, 8-15.

Svennerholm, L. (1976) Interaction of cholera toxin and ganglioside G(M1) Adv Exp Med Biol, 71, 191-204.

Swerdlow, D.L. and Ries, A.A. (1993) Vibrio cholerae non-O1--the eighth pandemic? Lancet, 342, 382-383.

Taylor, R.K., Miller, V.L., Furlong, D.B. and Mekalanos, J.J. (1987) Use of phoA gene fusions to identify a pilus colonization factor coordinately regulated with cholera toxin Proc Natl Acad Sci U S A, 84, 2833-2837.

Thompson, J.D., Higgins, D.G. and Gibson, T.J. (1994) CLUSTAL W: improving the sensitivity of progressive multiple sequence alignment through sequence weighting, position-specific gap penalties and weight matrix choice Nucleic Acids Res, 22, 4673-4680.

Vicente-Manzanares, M. and Sanchez-Madrid, F. (2004) Role of the cytoskeleton during leukocyte responses Nat Rev Immunol, 4, 110-122.

Voth, D.E. and Ballard, J.D. (2005) Clostridium difficile toxins: mechanism of action and role in disease Clin Microbiol Rev, 18, 247-263.

Waldor, M.K. and Mekalanos, J.J. (1996) Lysogenic conversion by a filamentous phage encoding cholera toxin Science, 272, 1910-1914.

Wang, Y., Zhao, S, Hill CW. (1998) Rhs elements comprise three subfamiilies which diverged prior to acquisition by Escherichia coli. J. Bacteriol., 180.

Waxman, L., Whitney, M., Pollok, B.A., Kuo, L.C. and Darke, P.L. (2001) Host cell factor requirement for hepatitis C virus enzyme maturation Proc Natl Acad Sci U S A, 98, 13931-13935.

Welch, R. (2001) RTX toxin structure and function: a story of numerous anomalies and few analogies in toxin Biology. Curr Topics Microbiol. Immunol., 88, 137-162.

Whitaker, J.R. and Perez-Villase nor, J. (1968) Chemical modification of papain. I. Reaction with the chloromethyl ketones of phenylalanine and lysine and with phenylmethyl-sulfonyl fluoride Arch Biochem Biophys, 124, 70-78.

WHO (2006) Cholera 2005 Weekly epidemiological record, Vol 81, pp. 297-308.

Wilderman, P.J., Vasil, A.I., Johnson, Z. and Vasil, M.L. (2001) Genetic and biochemical analyses of a eukaryotic-like phospholipase D of Pseudomonas aeruginosa suggest horizontal acquisition and a role for persistence in a chronic pulmonary infection model Mol Microbiol, 39, 291-303.

Wright, A.C., Simpson, L.M., Oliver, J.D. and Morris, J.G., Jr. (1990) Phenotypic evaluation of acapsular transposon mutants of Vibrio vulnificus Infect Immun, 58, 1769-1773.

Wu, Z., Nybom, P. and Magnusson, K.E. (2000) Distinct effects of Vibrio cholerae haemagglutinin/protease on the structure and localization of the tight junction-associated proteins occludin and ZO-1 Cell Microbiol, 2, 11-17.

Wu, Z., Yao, N., Le, H.V. and Weber, P.C. (1998) Mechanism of autoproteolysis at the NS2-NS3 junction of the hepatitis C virus polyprotein Trends Biochem Sci, 23, 92-94.

Xu, Q., Dziejman, M. and Mekalanos, J.J. (2003) Determination of the transcriptome of Vibrio cholerae during intraintestinal growth and midexponential phase in vitro Proc Natl Acad Sci U S A, 100, 1286-1291.

Yoshimori, T., Yamamato, A, Moriyami, Y, Futai, M, Tashiro, Y. (1991) Bafilomyin A1, a Specific Inhibitor of Vacuolar-type H+ ATPase, Inhibits Acidification and Protein Degradation in Lysosomes of Cultured Cells. J Biol Chem, 266, 17707-17712.

Appendix A

Sequence alignment of 19 putative cysteine protease domains.

```
Plu3324    AVVKPQSRPAVEDLEGLSGTNKGVEPTIIGDSHLKKPVD----GWQKVDVTPQTDG----
Plu3217    ---------AVEALDWLSGKNKRPEPTIIDDTHQDKKISRLLGDWQMEQVTPQADG----
Plu1341    -------------------PVTRFFNNELYGFKEDKNQD------RVKNSQQKNDN----
Plu1344    -------------------QYTDRIVSTLSDFQ-NKNRD------GVKNSWQKSDN----
XnRtx      ------------------IKKPLGDNSPESHIR-VNNHDVG-----SWENITVKPQPES----
XbRtx      -----------------VKVPLKDNLPEGVDRVVNNENVE----HWEPAFVKPQAEG----
VvRtx      -----------------PKITFKDSLSGANTALHNQNVN----DWERVVVTPTADG----
VcRtx      -----------------QVVDSKEALADG-KILHNQNVN----SWGPITVTPTTDG----
VsRtx      ------------------------SLNGSDDTVKNKDVN----SWERLIVSPQSDG----
FhaL4      -----------EIPATDTPTQQVATPVPAPDKLVIQQWH--SGAGAARPPSPQAQAQAPY
FhaL3      -----------ETTPPGAPPDAVAPPLAPVSARYLQQWRERSGVAQPRPPTPLGAEPPVH
FhaL2      -----------EFQRPGS---DTPSPQLPPHELLIRSWLASSAPVHALPLPPSSRGTLP-
FhaL1      -----------AAKAPALPLARPLTSVLAGPSSTSPTANPAAAPGIAAQPAPASPGRDAP
CstoxL     -----------RAKSQFEEYKKGYFEGALGEDDNLDFAQNTVLDKDYVS-KKILSS--MK
TcdB       --------------IQFEEYKKNYFEGALGEDDNLDFSQNTVTDKEYLL-EKISSS--TK
TcdA       --------------YQFEKYVRDYTGGSLSEDNGVDFNKNTALDKNYLLNNKIPSNNVEE
Cnalpha    -------LRSNIAEKEFQKLIKTYIGRTLNYEDGLNFNKWKRVTTSELL-KVIEEVNSTK
YpRtx      -----------------TGFLITTLDEPVVKYPDIVKVN----EWDLPAIANIDKT---A
YmMfp2     --------------------GETIDFSVWESPDQAYFT-------SLPNTPLEPE----
consensus  ----------------------------i------------------v---p--d-----

Plu3324    RETRFDGQIILQMEDDPIAARAAAANLAGKHPDSSVVIQLDANGKYRVVYGDLAKLS----
Plu3217    RETRFDGQIIIQMEDDPIVAKAAAANLAGKHSDSSVVVQLDSKGKYRVVYGDLTRLS----
Plu1341    RGTRFDGQIIIQMEDDPIVAKAAINLAGKHPDSSVVVKLDADGKYHVIDGDPAGLS----
Plu1344    RGTRFDGQIIIQMENDPIVAKAALNLASKHRKSSVVVKLDSNGKYHVIYGDPAGLS----
XnRtx      GDSRFSGQIIIQTENDPVAAKAAANLAGKHPDSSVIVQLDANGQYRVVYGDPADLSNK--
XbRtx      GDSRFNSQVIIQTENDPVAAKAAARLAGKHPDSSVIVQLDANGRYRVVYGDPATLS----
VvRtx      GESRFDGQIIVQMENDDVVAKAAANLAGKHPESSVVVQIDSDGNYRVVYGDPSKLD----
VcRtx      GETRFDGQIIVQMENDPVVAKAAANLAGKHAESSVVVQLDSDGNYRVVYGDPSKLD----
VsRtx      GETRFDGQIIIQMENDSSVSKAAENLAGKHPDSTVVVQLDSDGNYRVVYGDPSKLPKD--
FhaL4      GPDRYAHRVIVQLGSDTVTESAARRLFRKHAATSLWYGQTLEGTLMLKQGGDTPAA----
FhaL3      GPDRYGHRTIVQLGSDALTETAARRLFRKHAGNASWYSQDASGQLTQVRAPAAPAT----
FhaL2      GADPYALRSIVQLGTDAATARAAAALHGKHPANSNWYLQTRDGGLEPVRQAAGPAA----
FhaL1      KPDPYANRVIVQLAQDDVATQAAQALFHKHAEQSDWYRQADDGSLHPVHPLRAAAA----
CstoxL     TRNKEYIHYIVQLQGDKISYEASCNLFSKDPYSSILYQKNIEGSETAYYYYVADAEIKEI
TcdB       SSEGGYVHYIVQLQGDKISYEAACNLFAKNPYDSILFQRNIEDSEVAYYYNPTDSEIQEI
TcdA       AGSKNYVHYIIQLQGDDISYEATCNLFSKNPKNSIIIQRNMNESAKSYFLSDDGESILEL
Cnalpha    IYENYDLNMILQIQGDDISYESAVNVFGKNPNKSILIQG-VDDFANVFYFENG--IVQSD
YpRtx      TASQYDMQIVFQCENNPTVNRAATRLAGKHAKNSIIIQLDVDNNHRAFIIDDNIHAEWRE
YmMfp2     -GTHYEKTLIFQLQGDDTCFEASRALFNKHRYTSEWLQLGDGKPAEVFTWGETYKKFVYT
consensus  --trfd-qiilQme-d-i--raa-nlagKhp-ssvviqld-dg---vvygd-a-------

Plu3324    ----------------NKLRWQVVGHGRDTS-EQNNIRLSGYSADELAT-----KLKQFY
Plu3217    ----------------GKLRWQVVGHGRDTS-EQNNIRLSGYTADELAT-----RLTRFY
Plu1341    ----------------GKLRWQIVGHGRDES-TQNNTRLSGYRADELAI-----KLKQFS
Plu1344    ----------------GKLRWQIVGHGRNES-AQNNTRLSGYSADELAI-----KLKQFS
XnRtx      -------------LQSGKLRWQIVGHGREES-AQNHTRISGYSADELAL-----RLKQFS
XbRtx      ----------------GKLRWQIVGHGRDES-VQHHTRMSGYSADELAL-----KLKQFR
VvRtx      ----------------GKLRWQLVGHGRDDS-ESNNTRLSGYSADELAV-----KLAKFQ
VcRtx      ----------------GKLRWQLVGHGRDHS-ETNNTRLSGYSADELAV-----KLAKFQ
VsRtx      -------------KSTGQLRWQLVGHGRDES-ENNNTHLSGYSADELAV-----KLAAFN
FhaL4      ----------------GPLKIQFVGHG--GP-RYSMPLLGGNTPAELAQ-----MASTIQ
FhaL3      ----------------GPQKIQFVGHG--SI-LEGMPLLGGNNAAQLAR-----MLPAIR
FhaL2      ----------------GPHKVQFVGHG--DV-YHGVPLLGGNAAATLAD-----LLNQVE
FhaL1      ----------------GPTKIQLVGHG--SA-DR--QALSGHDGHAVAG-----IVQQLR
CstoxL     DKY----RIPYQISNKRNIKLTFIGHG--KS-EFNTDTFANLDVDSLSS-----EIETIL
TcdB       DKY----RIPDRISDRPKIKLTFIGHG--KA-EFNTDIFAGLDVDSLSS-----EIETAI
TcdA       NKY----RIPERLKNKEKVKVTFIGHG--KD-EFNTSEFARLSVDSLSN-----EISSFL
Cnalpha    NIN----NILSRFNDIKKIKLTLIGHG--EN-VFNPKLFGGKTVNDLYTNIIKPKLQHLL
YpRtx      ISHNELVTKLKIQPENGKIRWQVVGHGRSEGGNDKHPTLAGQRPEQLTA-----RLNQFS
YmMfp2     SPLKLD--------KEGKIRITLVGHGETEG---DTTTFGGMNAETLKG-----HLSSLF
consensus  ----------------gklrwqvvGHGr-es---n---lsg-sadela------kl--f-
```

```
Plu3324    QAAKLGKQAISKPDHISLVGCSLISD--NKRDGFARRFITELDK---------QGIRSDV
Plu3217    QDVNQGKSITHKPDHISIVGCSLISD--DKRDGFARRFITVLDK---------QGIRSDV
Plu1341    QDFEQAG----KPERISIVGCSLISD--DKQNGFAYRFMFALDK---------QGIRSEV
Plu1344    QNFEQAG----KPDRISIVGCSLISD--DKRNGFAYRFITALDK---------QGIRSEV
XnRtx      IDFKQAG----KPDHISLVGCSLISD--DKRNGFARRFISALNE---------QGVRTTV
XbRtx      TDFKQAG----SPDHISLVGCSLISD--DKRDGFARHFISELDK---------QGIRTTV
VvRtx      QSFNQAENINNKPDHISIVGCSLVSD--DKQKGFGHQFINAMDA---------NGLRVDV
VcRtx      QSFNQAENINNKPDHISIVGCSLVSD--DKQKGFGHQFINAMDA---------NGLRVDV
VsRtx      QAFSEAENVKASPDYISVVGCSLISD--DKQNGFGRLLIQSMGD---------NDIRSDV
FhaL4      HAGPPSQ-----LEKVTLVGCQTDCV--A-RPSLRKLFSTALAT-E-------HGLTPAV
FhaL3      QGLPATA----RVEKITLVGCNTGCA--S-RASLRNLLNHYLIT-T-------AGLSAEV
FhaL2      QHSPAGA----RLDKIALVGCDTDCT--G-RPSLREPFRQSLAARP-------DAPALTV
FhaL1      ERLPPAA----ALAKVALVGCDTDCA--S-GASLRGDVAQRLAADG-------AQPAPAV
CstoxL     NLAKADIS--PKYIEINLLGCNMFSYSISAEETYPGKLLLKIKDRVSELMPSISQDSITV
TcdB       GLAKEDIS--PKSIEINLLGCNMFSYSVNVEETYPGKLLLRVKDKVSELMPSMSQDSIIV
TcdA       DTIKLDIS--PKNVEVNLLGCNMFSYDFNVEETYPGKLLLSIMDKITSTLPDVNKNSITI
Cnalpha    EREGVILK--NKYLKINILGCYMFTPKVDINSTFVGKLFNKISRDLQPKG--FSKNQLEI
YpRtx      DYLQTEHQINISPQQVSLVGCAMSSS--DRYTSFAHKFMSHLNE---------NGIRTNV
YmMfp2     ARLGSSS-VLIKGITLNLTGCSLLNPKQPLADTLPGQLAIWLKQQAEILG--LDDSNWSV
consensus  q----g-----kpd-islvGCslis---dk--sfa-rfi--l-----------qgir--v

Plu3324    SARSSEVAVDATGRKFTRDENNQWVNNSP---MGRENWMFGGDGDDTAVVAGRINHVFMG
Plu3217    SARSSEVAVDVSGRKFTRDQNNQWVNNLPDNKIVLENWMFGGKGDDTAVVAGRINHVFMG
Plu1341    SVRRSDVAVDATGRKFTRDKNYQWVNRLD-------------------------------
Plu1344    SARRSEVAVDATGRKFTRDKNHQWVNKLD-------------------------------
XnRtx      SARSSEVAVDSIGRKYTKDAQDQWVHKLT-------------------------------
XbRtx      SARSSEVAVDSIGRKFTRNAEEQWVHKLM-------------------------------
VvRtx      SVRSSELAVDEAGRKHTKDANGDWVQKAE-------------------------------
VcRtx      SVRSSELAVDEAGRKHTKDANGDWVQKAE-------------------------------
VsRtx      SVRSSEVAVDSNGRKHTHDENGHWVQKEK-------------------------------
FhaL4      TGYAGRVDVDAAGRKRIVEQGGLNEPRAQ-----------------------------AGAST
FhaL3      KGYAGRVDVDAAGHKQIVEQGGLGNTPPP-----------------------------EAAP-
FhaL2      TGYIGRIDVDSAGRKRRVATGGLGDRPPA-----------------------------DEPAS
FhaL1      SGYIGRLEVDAAGRKHAVAQGGLGDVDPE-----------------------------ARAQG
CstoxL     SANQYEVRINEEGKREILDHSGKWINKEE-----------------------------SIIKD
TcdB       SANQYEVRINSEGRRELLDHSGEWINKEE-----------------------------SIIKD
TcdA       GANQYEVRINSEGRKELLAHSGKWINKEE-----------------------------AIMSD
Cnalpha    SANKYAIRINREGKREVLDYFGKWVSNTD-----------------------------LIAEQ
YpRtx      SASTKAIEVDPLGHKHDVDTPDIDSYNNK-----------------------------YLSS
YmMfp2     NARENDLLVLENGKKEIR-INDHWINKEVADIHGLVYFSTPINVQLDSRARTLIVPTLLD
consensus  sar--ev-vd--Grk---d--g-wvnk-------------------------------

Plu3324    EGNDQTFVFGEGGLIDAGNGQDYVVTSGNYNRVDTGAGQDYAVTIGN-------------
Plu3217    EGNDQTFVFGEGGFIDAGNGQDYVVTAGNYNRMDTGKGQDYAVIIGNNNQ----------
Plu1341    -DNKQVLCWNEEG------------------------------------------------
Plu1344    -DNKLVLRWNEQD------------------------------------------------
XnRtx      -DNKIVLGWNDKG------------------------------------------------
XbRtx      -DNKIVLGWNDKG------------------------------------------------
VvRtx      -NNKVSLSWDEQG------------------------------------------------
VcRtx      -NNKVSLSWDAQG------------------------------------------------
VsRtx      -SNKVTLSWDEQGEVTEKHER----------------------------------------
FhaL4      AAPNRIVQSVAHG-VALSQS-----------------------------------------
FhaL3      -AP-RVFR---HGNVTLSQSGEARQ------------------------------------
FhaL2      PRP-----------PAQPAA-----------------------------------------
FhaL1      TQP--VPRVFSHGPVNIAQSG----------------------------------------
CstoxL     ISSKEYISFNPKENKIIVKSKYLHELSTLLQEIRNNANSSDIDLEKKVMLTECE------
TcdB       ISSKEYI------------------------------------------------------
TcdA       LSSKEYI------------------------------------------------------
Cnalpha    ISNKYVVYWNEVENTLSARVEQLNKVAEFAKDINSIIQTTNNQELKQLDGNKYYFQSNSK
YpRtx      IKGTEKLYWNRWG------------------------------------------------
YmMfp2     DTERGKLFYQLIGNGGEYTLIMPSKTVAITITCADADKEHWIFDIEALIKQS--------
consensus  --nk--l-f---g------------------------------------------------
```

Curriculum Vita

Name: Kerri-Lynn Sheahan

Birthdate: August 10, 1976

Birthplace: Warwick, RI, USA

Education:

2006 — Ph.D., Biomedical Sciences
Northwestern University
Evanston, IL

1998 — Bachelor of Science, Biochemistry
Lehigh University
Bethlehem, PA

Research Experience:

2001-2006 — Doctoral Research
Laboratory of Dr. Karla Satchell
Northwestern University
Department of Microbiology-Immunology

1999-2001 — Research Technician
Laboratory of Dr. Sharon Rounds
Brown University
Department of Medicine

1998-1999 — Graduate Research Associate
Laboratory of Dr. Alexander Sulakvelidze
University of Maryland, Baltimore
Department of Epidemiology

Teaching Experience:

Fall 2004
Fall 2005 — Teaching Assistant for Medical Microbiology Laboratory
Northwestern University, Feinberg School of Medicine
Laboratory Coordinator: Dr. Karla J Fullner Satchell

Jan-May 1998 — Teaching Assistant for Introductory Chemistry
Lehigh University, Department of Chemistry.
Instructor for Laboratory and Lecture Recitation

Awards:

2003-2005 — Ruth L. Kirschstein NRSA Predoctoral Training Grant in Immunology and Microbial Pathogenesis (T32-AI007476-09)

September 2005 Best Student Poster Presentation
Microbiology-Immunology Department Retreat

Publications

Sheahan KL and Satchell KJ. Autoprocessing of the *Vibrio cholerae* RTX toxin by the cysteine protease domain. EMBO J. *In revision.*

Sheahan KL and Satchell KJ. Inactivation of the small Rho GTPasesby the multi-functional RTX toxin from *Vibrio cholerae*. Cell Micro. *In press.*

Sheahan KL, Cordero CL, and Satchell KJ. Identification of a Domain Within the Multi-functional *Vibrio cholerae* RTX Toxin that Covalently Cross-links Actin. Proc. Natl. Acad. Sci. USA (2004) 101:9798-803.

Kramer K, Harrington EO, Lu Q, Bellas R, Newton J, **Sheahan KL**, and Rounds S. Isoprenylcysteine carboxyl methyltransferase activity modulates endothelial cell apoptosis. Mol Biol Cell. (2003)14:848-57.

Bellas RE, Harrington EO, **Sheahan KL**, Newton J, Marcus C, and Rounds S. FAK blunts adenosine-homocysteine-induced endothelial cell apoptosis: requirement for PI 3-Kinase. Am J Phsiol Lung Cell Mol Physiol. (2002) 282:L1135-42.

Abstracts

Sheahan KL and Satchell KJ. (2005) Characterization of the Two Cell Rounding Activities of the *Vibrio cholerae* RTX Toxin: Actin Cross-linking and Rho Inactivation. The 12th European Conference of Bacterial Protein Toxins. Canterbury, England.

Sheahan KL, Cordero CL, and Satchell KJ. (2004) The Multi-functional RTX Toxin from *Vibrio cholerae* Covalently Cross-links Actin through a Novel Domain. 11th Annual Midwest Microbial Pathogenesis Meeting, East Lansing, Michigan.

Sheahan KL, Cordero CL, and Satchell KJ. (2004) The Multi-functional RTX Toxin from *Vibrio cholerae* Covalently Cross-links Actin through a Novel Domain. FASEB SRC, Microbial Pathogenesis: Mechanisms of Infectious Disease, Snowmass Village, Colorado.

Sheahan KL, Cordero CL, and Satchell KJ. (2003) *Vibrio cholerae* RTX Toxin Exhibits Bi-functional Activity: Actin Cross-linking and Rho Inactivation. The 1st Annual Chicago Cytoskeleton Conference, Chicago, Illinois.